ABSTRACT

PATIL, ROHAN RAMDAS. An Investigation into the Structure of Polymer Brushes using Degrafting as a Strategy. (Under the direction of Dr. Jan Genzer and Dr. Douglas Kiserow).

This PhD thesis aims to develop experimental protocols and measurements tools that provide detailed information about the properties of surface grafted polymer assemblies (SGPAs) on flat impenetrable surface. SGPAs, often colloquially referred to as polymer brushes, have become an active field of study in the recent two decades due to their potential in tailoring physico-chemical properties of material surfaces, and probing the effect of confinement due to substrate on controlled radical polymerization (*i.e.*, atom transfer radical polymerization, ATRP) originating from initiator centers anchored chemically to the surface (*i.e.*, "grafting from"). The two key attributes of polymer brushes we concentrate on in our study involve molecular weight distribution (MWD) and the grafting density (*i.e.*, areal density of polymeric grafts on the substrate), as they hold the key to comprehending the characteristics of SGPAs. We report on a novel and efficient way to degraft grafted polymer chains grown by the "grafting from" method from the surface. Specifically, we utilize tetrabutyl ammonium fluoride (TBAF) for degrafting poly(methyl methacrylate) (PMMA) brushes from silica based substrates. TBAF attacks selectively the Si-O bonds at the linker point between the substrate and the PMMA chain and does not cause any chemical changes to the polymer chain itself. We demonstrate that TBAF-governed cleavage removes nearly all PMMA grafts from the substrate. The cleaved chains are then collected and their MWD is characterized using size exclusion chromatography. Using MWD and dry thickness of the polymer layer we determine the grafting density of PMMA and find a value of 0.5 chains/nm^2, which is independent of the reaction conditions during the ATRP. This Thesis also attempts to shed light into the mechanism of degrafting by studying the kinetics of the process. The initial grafting density of

the polymers is found to play an important role. In addition, the degrafting process can be controlled by varying the incubation time, TBAF concentration in solution, and temperature. We demonstrate that it is possible to reuse this degrafted substrate for growing new polymer brush layers without using any physical or chemical cleaning/activation method. This notion is further utilized to create a variety of surface spatial patterns such as grafting density gradients or 2D patterns of homopolymer and copolymer brushes.

An Investigation into the Structure of Polymer Brushes using Degrafting as a Strategy

by
Rohan Ramdas Patil

A dissertation submitted to the Graduate Faculty of
North Carolina State University
in partial fulfillment of the
requirements for the degree of
Doctor of Philosophy

Chemical Engineering

Raleigh, North Carolina

2016

APPROVED BY:

_____	_____
Jan Genzer Co-Chair	Douglas Kiserow Co-Chair
_____	_____
Orlin Velev	Christopher Gorman

_____
Stefan Zauscher

DEDICATION

To my father, Ramdas

BIOGRAPHY

Rohan was born in a village named Soygaon in the state of Maharashtra, India. He moved to the small town of Jalgaon at an early age, where he went to high school at the St. Joseph's Convent School. He graduated with a degree in Chemical Engineering at the Institute of Chemical Technology, Mumbai in 2010. Following undergraduate studies he enrolled at Department of Chemical and Biomolecular Engineering at North Carolina State University, Raleigh, NC. He joined Prof. Jan Genzer's research group to pursue his PhD, where he studied polymers grafted on surfaces. He will be working at Intel Corporation as a Module Engineer following completion of his PhD.

ACKNOWLEDGMENTS

I would like to start by saying a big thank you to my advisor Dr. Jan Genzer, without his guidance this would not have been possible. His unwavering enthusiasm, curiosity, excitement about science combined with his jovial nature made my work as a doctoral student meaningful and fun. I would like to acknowledge Dr. Jiři Šrogl for coming up with the important idea about degrafting compound. I would also thank Dr. Henderson, Dr. Dickey, Dr. JP. Maria for letting me use the equipment in their labs.

A special thanks to Preeta, your guidance professional and otherwise has proved to be essential. I want to thank Dr. Erich Bain for teaching me all the basics of synthesizing polymers in the early part of my PhD, and thanks to Zuleyha for helping me out when I was not able to grow polymer brushes. Thanks to Edwin, Gilbert and Matt for keeping the lab safe and always striving for the best. Thanks to all the Genzer lab group members whose support has been integral for my work, thanks for repeatedly listening to my presentations and giving me valuable feedback.

A hearty thanks to Shiva, a loyal friend, an amazing roommate, and a great human being. Thanks to Janell, Manu, Yeongun, Stefanie, Sergej, Anurodh, Ishan for being amazing rock climbing buddies and thanks to all the roommates during my stay. Thanks to Chetan, Dishit and Shilpa for the support and all the interesting conversations. All of you made my stay in Raleigh enjoyable and I would forever miss those days.

Last but not least I am grateful to my father for always providing me the love and care a son wants. You have always given me the strength and inspiration I needed.

TABLE OF CONTENTS

LIST OF FIGURES

1. Introduction and Dissertation Scope

1.1 Introduction

Surface grafted polymer assemblies (SGPAs), often referred to, colloquially, as polymer brushes, have become an active field of research in the last two decades.[1,2] Such systems comprise polymer chains attached (physically or chemically) to a substrate or an interface. The polymer chains can be synthesized in bulk and attached to a surface, also known as "grafting to" polymerization. Alternatively, polymer brushes can be grown directly from the surface via a plethora of polymerization techniques; termed as "grafting from" polymerization. The work presented in this PhD Thesis pertains primarily to polymer brushes grown by "grafting from" polymerization on a flat silicon substrate. "Grafting from" is a more desirable method than "grafting to" when generating polymer brushes with high grafting densities.

The primary purpose of this PhD Thesis is an exploration into the techniques that can be utilized to measure the relevant properties of such a system. The determination of these properties is crucial for fundamental studies as well as for development of various applications involving polymer brushes. There is a correlation between the brush properties, such as the molecular weight and grafting density, to macroscopic properties such as friction coefficient, swelling, wettability, *etc*. For example, the friction coefficient of a fluorinated polymer brush is a strong function of the grafting density and molecular weight of the brush.[3] The swelling behavior of poly(methyl methacrylate) (PMMA) brushes in a poor solvent scales with the grafting density of the system.[4]

The results reported in this PhD Thesis are presented as four distinct chapters. Chapter 2 is a literature review of the various techniques that are available and utilized for measuring the various properties of polymer brushes. It will provide the reader with insight on the choice of the technique to investigate a grafted polymer system. The choice of the measurement technique depends on the desired property, the system attributes, *i.e.*, the geometry of the substrate, the physical, and chemical properties of grafted polymer such as its solubility in solution.

Chapter 3 offers a detailed insight into a novel technique to measure the molecular weight and grafting density of PMMA brushes grown on flat silicon substrates as displayed in **Figure 1.1**. The polymer is "degrafted" from the substrate quantitatively; *i.e.*, nearly all polymer chains are removed from the substrate in an efficient manner by cleaving the bond at the base of the polymer, without degrading the polymer itself. The compound called tetrabutyl ammonium fluoride (TBAF) is utilized to perform this task due to its specificity and low toxicity.[5,6] The polymer brushes are grown using atom transfer radical polymerization (ATRP) where the rate of polymerization can be controlled by varying the ratio of copper based catalysts. A grafting density value of 0.5 chains/nm^2 is determined which is independent of the ATRP conditions.

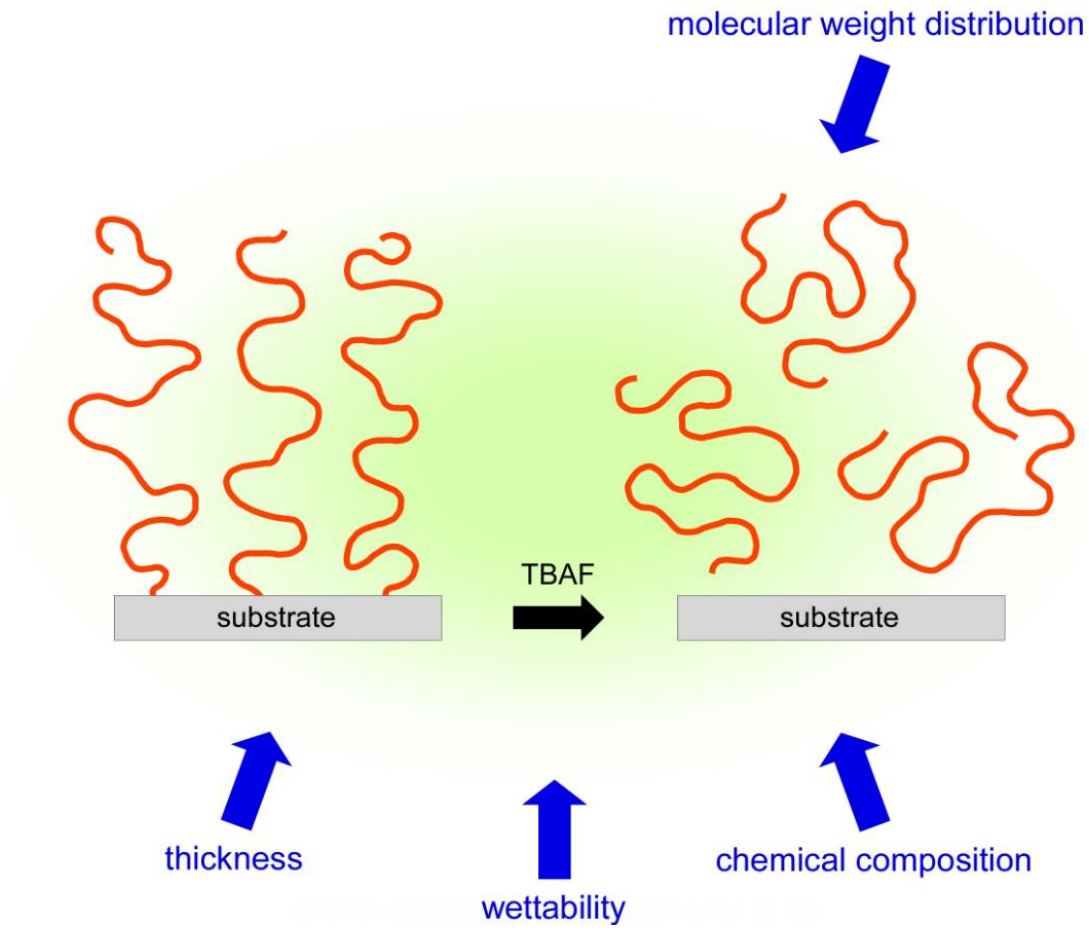

Figure 1.1. Scheme showing the degrafting of a polymer brush using TBAF and characterization of properties such as thickness, wettability and molecular weight distribution to get the complete picture.

The kinetics of the degrafting process is studied in more detail in Chapter 4. The degrafting characteristics of polymer brushes bear an analogy to chemical reaction kinetics. A chemical reaction involves changes in the concentration of chemical species as a function of time, which can be measured, and information about the rate constants and mechanism of the reaction can be inferred. In a similar manner, the grafting density can be monitored as a function of time to gain understanding of the mechanism of the degrafting process. By employing an orthogonal

gradient approach, we are able to study the degrafting for different initial grafting densities on a single sample.. The concentration of the TBAF in solution is large enough to be considered constant, hence, it has no effect on the reaction kinetics.

Application of the degrafting technique is demonstrated in Chapter 5. The degrafting process itself is chemically mild and the resulting substrate is reusable without activation by conventional ultraviolet ozone treatment for growing new polymer brush layer. Patterns such as continuous gradients can be created using the *dipping technique* in a TBAF solution. A hydrogel stamping technique similar to microcontact printing can be utilized to create localized patterns of desired shapes. The incubation time, temperature and concentration of TBAF solution are varied independently to obtain the desired polymer brush surface pattern. The degrafting method can be extended from brushes to organosilane monolayers to create surface patterns as well, because they have silane-based attachment with the substrate. We further discuss that organosilane monolayer surface patterns can themselves serve as a platform for creating polymer brush surface patterns.

Chapter 6 provides an outlook into future research work utilizing degrafting of grafted polymer brush systems. When growing a second polymer block on top of an existing polymer brush (*i.e.*, macroinitiator), synthesized by living polymerization, the conditions for initiation are different since the active chain end is not present on the free surface, as in the case of surface attached initiator. The *initiation* of this second polymer block depends on the physical properties of the first layer of polymer brush such as the solvent conditions, mobility of the chain end, *etc*. This effect can be studied by monitoring the thickness of the second block after

polymerization. A fluorescent dye can be attached by use of click chemistry to the active polymer ends before and after growing the second block, which can then be quantified using fluorescence microscopy. Information about the stability and attachment of silane-based monolayers can be obtained in a systematic manner by degrafting using TBAF. This can be carried out by varying the base group, the mesogen type/length, and the head group and observing their degrafting characteristics. Gradient approach can be integrated in each study to make the experiments more efficient and systematic.

1.2 References

(1) Milner, S. T. *Science* **1991**, *251* (4996), 905–914.

(2) Zhao, B.; Brittain, W. J. *Prog. Polym. Sci.* **2000**, *25*, 677–710.

(3) Bhairamadgi, N. S.; Pujari, S. P.; Leermakers, F. A. M.; Rijn, C. J. M. Van; Zuilhof, H. *Langmuir* **2014**, *30*, 2068–2076.

(4) Moh, L. C. H.; Losego, M. D.; Braun, P. V. *Langmuir* **2011**, *27* (7), 3698–3702.

(5) Patil, R. R.; Turgman-Cohen, S.; Šrogl, J.; Kiserow, D.; Genzer, J. *ACS Macro Lett.* **2015**, *4* (2), 251–254.

(6) Patil, R. R.; Turgman-Cohen, S.; Šrogl, J.; Kiserow, D.; Genzer, J. *Langmuir* **2015**, *31* (8), 2372–2381.

2. Determining the Attributes of Surface-anchored Polymer Assemblies using Analytical Methods

2.1 Introduction

The purpose of this chapter is to serve as a guide for everyone looking to characterize the properties of systems involving grafted polymer chains by providing insight into the choice of technique for a given system. There have been several review papers related to this topic. We incorporate some of that work here, especially the work of Hoshino *et al.*, which gives an excellent overview for how synchrotron radiation tools can be utilized for measuring properties of polymer brushes on flat and convex geometries.[1] We intend to provide an exhaustive picture focusing on the appropriate experimental technique for a given attribute or property of a grafted polymer system, with the help of examples that the reader can relate his system to.

The key properties that we are interested in involve the molecular weight (MW) distribution, the grafting density (σ) of the attached chains, the polymer chain orientation and the spatial distribution profile of certain species within the grafted layer. The techniques vary based on the property to be determined, the geometry of the substrate, the type of grafted polymer, chemistry, solubility, polymer length and grafting density. This chapter is divided into three parts on the basis of the geometry of the substrate which can be (i) flat, (ii) concave (e.g., inside pores) or (iii) convex (e.g., on nanoparticles). We first start with techniques that pertains to determining the properties of polymer brushes on flat substrates since it is the most commonly used platform. We then explore concave and convex geometries.

2.2 Flat substrates

Flat substrates are the most commonly used geometries because of the wide range of techniques that can be performed for characterization. They also serve as benchmarks or controls for other geometries. We have focused and divided the sections with titles mentioning the property/attribute along with the technique utilized to measure that property. We further discuss, citing examples in the literature, what systems this technique would be appropriate for and what are its limitations.

2.2.1 Direct measurement of molecular weight – Size Exclusion Chromatography (SEC)

Size exclusion chromatography (SEC) has been one of the most widely used technique for determining the molecular weight distribution (MWD) of bulk polymers because of its versatility and accuracy. However, for a grafted polymer system, we have two major problems for its utilization especially for polymer brushes grown by "grafting from" polymerization: (1) The polymer chains are chemically attached to the surface, hence we have to remove them from the surface and pass them through the SEC, the bulk polymer grown in the same solution as the brushes is sometimes utilized but the properties of those bulk-grown polymers are not the same as those grown from the substrate[2], (2) The amount of polymeric material present on the surface is extremely small and hence requires the use of very sensitive detectors, which also places a detection limit for the system studied.

We have approached to solve some of these problems in this PhD Thesis; the procedure will be described in detail in Chapter 3. Here is just a brief overview. For neutral poly(methyl

methacrylate) (PMMA) brushes grown on silicon substrate (with a thin layer on silica present on the top), we utilized a compound called tetrabutyl ammonium fluoride (TBAF) that *cleaves* selectively the Si-O bond at the base of the polymer substrate and etches away a part of the silica layer.[3,4] We refer to this process of cleaving near the substrate surface as 'degrafting'. The procedure is effective in removing nearly all the polymeric material and the reagent is mild enough so that the substrate is available for further use for re-deposition of a new initiator and growth of new polymer brush layer. The collected polymer can be passed through a SEC with sensitive differential refractive index (DRI) detector to obtain data which can then be converted to MWD using conventional calibration (**Figure 2.1**). The number average molecular weight (M_n) can be calculated from this MWD. We used THF instead of toluene as a solvent since the *dn/dc* of the polymer/solvent system is high and hence the sensitivity of the detection is increased. Spectroscopic ellipsometry was used in conjunction with SEC to obtain the dry thickness (h_P) of the brush films and using mass balance based Equation (2.1), the grafting density value of ~ 0.5 chains/nm^2 was calculated.

$$\sigma = \frac{h\rho N_A}{M_n} \tag{2.1}$$

Here ρ is the bulk polymer density and N_A is the Avogadro's number. Such a technique is useful if a large enough substrate of uniform polymer brush can be created. The substrate size utilized was 4.2 cm x 4.2 cm and the minimum thickness required was 48 nm. This size based on the detection limit of the DRI detector was determined by benchmark experiments carried out using bulk polystyrene PS of high polydispersity index (PDI). The degrafting technique is destructive in nature, as it severs the chemical attachment of the chains, but the substrate and

the polymer itself is left unharmed. A key limitation of this technique is that we may not have a good solvent for every polymer, especially polymers with lower critical solution temperature (LCST), e.g., poly(N-isopropyl acrylamide) (PNIPAM), poly(dimethylaminoethyl methacrylate) (PDMAEMA), may be harder to degraft since higher temperature will collapse the structure and make it harder for the TBAF molecule to reach the point of detachment. This places an upper limit on the degrafting temperature and hence an upper limit on the rate of degrafting. Some polymers may also be prone to forming complexes with TBAF itself which would change the MWD measured using SEC.

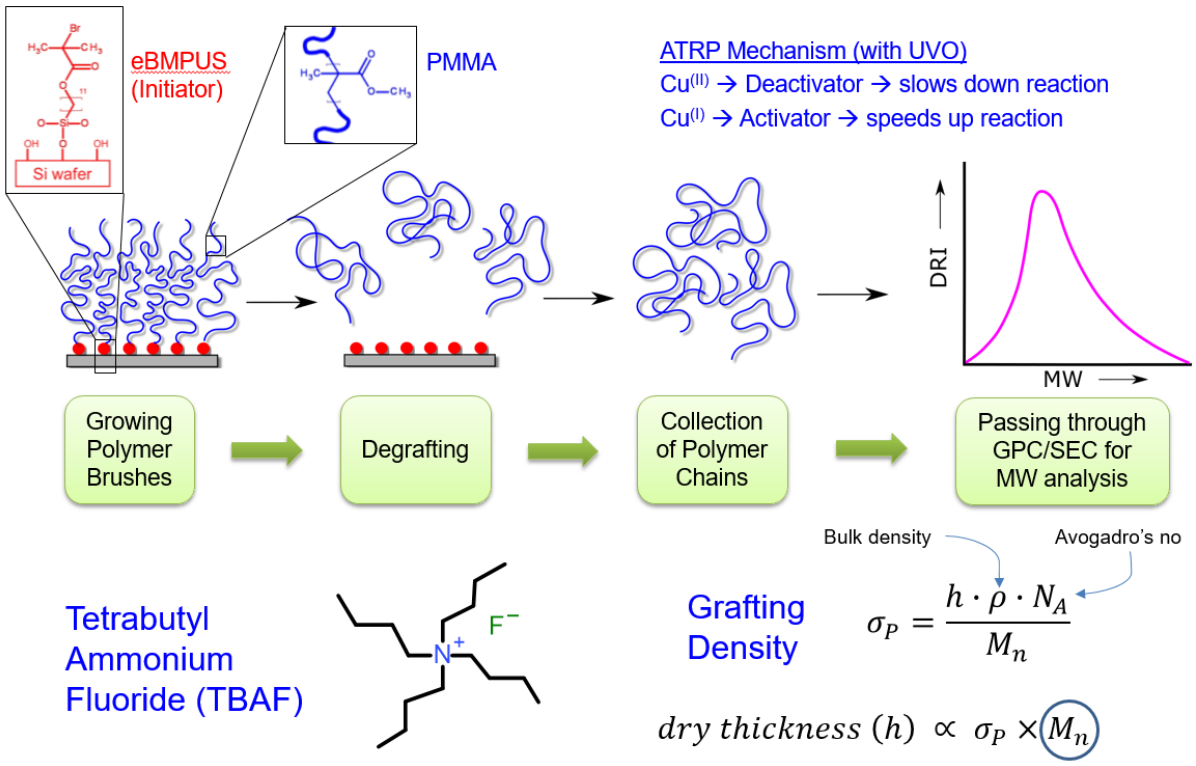

Figure 2.1. Scheme showing degrafting of poly(methyl methacrylate) (PMMA) brush layer from silicon substrates using tetrabutyl ammonium fluoride (TBAF) and further characterization using size exclusion chromatography (SEC).

The degrafting approach has also been implemented by Spencer *et al.* where they synthesized a custom initiator prone to cleaving upon irradiation with UV light.[5] The limitation here was that UV light is absorbed by nearly all organic compounds including polymer which may cause them to degrade or result into undesired side reactions. Concentrated sulfuric acid has also been employed to cleave polyelectrolyte brush such as Poly [{2(methacryloyloxy)ethyl} trimethylammonium chloride] (PMTAC) and further characterized using SEC to determine its MWD.[6]

In the case of gold or metal substrate, thiol based initiators are commonly used. The strength of the sulfur/Au bond is weaker in comparison to siloxane bond on silica surface. The polymer chains grown here could be degrafted by simply heating the system in a good solvent[7] although a reductive environment such as in the presence of bromine is favorable. Polymer chains can then be collected and analyzed using a SEC.

2.2.2 Optical Properties – Ellipsometry – Thickness and More

Ellipsometry has become one of the most popular techniques and true "work horses" for quick and reliable measurement of thin film properties. In the commonly used reflective mode, we measure the change in the polarization of the incident light. The complex reflection coefficient is given as

$$\rho = \frac{R_P}{R_S} = \tan\Psi\, e^{i\Delta} \tag{2.2}$$

Where Ψ and Δ are ellipsometric parameters such that tanΨ is amplitude ratio and Δ is the phase difference.[8] Ellipsometry measures the change in the polarization of the incident light on the sample which depends on its optical properties and geometric arrangement of optically distinguishable layers.

The *thickness* of the film is the most common measurement that is obtained by a model fit although a lot more information such as the amount of embedded moisture[9], co-solvency[10] can be obtained. The limitation of ellipsometry (or any reflectivity or scattering technique, be it visible light, X-ray, electrons or neutrons) is that it is highly dependent on model fitting. If one has a good understanding of the nature of the system, the fit to the data is reliable and meaningful. Characterizing a brand new system can be challenging and should always be backed by measurements from other non-model based techniques. For example, a reliable way to know the thickness of a polymer brush (or any polymer) film would be by AFM using the *scratch technique*.[11] Although it is cumbersome and time consuming, it is worth checking a few samples to be consistent.

The measured change in the polarization depends on the dielectric constant of the film, thickness and arrangement of layers in the sample. In the visible range (i.e, 300-800 nm), most polymers exhibit no absorption, thus the dielectric constant can be represented by a simple refractive index (RI) value. Most polymer brush films can be fitted using simple Cauchy Model which gives RI as a function of wavelength of light for a given material. Spectroscopic ellipsometry instruments are capable of doing measurements over a wide range of wavelengths and the choice of range depends on the system under consideration. The refractive indices (n) of most polymers lie between the values of 1.4 and 1.6 but the exact value can be determined by a fit with ellipsometric data. If the exact value of the n for pure polymer is known then the fitted value can be used to determine the amount of a different component, for example, water present in the system which has a significantly different refractive index (n_{water} = 1.33) can be estimated. Variable angle spectroscopic ellipsometric (VASE) setups (like the VASE by J. A. Woollam) also allow measurement over a wide range of angle to eliminate the effects of incident/reflection angle.

The RI is affected by the density and composition of the polymeric film, for example due to presence of water which may have a different RI. Kooij *et al.* utilized this fact to get an optical segment density profile of PNIPAM brush layer to monitor its temperature induced transition *in situ*.[12] They modeled the PNIPAM film as consisting of two layers, a dense layer near the underlying substrate and a dilute layer exposed to solvent. An effective medium approximation was assumed for the dilute layer which considers the RI of both solvent and the polymer. Since the thermal transition is relatively faster than spectroscopic measurement time

(on the order of minutes) a single wavelength and fixed angle measurement was carried out for faster measurements while temperature was varied. A RI profile for high, medium and low grafting density brush layers was obtained in the z-direction at temperatures ranging around the LCST.[12] The advantage of doing ellipsometry here is that it is relatively simple in comparison to more advanced techniques like neutron reflectivity which essentially provides a scattering density z-profile.

The IR-VASE made by J.A. Woollam Inc. can measure ellipsometric data in the infrared wavelength regime. Since most polymeric materials absorb in IR region of the spectra, the absorption part of the dielectric constant contains features that are analogous to a FTIR spectra. This absorbing region of the spectrum provides information about the chemical nature of the polymer while the non-absorbing region can be utilized to determine the thickness of the polymer film. The limitation here is that the sensitivity is lower than regular ellipsometry hence the measurements times are much longer (usually on the order of hours).

2.2.3 Optical Properties – Surface Plasmon Resonance – Thickness and More

Surface plasmon resonance (SPR) measures the change in refractive index of an interfacial region between a noble metal and a liquid. Balamurugna *et al.* studied the LCST transition of thermoresponsive PNIPAM brushes on gold substrate using SPR.[13] The transition above the critical temperature into an insoluble state increases the density of PNIPAM due to collapse which increases the refractive index of the film near gold substrate. They observed that the local concentration of polymer in the brush and their confinement to the surface imparts unique

film behavior. The result is that PNIPAM brushes do not exhibit a sharp transition at LCST; rather it is a broad transition extending from 10 – 40°C depending on the properties of the brush.[13,14] The advantage of using SPR here is that *in-situ* monitoring can be carried out, the temperature and fluid environment can be controlled with time to obtain dynamic behavior. The disadvantage is that the surface has to be a noble metal, i.e., Au or Ag (for visible light), or a more exotic substrate, *i.e.*, Al-doped ZnO (for IR light), and the sensitivity is limited. For most cases related to measuring grafted polymer optical properties, ellipsometry is preferred over SPR.

2.2.4 Polymer Brush Conformation – Optical Reflectance

Varma *et al.* have developed a microscope-based optical setup to monitor the conformation of thermoresponsive behavior of PNIAM brushes on glass substrate.[15] Density profiles were fitted to the spectral reflectivity data in optical range using a simple model, as shown in **Figure 2.2**. They confirmed the process of vertical phase separation that takes place during the temperature transition across LCST. Okada *et al.* utilized reflectometric interference spectroscopy (RIfS) on thin PNIPAM hydrogel attached to a surface in a custom microfluidic setup to determine its dynamic transition properties.[16] This technique can be extended to brushes if they are grown on the surface by grafting from polymerization.

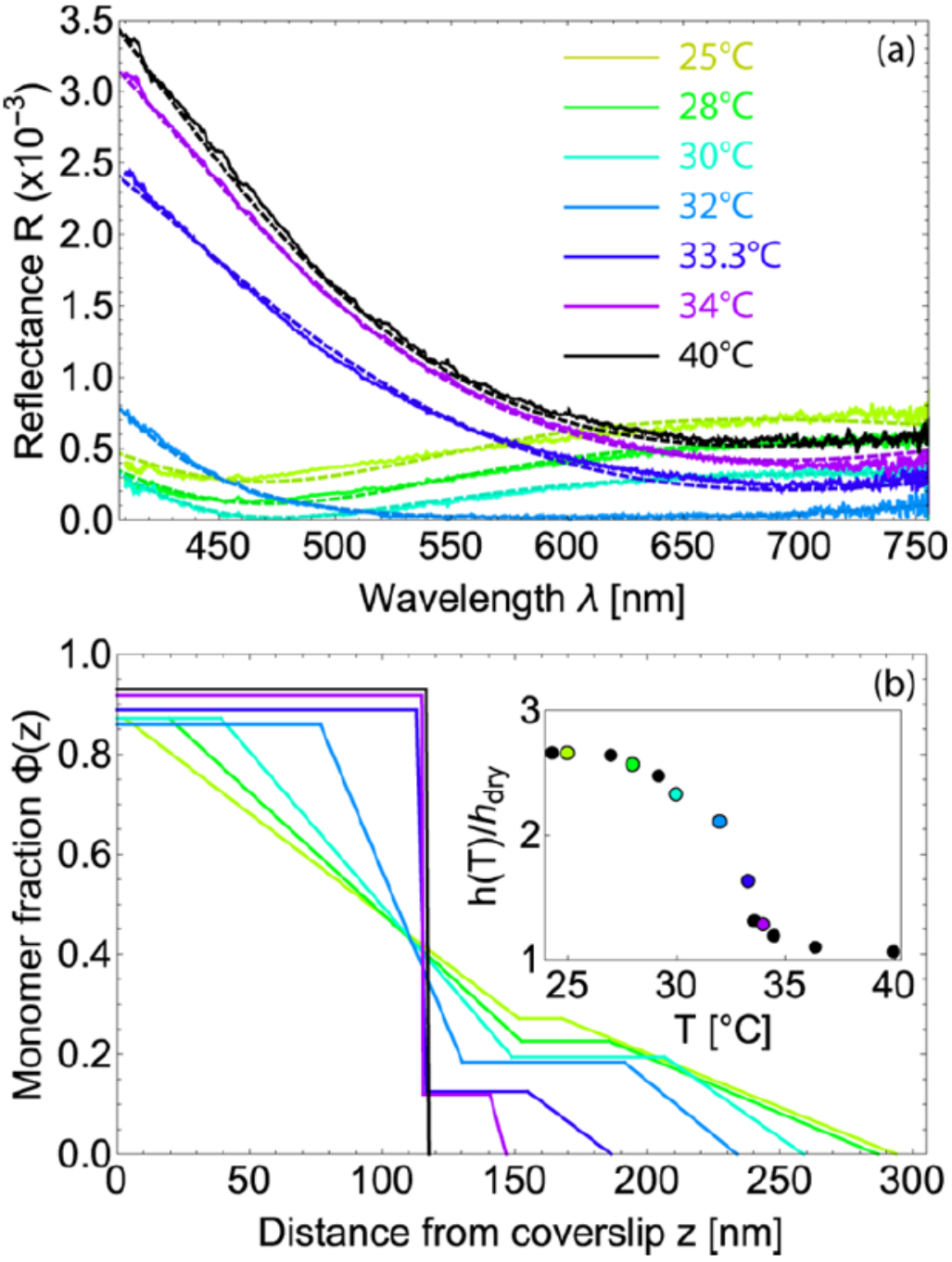

Figure 2.2. (a) Reflectance spectra obtained from high grafting density brush of thickness 108 nm as a function of temperature. Solid lines are the measured spectra, dashed lines are the best fits obtained with the profiles displayed in panel (b). (Inset) Swelling ratio as a function of temperature, showing a marked transition around the LCST.[15]

2.2.5 Molecular weight, grafting density and more – Atomic Force Microscopy

Atomic Force Microscopy (AFM) is a powerful method used to determine the local properties of a grafted polymer system. The adhesion profile of the end-grafted polymer chain to the AFM tip can be obtained from approach/retraction of the tip. Such a measurement involves the adsorption of the polymer chain to the tip usually by direct approach (*cf.* **Figure 2.3**), the stretching of the polymer at the free end away from the surface gives the force profile, while the separation at the bond rupture is used to estimate the contour length of the polymer. If the grafting density is sufficiently low then a single molecule can be adhered to the tip, this is referred to as *single molecule force spectroscopy*. A distribution of the contour lengths is generally obtained by repeating this procedure a large number of times over the entire substrate, this data can then be converted into M_n and polydispersity index (PDI) knowing the length of each monomer. However, when the grafting density is higher, the estimation of contour lengths is harder since multiple chains adhere to the tip of the AFM at the same time. Moreover, the tip may not be able to penetrate the layer completely and as a result, contour length is not measured for the entire graft.

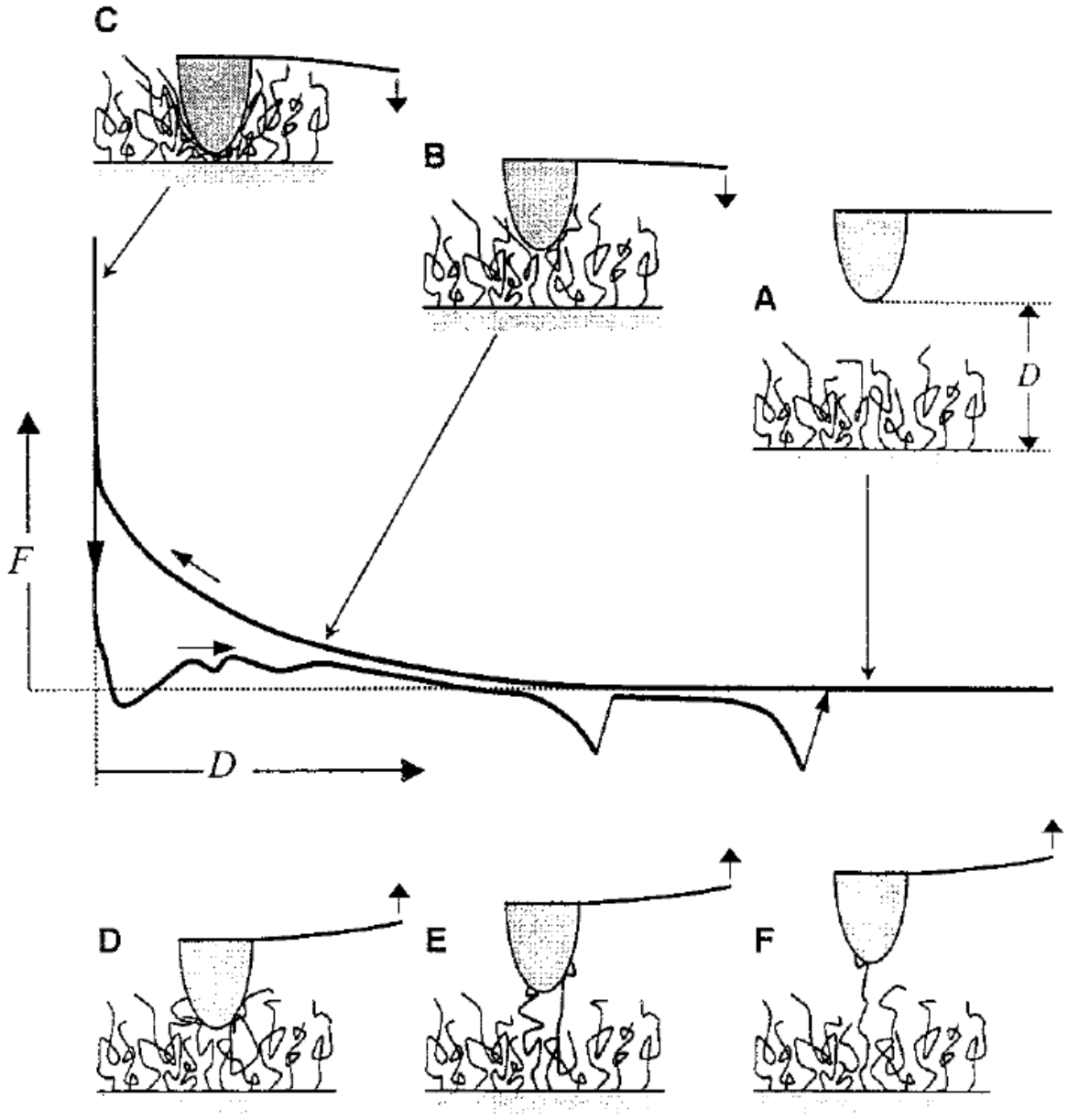

Figure 2.3. Schematic of Steps during Force Spectroscopy Measurements[17]

Butt *et al.* studied the stretching force *vs* distance curves for polystyrene (PS) grafted on silicon surface in cyclohexane and poly(ethylene oxide)/poly(methacrylic acid) (PEO/PMAA) diblock copolymer adsorbed with the PMAA block to aluminum oxide surface in aqueous medium.[17] Force spectroscopy measurements involving adhesion of the attached polymer chain to the AFM tip and subsequent approach/retraction gives us the stretching force profile as a function of the distance from the surface shown in **Figure 2.3** and **Figure 2.4**. They derived a simplified version of the de Gennes[18] expression based on Alexander[19] for the force between the AFM tip and surface grafted polymer chains given below for $0.2 < D/L_0 < 0.9$.

$$f \approx 50 k_B T \Gamma^{3/2} e^{2\pi D/L_0} \tag{2.3}$$

Here Γ is the grafting density, D is the separation between the two surface (the grafting substrate and the AFM tip), L_0 is the equilibrium thickness of the polymer brush, T is the absolute temperature and k_B is the Boltzmann constant. The grafting density calculated here for the grafted PS chains was a moderate value of 0.011 chains/nm^2. The tip of the AFM was roughly parabolic in the direction perpendicular to the grafting substrate, while the radius of curvature of was ~50 nm. These are well studied geometries and hence a simple expression for force profile can be obtained.[20] The force per unit area for the parabolic AFM cantilever tip was obtained using this equation

$$F \approx 50 k_B T L_0 \Gamma^{3/2} e^{2\pi D/L_0} \tag{2.4}$$

A simple geometric model gave a good qualitative estimate but not an accurate value for the zero distance or "offset" between the grafting surface and the AFM tip. Determining the offset distance is one of the key problems of this technique. Fitting the data to a worm-like chain

(WLC) model gave a more accurate value of the persistence length (~1 nm) and the contour length (L_0) of the chain. A distribution of the contour length was obtained by repeating the approach/retraction multiple times, this give us the distribution of the chains (PDI).

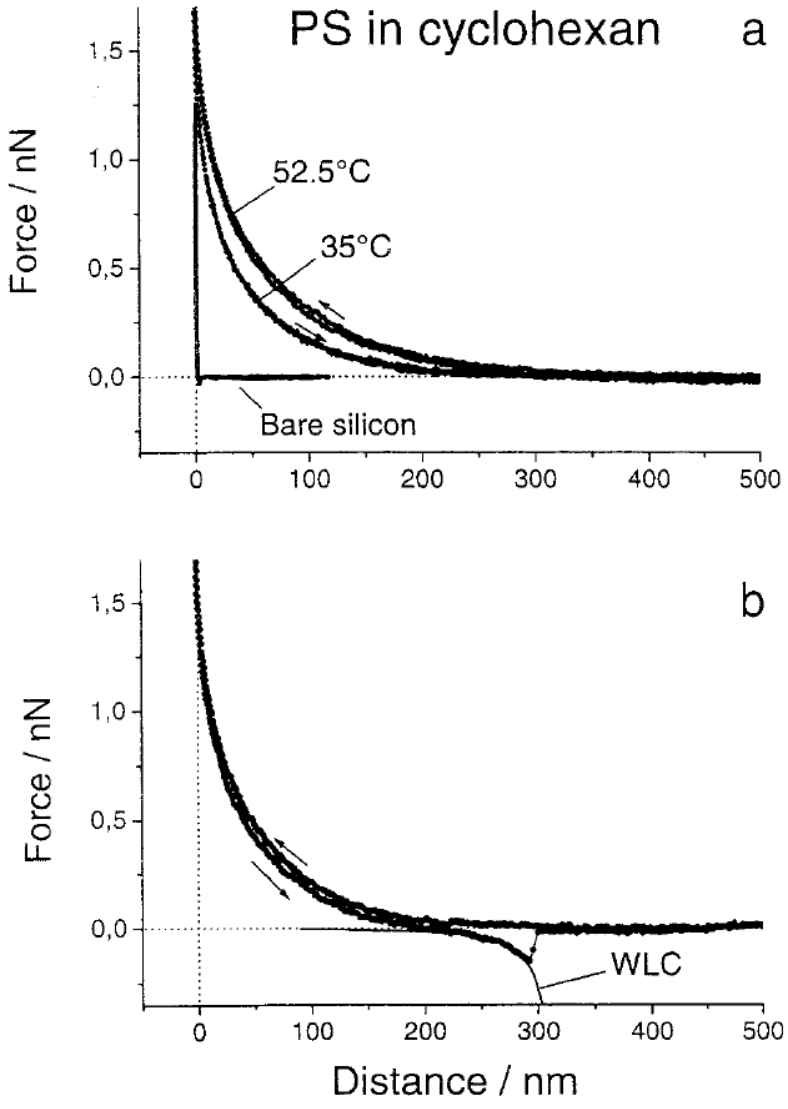

Figure 2.4. Force curve measured between polystyrene grafted to silicon and silicon nitride AFM tip in cyclohexane at the θ-temperature of 35 °C and at 52.5 °C. Approach and retraction usually showed an exponentially decaying repulsive force (a). In about 15% of the force curves, adhesion peaks were observed when retracting the tip (b) done at 24 °C.[17]

Yamamoto *et al.* were the first to study and measure properties of high grafting density poly(methyl methacrylate) (PMMA) brushes, of about 0.4 chains/nm^2, using force spectroscopy measurements.[11,21] A spherical silica particle probe attached to the cantilever was utilized under toluene as solvent. They obtained the true distance between the surface and AFM tip by using the *scratch technique*, where the region at the boundary between a scratched and unscratched area is imaged. This is probably one of the most accurate and reliable measurements that can be obtained for the thickness of polymer brushes and has been used widely by AFM users.[22] The true equilibrium thickness (L_e) of the brush was obtained which is the critical distance at which the repulsive force is detectable. The weight average contour length ($L_{c,w}$) was obtained from M_w obtained from SEC of free polymer grown in the same bulk solution as the brush, knowing the monomer unit length (0.25 nm). We now know that this M_w is not an accurate representation of a grafted polymer system[2], nevertheless the qualitative trends still hold. The results showed that longer chains are more resistant to compression. In a related study, Yamamoto *et al.* investigated PMMA brushes with varying grafting denisty ($0.07 < \sigma < 0.7$ chains/nm^2) but constant full chain length (L_c).[21] L_e/L_c scaled as σ^n where n varied from 0.3 to 0.5 nm with increasing σ. Force spectroscopy measurements were utilized to obtain the contour length (L_c).

Al-Maawali *et al.* studied the polydispersity of poly(dimethyl siloxane) (PDMS) chains attached by 'grafting to' method on a silica surface.[23] Since the grafting density was low, single molecule force spectroscopy was performed and a reasonably good match between the AFM and SEC data was obtained. Goodman *et al.* also used force spectroscopy measurements for

PNIPAM brushes of moderate grafting density (0.037 – 0.067 chains/nm^2).[24,25] A Si_3N_4 tip was used and the decompression profile of the adsorbing brush was studied. The separation between the AFM tip and the surface underlying polymer brushes at the maximum force corresponds to the maximum fraction of adsorbed chains and gives a good approximate for the contour length of the chain. PDI was then calculated from the weight fraction as a function of molecular weight which was obtained from the derivative of the force profile and by fitting a log-normal distribution. They also obtained the M_n and PDI by cleaving the polymer brushes from the surface and using SEC to obtain the entire distribution independently. It was realized that the M_n obtained from the force spectroscopy method is dependent on the σ of the polymer brushes, for lower σ the values were significantly underestimated. This was because in the high σ brush regime (where the distance between the neighboring chains is less than twice the radius of gyration) the formation of a large number of segment-tip contacts having separation smaller than the contour length is enabled.

AFM can be a suitable technique for characterizing polymer brushes locally, i.e., on a specific location of a sample. To this end, they can be convenient for characterizing grafted polymer assemblies a gradient sample, where at least one of the brush attributes (i.e., σ, MW, branching, etc) varies gradually across the sample in either unidirectional or (for the case of two attributes) orthogonal directions. The method to determine the M_n and σ by degrafting approach does not work when there are local changes on the sample, for example, on a gradient sample created by the dipping technique or vapor deposition of chlorosilanes. If we are to study the M_n and σ dependence on the position or time then an AFM with force spectroscopy method

can be applied to measure them at the every position on the sample. If the sample is larger than what is measurable by the AFM it can be broken down into smaller pieces and each of them measured separately and a complete profile can be created.

2.2.6 Scattering Length Density Profiles - Synchrotron Radiation Based Techniques

Neutron Reflectivity (NR) is a powerful method for determining the concentration profiles (and hence conformation) of grafted polymer systems at a nanometer scale on flat surfaces. The advantages of using NR for characterization are that (i) it is a non-destructive technique, because the neutrons interact only with the nuclei of the atoms, (ii) it can provide contrast between the molecules of similar chemical species but different isotopes (deuterium vs hydrogen), (iii) they can penetrate thick substrates and provide information about buried interfaces. The disadvantages are (i) large (5 cm and higher in diameter) ultra-flat substrates are required, (ii) the reflectivity data is usually complex to fit, (iii) access to NR measurements is difficult due to limited number of facilities present. In NR, the specular neutron reflectivity is obtained as a function of wave vector transfer $q_z = 4\pi\sin\theta/\lambda$ where θ is the angle of incidence or reflection of the neutron beam. A scattering length density (SLD) profile can then be fitted based on assumption of a model.

The use of NR started in the 1990s with work from polymer brush characterization by Hamilton, Satija, Fetters *et al.* beginning with the study of the segment density profiles of adsorbed diblock copolymers, a system similar to grafted polymer brushes.[26–28] Fetters *et al.* studied the density profile of end grafted polystyrene in good and theta solvent.[29] Deuterated

solvents i.e. *d*-toluene (good solvent) and *d*-cyclohexane (poor solvent) were used to obtain sufficient contrast and the measurements were done over a range of temperatures. They were able to obtain a z-density profile where they observed stretching and contracting of the brush layer under different solvent and temperature conditions. A number of different grafted polymer systems were studied using NR in this manner in the following years.

Ivkov *et al.*[30] studied the brush height and chain density profile of *d*-PS brushes under solvent flow. Hamilton *et al.*[31] studied the density profile of opposing polymer brush layers under confinement. Ell *et al.*[32] studied the density profiles of PS brushes of different MW grown by ATRP on silica substrates from which they obtained the scattering length density (SLD) profiles. They obtained a parabolic density distribution for the polymer volume fraction as a function of the distance from the surface shown in **Figure 2.5**.

Hoshino *et al.* carried out NR studies of poly zwitterionic polymer brushes namely poly[3-(N-2-methacryloyl-oxyethyl-N,N-dimethyl) ammonatopropanesulfonate] (PMAPS), poly(2-methacryloyloxyethyl phosphorylcholine) (PMPC) and polyelectrolyte brush of poly[2-(methacryloyloxy)ethyltrimethylammonium chloride] (PMTAC).[1] SLD profiles for these layers was studied under different salt concentration (NaCl in D_2O) ranging from 0 to 0.5 M. They successfully estimated the volume fraction profiles and the balance of polymer-polymer and polymer-solvent interactions was studied with dependence on salt concentration. Galvin *et al.* were able to measure the SLD profiles for PDMAEMA brushes at various relative humidities (RH) ranging from 10% to 95%.[9] D_2O was used to obtain contrast between the hydrogen in the polymer layer and deuterium in the water vapor.

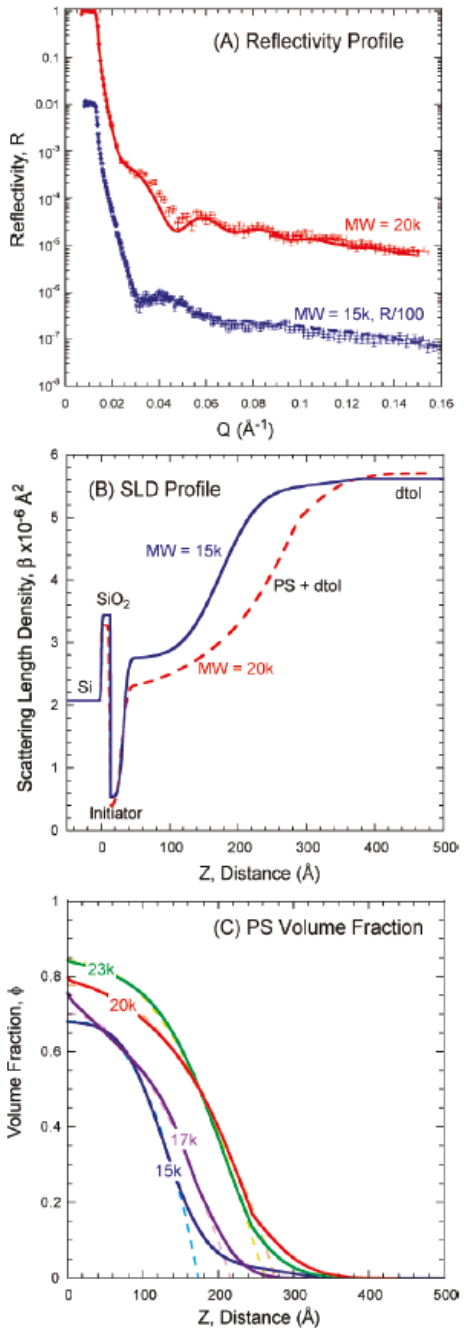

Figure 2.5. (A) Reflectivity profile for two different molecular weight PS dry films. The 20K reflectivity profile is decreased by 2 orders of magnitude for clarity. Line fits to the data are based on the SLD profiles shown in (B). (C) Volume fraction profiles of PS for four different MW with power law fits (dashed).[32]

2.2.7 Some Tools for Thermally Responsive Polymer Brush Characterization

Recently there has been significant interest in the study of thermally responsive polymers, such as PNIPAM, which show an LCST transition behavior. Above the LCST the polymer is collapsed, while below the LCST the polymer is expanded. This coil-to-globule transition which occurs close to human body temperature, is of interest for various applications such as tissue engineering, permeation-controlled filters, actuators.[33–37]

The nature of the transition itself is of importance for grafted polymer brushes with LCST, and it can be characterized in a number of ways since it involves changes in the film thickness, density, composition and a resulting change in optical and mechanical properties that is measurable. Monitoring the system using force sensing techniques such as AFM or surface force apparatus is a good way to understand the range of adhesive and repulsive forces. Some other techniques that have been utilized for temperature transition are *in-situ* ellipsometry, neutron reflectivity, quartz crystal microbalance and surface-plasmon resonance spectroscopy.

Malham *et al.* used scaling analysis of the ratio of thickness between polymer brushes swollen in good solvent and dry thickness to determine the grafting density and chain length of the grafted PNIPAM chains.[38] They used surface force apparatus (SFA) in a manner where PNIPAM brushes were decorated on both a flat surface and the probe to measure the force-distance curves. Within the frame work of Alexander-deGennes[19,39] they derived the following expression for swelling ratio in a good solvent

$$\alpha = \frac{h_{swell}}{h_{dry}} = \left(\frac{d}{a}\right)^{3-\frac{1}{\nu}} \tag{2.5}$$

Where ‘a’ is the monomer size (nm, measure of volume), ν is an exponent that is a function of the grafting density and d is the distance between the grafts and it gives σ. For high grafting density, the value of ν = ½ was found to give the best fit, which suggests that the blobs are Gaussian in nature. The calculated values of σ were in the range of 0.09 – 0.4 chains/nm^2. The pull-off forces obtained from the SFA apparatus also gave some idea about the mechanism of the adhesion and were found to be independent of σ. The limitation of this method is that it requires the use of a good solvent conditions and the appropriate value of the exponent ν. The great advantage is that measuring swelling ratio is relatively simple by measuring thickness using ellipsometry or optical reflectivity.[15]

Orski *et al.* have attempted to get an understanding of the thermodynamics and grafting density of PMMA brushes by swelling them in various solvents and characterizing by X-Ray Reflectivity (XRR) though they were unable to calculate an accurate value of σ.[40]

2.2.8 Mass changes – Quartz Crystal Microbalance (QCM)

QCM measures changes in the mass loading and/or the changes in viscoelastic properties. The polymer brush layer that is to be characterized is usually grown on a silica sensor surface and the change in the fundamental resonance frequency (Δf) of vibration and the dissipation (D) is monitored. Sugnaux *et al.* created poly (3-methacrylamido phenylboronic acid) (PMAPBA) modified QCM sensors and monitored glucose absorption from solution.[41] The shift in Δf was established as a nearly linear function of the glucose concentration in the surrounding solution. In a similar manner, the degree of post polymerization reaction may be monitored when the polymer brush film on QCM sensor is exposed to reaction environment since it could result in a change in mass of the system. John *et al.* studied the LCST transition for PNIPAM brushes grown on the quartz sensor coated with silicon dioxide.[42]. The depression in phase-transition temperature for grafted PNIPAM was found to be a non-linear function of the salt concentration. Others have used QCM to monitor thermal transition such as collapse above the LCST for polymers such as $PMEO_2MA$[43] and PNIPAM[44–48].

2.2.9 Qualitative surface chemistry determination

For benchmarking and various other reasons, the chemistry of the polymer brush needs to be characterized at different stages of a given process. Some of the commonly used techniques are X-ray Photoelectron Spectroscopy (XPS), time of flight secondary ion mass spectrometry (TOF-SIMS), transmission and reflection mode Fourier transform infrared spectroscopy (FTIR) and ultraviolet-visible spectroscopy (UV-Vis).

XPS is sensitive to the top ~10 nm organic and ~1 nm inorganic surface. The incident X-rays themselves can penetrate much deeper but the photoelectrons that are ejected from the inner shells of atoms, which carry the chemical information, cannot travel more than the above mentioned distances. This places limitation on how deep we can probe the surface, however the sensitivity is very high near the surface, and in fact, by increasing the angle of incidence (measured from the normal to substrate), the sensitivity can be increased even more. The data obtained from XPS does provide a direct proof of the presence of certain atoms and their rough composition in the film. Using high resolution measurements for certain key peaks, one could also obtain information about chemical bonding.[3,4] The limitation of XPS is that the measurements need to be carry out in high vacuum, thus without the presence of solvent.

In TOF-SIMS, the surface is irradiated with pulsed ion beam usually with energy of ~25 keV, and the emitted secondary ions are characterized using mass spectrometry. The technique is sensitive to the top 1-2 nm surface and both positive and negative ion spectra can be collected, which often reveal different information. The disadvantage is that since it is a mass spectrometry based detection, we detect the ion fragments and the chemical information

obtained is indirect and depends on the peak assignment. One has to be careful with assigning the peaks of a given m/z ratio to a chemical fragment. Proper calibration helps with the accuracy but the data should be treated qualitatively since the instrument operating conditions have a strong influence on the data obtained. Similar to the XPS, TOF-SIMS measurements are carried out in high vacuum. In some instances, TOF-SIMS measurements can be carried out in a cryogenic set-up, which would facilitate having solvent entrapped in the sample. However, we are not aware on any report that would utilize this mode of TOF-SIMS in measuring the properties of grafted polymer layers.

FTIR for polymer brushes can be carried out in reflection, transmission and attenuated total reflectance (ATR) mode. The sensitivity is limited due to the small amount of material present. A preferable configuration to maximize the signal to noise ratio is using transmission mode for a polymer brush film grown on both sides of a substrate, for example, a double sided polished Si wafer. UV-Vis spectroscopy can also be carried out on polymer brushes grown on quartz surface. This gives some chemical information based on absorption peaks in UV regime but the sensitivity is limited such as that for FTIR.

Sum frequency generation[49] is another technique sensitive to the chemistry of the very top monolayer of a surface or an interface. Uosaki *et al.* studied the interfacial structure of poly(vinylpyridine) brushes with various side chains lengths exposed to dry nitrogen, water vapor, liquid water and aqueous electrolyte solution.[50] Information about the presence of chemical moieties such as OH group and the conformation/orientation of the side chain on the top layer was obtained.

2.3 Concave surface

Polymer brush grown on concave surfaces, such as pores, find applications in creating switchable permeable membranes[51], enhancing nanoscale transport[52] and more. We provide here a few examples where the properties of the system were determined.

Gorman *et al.* studied the growth of PMMA inside the concave substrates namely porous silica and anodic aluminum oxide with pore sizes 50 nm and 200 nm respectively.[53] The porous silicon was used as a support to study the molecular weight distribution of polymers by utilizing desorption ionization on silicon mass spectrometry (DIOS-MS). It is a variant of an established technique called matrix- assisted laser desorption ionization (MALDI-MS) which requires the use of an organic matrix to immobilize the polymer to be studied, and this reduces the signal of interest. DIOS-MS overcomes this limitations since it does not require any matrix and hence relatively small amount of polymer can be detected. The MS detector here gave direct information about the MW distribution however a practical upper limit of 15 kDa was found, due to significant increase in the signal to noise ratio above it. They concluded that the increase in the confinement, *i.e.* going from convex to flat to concave substrate lead to decrease in the molecular weight of the grown polymer brush.

PNIPAM grown in nanopores of track-etched PET were studied using AFM to obtain both MW and σ. Radji *et al.* grew PNIPAM brushes by ATRP inside the PET pores of size 80 nm and 330 nm, respectively.[54] The PET film was then cryo-microtomed to expose the pores and it was further studied using AFM under water. The approach force *vs* distance profile was fitted with Alexander and de Gennes model to get the grafting density, and a worm like chain

model was used to estimate the chain length from the retract profiles as described in section 2.2.5. The properties were earlier studied by Alem *et al.* for PNIPAM grown in track-etched PET for the same pore diameters using AFM and TEM coupled with electron energy loss detector.[36] They used XPS to first confirm the growth of the PNIPAM brushes on the outside surface of the PET film, AFM was utilized to find the thickness of the film by *force spectroscopy experiments*. The morphology of the PNIPAM brushes inside the nanopores was determined using scanning electron microscopy (SEM) and transmission electron microscopy (TEM) equipped with electron energy loss spectroscopy detector (EELS).

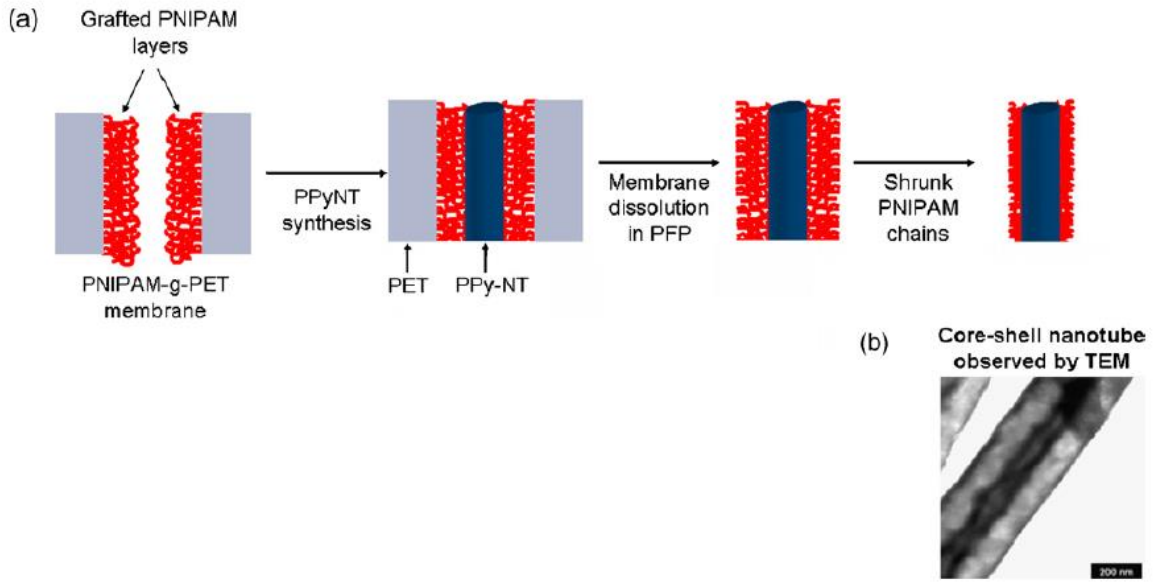

Figure 2.6. Schematic representation of the process used to prepare PNIPAM-PPy core–shell nanotubes and TEM picture of stained PNIPAM-PPy nanotubes.[36]

The thickness of the brushes inside the pores was determined using original template-based method shown in **Figure 2.6**.[36] Polypyrrole (PPy) nanotubes were synthesized inside the nanopores above the PNIPAM brushes by a reaction between $FeCl_3$ and pyrrole solution. The membrane was placed between two half cells containing the respective solutions and the reaction between them created a polymeric nanotube. The PET film was then dissolved in pentafluorophenol (PFP) at 30°C and the resulting core shell nanotubes were deposited on a carbon grid. The Polypyrole nanotubes (PPy-NT) were then stained with RuO_4 and then analyzed using TEM. Knowing the average pore diameter before PNIPAM was grown and comparing that with the diameter of the nanotubes obtained from TEM the thickness of the PNIPAM brush layer inside the nanopores was obtained. In the same paper, Alem *et al.* also reported the temperature sensitive properties such as the permeability though the PNIPAM nanopore coated PET films, by measuring the conductivity across the pores. The method was based on detecting the changes in the membrane pore size by monitoring changes in electrical resistivity with temperature.

2.4 Convex Substrate

Convex surfaces, such as that of nanoparticles, decorated with grafted polymer chains form an important class of materials owing to their versatility in controlling inter-particle interactions in colloidal suspensions, and potential applications that make use of the optical absorption or electron transport properties of the polymer and nanoparticle material. The distribution of the nanoparticles inside the polymer matrix is also important and polymer brushes immobilized particles are commonly used to enhance compatibility or to control the separation of particles. Determination of the conformation of the polymer brushes is important for such applications. Various scattering techniques that utilize visible, X-ray light and neutrons can be used for measuring the properties and are discussed in this section. Some techniques like dynamic light scattering (DLS) and X-ray photon correlation spectroscopy (XPCS) could perform time dependent measurement and provide us with information about the dynamical properties of a polymer brush. Direct removal of polymer brushes by cleaving the bond followed by use of SEC has been done to obtain direct measurement of the MW of the polymer brushes, if they were grown by "grafting from" polymerization.[55–59] A method can be chosen depending on the length and time scale of the phenomena of interest, **Figure 2.7** taken from Hoshino *et al.*[1] shows the various techniques that are available.

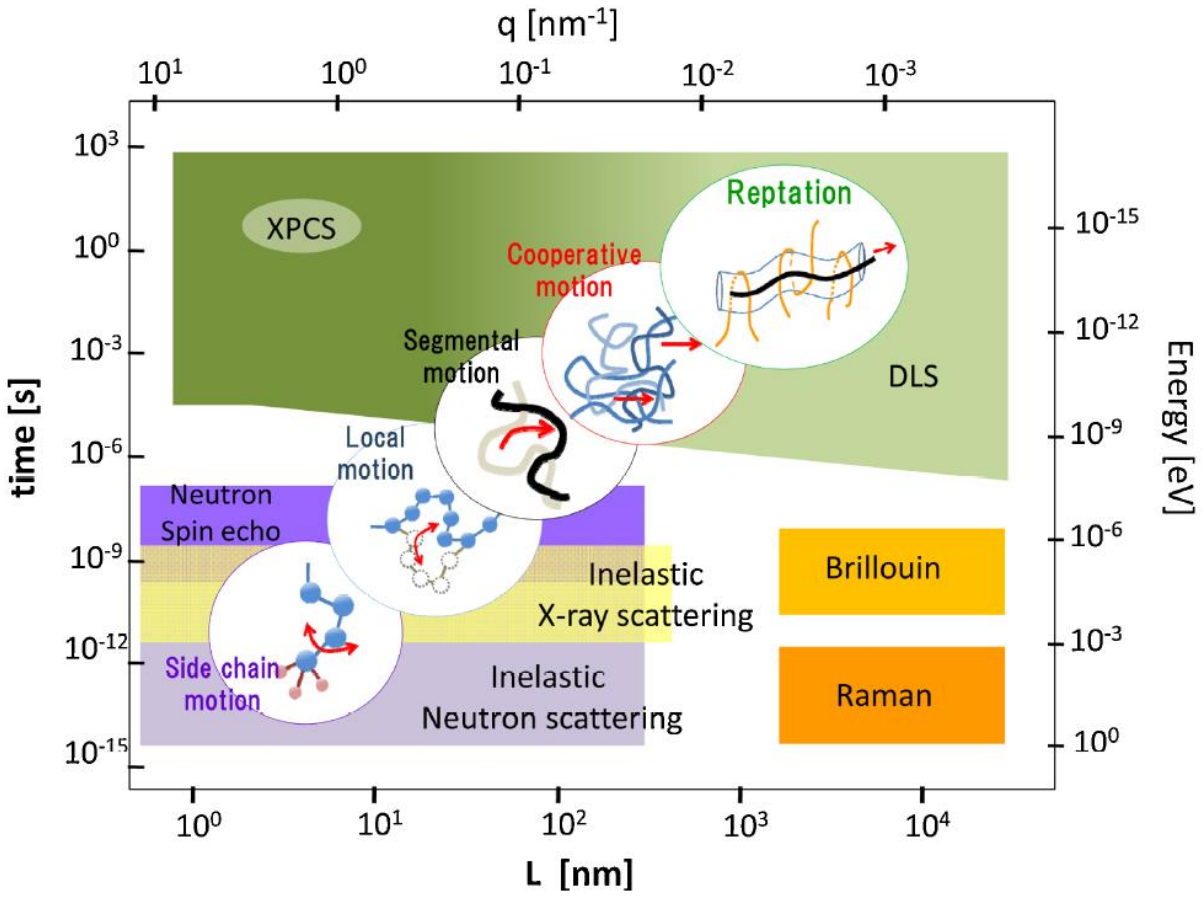

Figure 2.7. Time and length scale of a hierarchal dynamical structure in polymers and the corresponding analytical techniques that can be used to measure it.[1]

2.4.1 Dynamic Light Scattering (DLS)

Due to the geometry of nanoparticles causing an increase in the available volume for the polymer chains there are changes in regime observed as we go outwards and away from the surface of the particles. A nanoparticle with concentrated polymer brush (CPB) regime near the surface has a critical distance r_c above which the regime is semi-dilute polymer brush (SDPB). This argument was originally presented by Daoud and Cotton[60] for star shaped

polymers emerging from a point, and later extended to polymer brushes on nanoparticles with radius r_0 by Ohno.[61] The brush height scales in a different manner for each regime and this is important because it affects the apparent particle size and the inter-particle interaction. DLS is a simple way to obtain the brush height by measurement of hydrodynamic radius (R_H) in a dilute solution. This has been utilized by various groups to study scaling of polymer brushes.[62] Since the measurements are carried out in a solution in which the polymeric nanoparticles are dispersed one should be careful that R_H depends on the type of solvent, and in case of aqueous solution the salt concentration and pH should be noted. Thermogravimetric analysis and direct measurement of MW by SEC are often used in conjunction to DLS to verify the MW of the polymer chains especially if they are synthesized by "grafting from" polymerization.[63]

2.4.2 Morphology - Transmission Electron Microscopy

The core of the nanoparticles (usually silica or metal) often has very different electron density from that of the outer layer which is a grafted polymer. Due to the spherical geometry of a nanoparticle the grafted polymer brush exhibits two regimes, concentrated polymer brush (CPB) and semi-dilute polymer brush (SDPB) based on aforementioned Daoud and Cotton model.[60] This fact is utilized to create flexible nanoparticle array *superlattice* structures.[64] Such a system could have superior mechanical properties, which were studied using TEM. Here the chain entanglement and the phenomena of *crazing*, common in bulk polymeric material, was observed and is seen in the TEM image in **Figure 2.8**. The interaction between the polymer chains grafted on the particles, the grafting density and length of the chains define the ordering

of particles and the inter-particle spacing. Studying the macroscopic properties like elastic modulus is critical here and TEM can be a useful tool for studying it.[65]

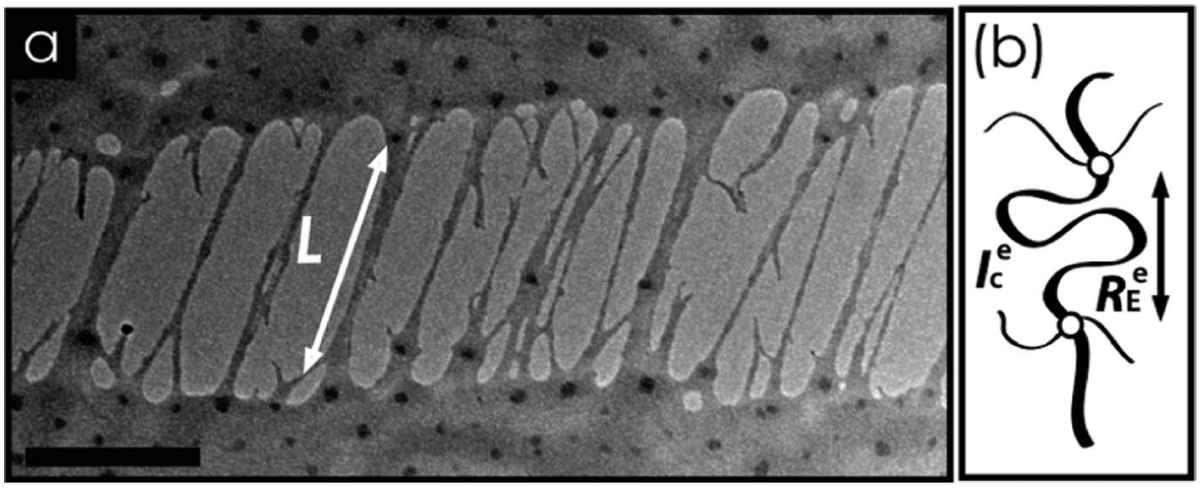

Figure 2.8. TEM of SiO_2-S770 thin film depicting craze formation. The fibril length L is determined as the maximum (observable) length of fibrils formed between two particle centers. Scale bar is 200 nm. (b) Illustration of the structural parameters of entanglement network. R_E^e and l_c^e denote the end-to-end distance and contour length of a chain segment between entanglement points, respectively.[64]

2.4.3 Neutron and X-ray scattering techniques

Kikuchi *et al.* studied the dimensions of two zwitterionic polyelectrolyte brushes namely poly[3-(N-2-methacryloyloxyethyl-N,N-dimethyl) ammonatopropanesulfonate] (PMAPS) and poly(2-methacryloyloxyethyl phosphorylcholine) (PMPC) immobilized on silica nanoparticles using Small Angle X-ray Scattering (SAXS). PMPC is soluble in deionized water at room temperature while PMAPS is not and it has an upper critical solution temperature (UCST). The extension of the chains as a function of the concentration of NaCl electrolyte solution was established.[1,66] The dimensions of the chains in salt solution with varying concentrations were actualized by looking at the scattering length density profiles. Above a certain concentration of NaCl, the PMAPS chains swell due to charge shielding causing a decrease in the inter-chain attraction. On the other hand, no significant swelling is observed for PMPC since the inter-chain attraction is unaffected.

Hore *et al.* studied the conformation of deuterated PMMA nanocomposite containing PMMA-grafted Fe_3O_4 nanospheres using Small-angle neutron scattering (SANS) combined with self-consistent field theory (SCFT) calculations.[67] Studying the conformation is important to understand and predict the diffusion of polymers within the nanocomposite. Using the SANS measurements they were able to directly probe the concentrated polymer brush (CPB) and semi-dilute polymer brush (SDPB) regions of the grafted polymer interface. Chevginy *et al.* in multiple publications have demonstrated the utility of SANS, SAXS and TEM for studying the system of polymer corona grafted on particles inside a polymer matrix along with theoretical modeling.[68–70]

2.4.4 Measuring Dynamical Properties

X-ray photon correlation spectroscopy (XPCS) is a technique similar to DLS that utilizes partially coherent X-rays to obtain information about microscopic dynamic phenomena (*cf.* **Figure 2.9**). Akgun *et al.*[71], Hoshino *et al.*[1], and others have demonstrated the practicality of this technique by measuring the properties of polymer brushes on flat surface and silica nanoparticles. The scattered intensity from a random arrangement of *scatterers* exhibits a speckled pattern which is a function of the instantaneous arrangement, and there are changes in this pattern over time, hence it contains information about the dynamics of the system. Although the technique is similar to DLS, the use of X-rays which have a shorter wavelength allows the study of smaller length scales on the order of nanometers. The disadvantage is that since high brilliance of X-rays is necessary, a synchrotron source is required to do the measurements. X-rays also have a high transmittance because of which multiple scattering is often negligible. Due to this XPCS has been utilized to study various concentrated colloidal suspensions.[72–74]. Akgun *et al.*[71] revealed surface fluctuation in polystyrene and poly(n-butyl acrylate) "brushes" on the order of 620 – 3100 nm above the glass transition temperature and no relaxation was observed in the time window of 0.1 – 1000 s. Hoshino *et al.*[1] obtained information about the relaxation times and sub-diffusive motion of PS grafted silica nanoparticles. They observed the so called "de Gennes narrowing" demonstrating the slow decay of the most probable density fluctuations due to caging by neighboring particles.

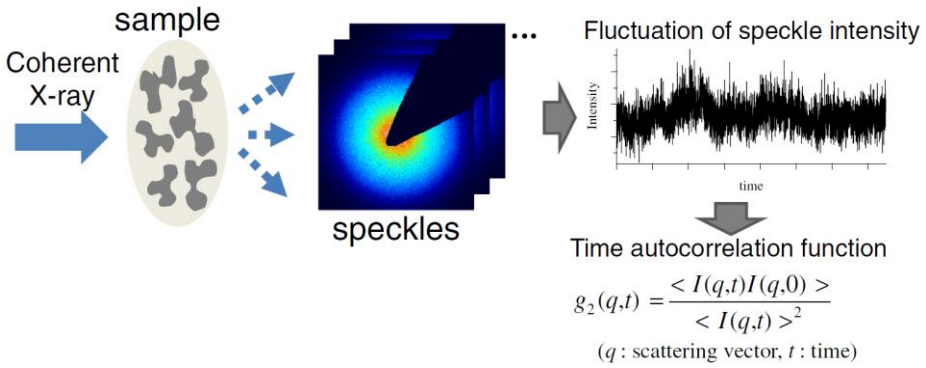

Figure 2.9. Schematic of X-ray photon correlation spectroscopy (XPCS) measurement technique.[1]

2.5 Conclusions

We have assembled a number of examples as a guide and a list of techniques that are utilized in measuring the properties of grafted polymer systems. The choice of a technique is made not only based on the measurable property but also the ease in terms of the amount of time and resources required. We have attempted to highlight various problems one could encounter and the range of properties that can be measured for a grafted polymer system.

2.6 References

(1) Hoshino, T.; Tanaka, Y.; Jinnai, H.; Takahara, A. *J. Phys. Soc. Japan* **2013**, *82* (2), 1–12.

(2) Genzer, J. *Macromolecules* **2006**, *39*, 7157–7169.

(3) Patil, R. R.; Turgman-Cohen, S.; Šrogl, J.; Kiserow, D.; Genzer, J. *ACS Macro Lett.* **2015**, *4* (2), 251–254.

(4) Patil, R. R.; Turgman-Cohen, S.; Šrogl, J.; Kiserow, D.; Genzer, J. *Langmuir* **2015**, *31* (8), 2372–2381.

(5) Kang, C.; Crockett, R. M.; Spencer, N. D. *Macromolecules* **2014**, *47* (1), 269–275.

(6) Kobayashi, M.; Terada, M.; Terayama, Y.; Kikuchi, M.; Takahara, A. *Macromolecules* **2010**, *43* (20), 8409–8415.

(7) Park, C. S.; Lee, H. J.; Jamison, A. C.; Lee, T. R. *ACS Appl. Mater. Interfaces* **2016**, *8* (8), 5586–5594.

(8) Azzam, R. M. A.; Bashara, N. M. *Ellipsometry and Polarized Light*; North-Holland Publishing Company: New York, 1977.

(9) Galvin, C. J.; Dimitriou, M. D.; Satija, S. K.; Genzer, J. *J. Am. Chem. Soc.* **2014**.

(10) Edmondson, S.; Nguyen, N. T.; Lewis, A. L.; Armes, S. P. *Langmuir* **2010**, *26* (10), 7216–7226.

(11) Yamamoto, S.; Ejaz, M.; Tsujii, Y.; Matsumoto, M.; Fukuda, T. *Macromolecules* **2000**, *33* (15), 5602–5607.

(12) Kooij, E. S.; Sui, X.; Hempenius, M. A.; Zandvliet, H. J. W.; Vancso, G. J. *J. Phys.*

Chem. B **2012**, *116* (30), 9261–9268.

(13) Balamurugan, S.; Mendez, S.; Balamurugan, S. S.; O'Brie, M. J.; López, G. P. *Langmuir* **2003**, *19* (7), 2545–2549.

(14) Harmon, M. E.; Jakob, T. a. M.; Knoll, W.; Frank, C. W. *Macromolecules* **2002**, *35*, 5999–6004.

(15) Varma, S.; Bureau, L.; Débarre, D. *Langmuir* **2016**, *32* (13), 3152–3163.

(16) Okada, F.; Akiyama, Y.; Kobayashi, J.; Ninomiya, H.; Kanazawa, H.; Yamato, M.; Okano, T. *J. Nanoparticle Res.* **2015**, *17* (3), 148.

(17) Butt, H. J.; Kappl, M.; Mueller, H.; Raiteri, R.; Meyer, W.; Ruhe, J. *Langmuir* **1999**, *15* (7), 2559–2565.

(18) de Gennes, P. G. *Adv. Colloid Interface Sci.* **1987**, *27* (3-4), 189–209.

(19) Alexander, S. *J. Phys.* **1977**, *38* (8), 983–987.

(20) Israelachvili, J. *Intermolecular and Surface Forces (Third Edition)*, 3rd ed.; Elsevier Inc.: San Diego, 2011.

(21) Yamamoto, S.; Ejaz, M.; Tsujii, Y.; Fukuda, T. *Macromolecules* **2000**, *33* (15), 5608–5612.

(22) Schuh, C.; Lomadze, N.; Rühe, J.; Kopyshev, A.; Santer, S. *J. Phys. Chem. B* **2011**, *115* (35), 10431–10438.

(23) Al-Maawali, S.; Bemis, J. E.; Akhremitchev, B. B.; Leecharoen, R.; Janesko, B. G.; Walker, G. C. *J. Phys. Chem. B* **2001**, *105* (18), 3965–3971.

(24) Goodman, D.; Kizhakkedathu, J. N.; Brooks, D. E. *Langmuir* **2004**, *20* (15), 6238–6245.

(25) Goodman, D.; Kizhakkedathu, J. N.; Brooks, D. E. *Langmuir* **2004**, *20* (8), 3297–3303.

(26) Satija, S. K.; Majkrzak, C. F.; Russell, T. P.; Sinha, S. K.; Sirota, E. B.; Hughes, G. J. *Macromolecules* **1990**, *23* (16), 3860–3864.

(27) Field, J. B.; Toprakcioglu, C.; Ball, R. C.; Stanley, H. B.; Dai, L.; Barford, W.; Penfold, J.; Smith, G.; Hamilton, W. *Macromolecules* **1992**, *25* (1), 434–439.

(28) Auroy, P.; Mir, Y.; Auvray, L. *Phys. Rev. Lett.* **1992**, *69* (1), 93–95.

(29) Karim, a.; Satija, S.; Douglas, J.; Ankner, J.; Fetters, L. *Phys. Rev. Lett.* **1994**, *73* (25), 3407–3410.

(30) Ivkov, R.; Butler, P. D.; Satija, S. K.; Fetters, L. J. *Langmuir* **2001**, *17* (10), 2999–3005.

(31) Hamilton, W. A.; Smith, G. S.; Alcantar, N. A.; Majewski, J.; Toomey, R. G.; Kuhl, T. L. *J. Polym. Sci. Part B Polym. Phys.* **2004**, *42* (17), 3290–3301.

(32) Ell, J. R.; Mulder, D. E.; Faller, R.; Patten, T. E.; Kuhl, T. L. *Macromolecules* **2009**, *42* (24), 9523–9527.

(33) Sui, X.; Di Luca, A.; Gunnewiek, M. K.; Kooij, E. S.; Van Blitterswijk, C. A.; Moroni, L.; Hempenius, M. A.; Vancso, G. J. *Aust. J. Chem.* **2011**, *64* (9), 1259–1266.

(34) Xu, F. J.; Zhong, S. P.; Yung, L. Y. L.; Kang, E. T.; Neoh, K. G. *Biomacromolecules* **2004**, *5* (6), 2392–2403.

(35) Mitsuishi, M.; Koishikawa, Y.; Tanaka, H.; Sato, E.; Mikayama, T.; Matsui, J.; Miyashita, T. *Langmuir* **2007**, *23* (14), 7472–7474.

(36) Alem, H.; Duwez, A. S.; Lussis, P.; Lipnik, P.; Jonas, A. M.; Demoustier-Champagne, S. *J. Memb. Sci.* **2008**, *308* (1-2), 75–86.

(37) Lokuge, I.; Wang, X.; Bohn, P. W. *Langmuir* **2007**, *23* (1), 305–311.

(38) Malham, I. B.; Bureau, L. *Langmuir* **2010**, *26* (7), 4762–4768.

(39) Gennes, P. G. De. **1980**, *1075* (19), 1069–1075.

(40) Orski, S. V.; Sheridan, R. J.; Chan, E. P.; Beers, K. L. *Polym. (United Kingdom)* **2015**, *72*, 471–478.

(41) Sugnaux, C.; Klok, H. A. *Macromol. Rapid Commun.* **2014**, *35* (16), 1402–1407.

(42) Jhon, Y. K.; Bhat, R. R.; Jeong, C.; Rojas, O. J.; Szleifer, I.; Genzer, J. *Macromol. Rapid Commun.* **2006**, *27* (9), 697–701.

(43) Laloyaux, X.; Mathy, B.; Nysten, B.; Jonas, A. M. *Langmuir* **2010**, *26* (2), 838–847.

(44) Ishida, N.; Biggs, S. *Macromolecules* **2010**, *43* (17), 7269–7276.

(45) Ma, H.; Fu, L.; Li, W.; Zhang, Y.; Li, M. *Chem. Commun. (Camb).* **2009**, No. 23, 3428–3430.

(46) Annaka, M.; Yahiro, C.; Nagase, K.; Kikuchi, A.; Okano, T. *Polymer.* **2007**, *48* (19), 5713–5720.

(47) Ishida, N.; Biggs, S. *Langmuir* **2007**, *23* (22), 11083–11088.

(48) Liu, G.; Zhang, G. *J. Phys. Chem. B* **2005**, *109* (2), 743–747.

(49) Shen, Y. R. *Nature* **1989**, *337* (6207), 519–525.

(50) Uosaki, K.; Noguchi, H.; Yamamoto, R.; Nihonyanagi, S. *J. Am. Chem. Soc.* **2010**, *132* (48), 17271–17276.

(51) de Groot, G. W.; Santonicola, M. G.; Sugihara, K.; Zambelli, T.; Reimhult, E.; Vörös, J.; Vancso, G. J. *ACS Appl. Mater. Interfaces* **2013**, *5* (4), 1400–1407.

(52) Chen, Q. *Langmuir* **2014**, *30* (27), 8119–8123.

(53) Gorman, C. B.; Petrie, R. J.; Genzer, J. *Macromolecules* **2008**, *41*, 4856–4865.

(54) Radji, S.; Alem, H.; Demoustier-champagne, S.; Jonas, A. M.; Cuenot, S. *Macromol. Chem. Phys.* **2012**, *213*, 580–586.

(55) von Werne, T.; Patten, T. E. *J. Am. Chem. Soc.* **2001**, *123*, 7497–7505.

(56) Bo, H. G.; Beers, K.; Matyjaszewski, K.; Sheiko, S. S.; Mo, M. **2001**, 4375–4383.

(57) Tsujii, Y.; Ejaz, M.; Sato, K.; Goto, A.; Fukuda, T. **2001**, No. Figure 1, 8872–8878.

(58) Baum, M.; Brittain, W. J. *Society* **2002**, 610–615.

(59) Ohno, K.; Akashi, T.; Huang, Y.; Tsujii, Y. *Macromolecules* **2010**, *43* (21), 8805–8812.

(60) Daoud, M.; Cotton, J. P. *J. Phys.* **1982**, *43* (3), 531–538.

(61) Ohno, K.; Morinaga, T.; Takeno, S.; Tsujii, Y.; Fukuda, T. *Macromolecules* **2007**, *40* (25), 9143–9150.

(62) Dukes, D.; Li, Y.; Lewis, S.; Benicewicz, B.; Schadler, L.; Kumar, S. K. *Macromolecules* **2010**, *43* (3), 1564–1570.

(63) Matsuda, Y.; Kobayashi, M.; Annaka, M.; Ishihara, K.; Takahara, A. *Langmuir* **2008**, *24* (16), 8772–8778.

(64) Choi, J.; Dong, H.; Matyjaszewski, K.; Bockstaller, M. R. *J. Am. Chem. Soc.* **2010**, *132* (36), 12537–12539.

(65) Choi, J.; Hui, C. M.; Schmitt, M.; Pietrasik, J.; Margel, S.; Matyjazsewski, K.; Bockstaller, M. R. *Langmuir* **2013**, *29* (21), 6452–6459.

(66) Kikuchi, M.; Terayama, Y.; Ishikawa, T.; Hoshino, T.; Kobayashi, M.; Ogawa, H.;

Masunaga, H.; Koike, J.; Horigome, M.; Ishihara, K.; Takahara, A. *Polym. J.* **2012**, *44* (1), 121–130.

(67) Hore, M. J. a; Ford, J.; Ohno, K.; Composto, R. J. **2013**, 1–26.

(68) Chevigny, C.; Gigmes, D.; Bertin, D.; Jestin, J.; Boué, F. *Soft Matter* **2009**, *5* (19), 3741.

(69) Chevigny, C.; Jestin, J.; Gigmes, D.; Schweins, R.; Di-Cola, E.; Dalmas, F.; Bertin, D.; Boué, F. *Macromolecules* **2010**, *43* (11), 4833–4837.

(70) Chevigny, C.; Dalmas, F.; Di Cola, E.; Gigmes, D.; Bertin, D.; Boué, F.; Jestin, J. *Macromolecules* **2011**, *44* (1), 122–133.

(71) Akgun, B.; Uğur, G.; Jiang, Z.; Narayanan, S.; Song, S.; Lee, H.; Brittain, W. J.; Kim, H.; Sinha, S. K.; Foster, M. D. *Macromolecules* **2009**, *42* (3), 737–741.

(72) Lurio, L. B.; Lumma, D.; Sandy, a R.; Borthwick, M. a; Falus, P.; Mochrie, S. G.; Pelletier, J. F.; Sutton, M.; Regan, L.; Malik, a; Stephenson, G. B. *Phys. Rev. Lett.* **2000**, *84* (4), 785–788.

(73) Banchio, A. J.; Gapinski, J.; Patkowski, A.; Häußler, W.; Fluerasu, A.; Sacanna, S.; Holmqvist, P.; Meier, G.; Lettinga, M. P.; Nägele, G. *Phys. Rev. Lett.* **2006**, *96* (13), 1–4.

(74) Riese, D. O.; Wegdam, G. H.; Vos, W. L.; Sprik, R.; Fenistein, D.; Bongaerts, J. H. H.; Grübel, G. *Phys. Rev. Lett.* **2000**, *85* (25), 5460–5463.

3. Degrafting of Polymer Brushes and Study of Their Molecular Weight and Grafting Density*

3.1 Introduction

Polymer chains tethered to a surface by one or more covalent bonds form surface grafted polymer assemblies (SGPA). Grafting of macromolecules to surfaces results in a loss of translational entropy of the chains and has, in turn, profound effect on chain structure and conformation of the macromolecules. The grafted polymers adopt a so-called "mushroom" conformation if the distance between neighboring grafts is greater than the radius of gyration of the chain (R_g). When the average distance between two neighboring grafts is less than R_g, the macromolecular grafts enter the so-called "brush" conformation, in which steric effects due to neighboring chains cause the polymers to stretch perpendicularly to the surface, as explained by Alexander and de Gennes.[1–4] In spite of the aforementioned classification schemes, often times all grafted polymer systems are colloquially referred to as 'polymer brushes'. The interplay among the microscopic properties of polymer brushes, such as, the molecular weight, the grafting density (*i.e.*, the number of grafted polymers per surface area), the chemical composition of the grafts as well as the sequence distribution of the chemical units along the grafted chain, influences the macroscopic behavior in SGPA (*i.e.*, wettability, lubricity, modulus, response to stimulus).

* This chapter contains material published in ACS Macro Letters, vol. 4(2), pp. 251-254, 2015 and ACS Langmuir, vol. 31(8), pp. 2372-2381, 2015, © 2015 American Chemical Society. It is reprinted here with permission from the publisher.

For those reasons polymer brushes have been studied extensively with regard to creating surfaces that respond to external stimuli [5–7], can be patterned[8,9], or can exhibit anti-biofouling[10–12], ultralow friction[13–16] and highly adhesive[17] characteristics. Two general favored methods exist to prepare grafted polymer chains. The "grafting to" methodology involves growing polymer chains in bulk solution followed by deposition on the surface through physisorption or chemisorption. While the molecular weight (M_n) of the chains can be determined in advance the process yields polymer grafts with a low grafting density (σ_p) due to the steric hindrance of adsorbing chains. In the more commonly used "grafting from" method, the polymer chains grow directly from initiator centers attached to the surface. While this method gives a higher σ_p, it is laborious and challenging to accurately determine σ_p and M_n. For growing well-defined surface initiated (SI) polymers, aside from free radical polymerization (FRP), a wide range of controlled radical polymerization (CRP) techniques are available, such as atom transfer radical polymerization (ATRP)[18–21], reverse atom transfer radical polymerization (R-ATRP)[22], reversible addition fragmentation chain transfer polymerization (RAFT)[23], and nitroxide mediated radical polymerization (NMRP)[24]. ATRP has been widely used given its versatility and relatively benign reaction conditions and is expected to give a narrow molecular weight distribution (MWD) of SGPAs.

The conformations of polymer brushes on surfaces are governed by the complex interplay among M_n and σ_p, solvent quality, and the curvature of the substrate.[25] σ_p is difficult to access directly through experiments. Often, the mass balance equation is employed, in which σ_p is calculated using the known values of dry polymer thickness (h_p) and M_n:

$$\sigma_p = \frac{h_p \cdot \rho \cdot N_A}{M_n} \quad , \tag{3.1}$$

In Equation (3.1), N_A is Avogadro's number and ρ is the bulk density. Determining σ_p for polymeric grafts prepared by the "grafting onto" methodology is straightforward because M_n is measured directly for polymers synthesized in bulk and h_p is assessed after grafting onto dry samples. In contrast, calculating σ_p for systems prepared by the "grafting from" approach is more challenging because M_n is unknown a priori. Previous attempts to remove polymer brushes from substrates after "grafting from" polymerization used strong chemical agents or specialty initiators that would cleave after being exposed to external radiation (*i.e.*, UV light). The miniscule amount of degrafted material generated from the thin film also leads to problems in the accurate characterization of molecular weight. For this reason, several research groups estimated M_n of the grafts by measuring the M_n of polymers made simultaneously in solution using sacrificial initiators.[26–29] This approach has limitations in that surface- and bulk-initiated polymers do not experience the same reaction environment (*i.e.*, confinement, monomer or/and catalyst concentration, *etc.*). Recent computer simulations have revealed that the molecular weight distribution of densely grafted polymers prepared by the "grafting from" approach can differ significantly from that of polymers synthesized under identical conditions in bulk. The SGPAs tend to have lower M_n and a higher polydispersity index (PDI), especially for systems with a high σ_p.[30] M_n of polymer brushes has also been measured indirectly using swelling ratio[16] in a good solvent but this method cannot provide information about both MWD and PDI of the system. Other methods have employed nanoparticles[31,32] or porous materials[33] as substrates with large surface areas to grow sufficient amounts of polymer for analysis. The

potential drawback of these curved geometries is that the curvature of the surface may impose varying degrees of confinement. The degree of confinement may in turn affect the delivery of monomer and catalyst to reactive centers or may otherwise change the reaction environment.[25,34]

To overcome the aforementioned limitations associated with determining M_n for "grafted from" polymers, it is crucial to measure the properties of SGPAs on flat surfaces by direct analytical methods on the same surface on which the grafts were formed. As mentioned earlier, one method of characterizing the molecular weight distribution (including M_n) is to degraft the polymer chains from a large surface area and collect a sufficient amount of material to analyze using a sensitive analytical method, such as MALDI-TOF or size exclusion chromatography (SEC). Silicon (Si) substrates are commonly used as model surfaces for growing SGPAs, where the monolayer of surface initiators is attached by a $Si_{initiator}$–O–$Si_{substrate}$ bond to the thin layer of silica at the base. Hydrofluoric acid (HF) solution has been used to degraft polymer chains by breaking the Si–O bonds and dissolving the silica layer on the substrate.[32,33,35] However, HF is toxic and its use requires special protection and training. Initiators with certain cleavable functional groups[36] have also been used for degrafting. These methods utilized strong acids[37], bases[38] or an external energy source, such as UV light,[39,40] and hence cannot be employed for all initiator-polymer systems. Moreover, in certain instances the application of a harsh chemical for chain degrafting may degrade the polymer and may not cleave the bond at the linkage site on the substrate. In other instances, degrafting may not be

quantitative such that a small amount of the grafted chains remains on the substrate, which introduces error in determining M_n and ultimately σ_p.

In this work, we employ SI-ATRP to grow poly(methyl methacrylate) (PMMA) brushes on silica surfaces and utilize tetrabutyl ammonium fluoride (TBAF) to remove quantitatively the polymeric grafts from the substrate by cleaving the linkage between the initiator and the silica support. TBAF is a common source of fluoride (F^-) ions[41] and is available in THF solution with small amounts of water present for dissociation. The F^- ions have a strong tendency to attack Si atoms in Si–O bonds. The Si–F bond has a considerably high energy of formation (bond energy = 644 kJ/mol)[42] and hence it is thermodynamically favored. The C–F bond also has a high energy of formation (bond energy = 484 kJ/mol)[43] but the process is much slower and does not result in degradation of polymer chains (at least not in a short period of time, *i.e.*, ~24 hours, see Appendix A). We further show that polymers grown on a flat silica wafer as small as 4.2 x 4.2 cm^2 can be employed to degraft and collect a sufficient amount of polymer (minimal dry thickness 48 nm) whose MWD can be determined by SEC equipped with a sensitive differential refractive index (DRI) detector. We use the values of M_n determined from the SEC studies in conjunction with dry thicknesses measured by ellipsometry to calculate σ_p using Equation (3.1). The PDI values of the degrafted polymers range between 1.05 and 1.35 and do not exhibit any strong correlation with either the $Cu^{(II)}/Cu^{(I)}$ ratio or the polymerization time. We also detect a small dependence of σ_p on $Cu^{(II)}/Cu^{(I)}$. Specifically, we report that σ_p increases slightly with increasing $Cu^{(II)}/Cu^{(I)}$. We

attribute this behavior to smaller number of chain terminations under more controlled reaction conditions, *i.e.*, higher $Cu^{(II)}/Cu^{(I)}$.

3.2 Experimental Section

All chemicals were purchased from Sigma-Aldrich and used without further purification unless otherwise specified. Methyl methacrylate (MMA) was passed through columns of inhibitor remover to remove monomethyl ether hydroquinone. Deionized water (DIW, 120 MΩ) was obtained using Millipore Elix 3. Anhydrous toluene was prepared using molecular sieves (4 Å), which were activated under vacuum by heating them for 25 minutes using a heating gun. Copper (II) chloride was purified by dissolution in ethanol and precipitation in hexanes. The surface initiator (11-(2-bromo-2-methyl)propionyloxy undecyltrichlorosilane) (eBMPUS) was synthesized as described in the literature.[44] ACS grade methanol was purchased from Fisher Scientific. Silicon wafers (p-doped, orientation<100>) were purchased from Silicon Valley Microelectronics. TBAF was purchased as a 1 M solution in THF from Sigma-Aldrich.

Initiator deposition

A monolayer of eBMPUS was deposited on the silicon substrates (4.2 cm × 4.2 cm area). The substrates were cleaned by rinsing with methanol followed by sonication in methanol for 10 mins and then drying under a stream of nitrogen gas. The wafers were then placed in an ultraviolet-ozone (UVO, wavelengths 184.9 nm and 253.7 nm) chamber for 15 mins to generate free hydroxyl (–OH) groups at the surface. The eBMPUS solution was prepared by

adding 80 µl of a 5% w/w of e-BMPUS (in toluene) stock solution to 80 ml of anhydrous toluene. Two back-to-back, UVO-treated silicon wafers were placed in a glass container that was filled with eBMPUS solution, capped with argon, sealed, and placed in freezer at -18°C for 24 hours. After deposition was complete, the wafers were thoroughly rinsed with toluene and dried under nitrogen.

Growing the surface-grafted PMMA brush layer

ATRP solutions of four different catalyst ratios of $CuCl_2$/CuCl ($Cu^{(II)}/Cu^{(I)}$) were made. The concentration of CuCl was kept constant and only the amount of $CuCl_2$ was varied. Each batch was made by adding MMA (176.34 g, 1.76 mol), methanol (137.51 g, 4.29 mol), DIW (37.75 g, 2.1 mol), 2,2′-bipyridyl (11.11 g, 71.1 mmol), CuCl (3.55 g, 35.6 mmol), and $CuCl_2$ (4 different amounts for 4 solutions). The four $Cu^{(II)}/Cu^{(I)}$ ratios were 0, 0.005 ($CuCl_2$: 24.2 mg, 0.18 mmol), 0.01 (48.3 mg, 0.36 mmol), 0.015 (96.7 mg, 0.72 mmol). The solutions were mixed and degassed by bubbling with argon for 25 minutes. Each solution was then transferred to 4 different custom reaction chambers; each with one pair of back-to-back, eBMPUS coated wafers located ~1.5 cm above from the base allowing space for a stir bar. About 80 ml of MMA ATRP solution was added to each chamber, and the stir-bar insured proper mixing of the solution for homogeneous concentrations throughout the reaction mixture. The reaction chamber design also enabled an argon flow for a few minutes before being sealed and isolated from the outside atmosphere. The reaction was carried out at room temperature for 6, 9, 12, 16, 20 and 24 hours to obtain 4 or 6 different thickness (and hence M_n) for the PMMA brushes.

The reaction was stopped by opening the apparatus to air, rinsing the wafers with excess methanol followed by sonication in methanol for 5 minutes and drying with a stream of nitrogen gas. Finally the wafers were cleaned by rinsing with acetone and drying with nitrogen.

Degrafting the PMMA brush layer

Each wafer piece was put in a glass jar containing a 25 ml solution of 0.04 M TBAF in HPLC grade THF. Flat bottomed glass jars were used to minimize the amount of degrafting solution. The samples were incubated at 55°C using a water bath for 24 hours. The solution was then collected and rotovaped to ~1 ml of concentrate, which was then filtered through 0.2 μm polytetrafluoroethylene (PTFE) filters and passed through the SEC with THF. For the kinetic study, small samples (1 cm x 0.8 cm) were cut from a large 1 cm x 8 cm parent wafer containing the PMMA brush layer and the individual samples were subjected to different conditions by varying the TBAF concentration, the temperature of solution, and the incubation time. In the Appendix A we provide evidence that TBAF does not affect the properties of PMMA chains (*i.e.*, no chain cleavage).

Characterization

Size exclusion chromatography (SEC) was carried out using a Waters 2695 separations module. A light scattering detector (MiniDawn, Wyatt Technology Co.) and a differential refractive index (DRI) detector (Optilab Rex, Wyatt Technology Co.) were attached in series, however only data from DRI was used for M_n analysis. The setup had 3 columns in series (M_n ranges: 0.5~30, 0.05~100, 5~600 kDa) and the mobile phase was THF with a flow rate of 0.3

ml/min. The columns and detectors were maintained at 25°C. Conventional calibration was done using nine polystyrene standards from Fluka ranging from 2 to 400 kDa. The static water contact angle was measured using a contact angle goniometer (model 100-00, Ramé Hart) with DIW as the probe liquid. The thickness of polymer grafts on the substrate was determined using variable angle spectroscopic ellipsometry (VASE, J.A. Woollam Co., Inc.) with 3 angles of incidence (65, 70, 75°) and measurements at 5 spots for each large sample (4.2 cm x 4.2 cm) at varying $Cu^{(II)}/Cu^{(I)}$ ratios. The polymer layer thickness was obtained by fitting the ellipsometry data using a 3-layer model with silicon primarily at the bottom, intermediate silica (SiO_x) layer, and a top polymer 'Cauchy' layer. For the kinetic study, the thickness was measured using a fixed angle (70°) ellipsometer (Auto EL, Rudolph Research) with three measurements per small sample (size: 1 cm x 0.8 cm). X-ray photoelectron spectroscopy (XPS) was carried out using a SPECS FlexMod instrument with Al K-α source (excitation energy 1486.7 eV). The take-off angle measured from normal to the surface was 30°. Energy calibration was established by referencing to adventitious Carbon (C1s line at binding energy of 285.0 eV). Survey scans were taken with 0.5 eV steps and 0.04 s dwell per point and a pass energy (E_{pass}) setting of 24. High resolution XPS scans were taken with 0.1 eV steps and 0.5 s dwell per point with E_{pass} setting of 20.

Time-of-flight secondary ion mass spectrometry (TOF-SIMS) was employed to determine elemental and molecular information from the surface of the material with high spatial and mass resolution. A finely focused, pulsed primary ion beam was rastered across the surface of the sample and the secondary ions emitted at each irradiated point or pixel were

extracted into a time of flight mass spectrometer, mass filtered, and counted. The analysis was conducted using a TOF-SIMS V (ION TOF, Inc. Chestnut Ridge, NY) instrument equipped with a Bi_n^{m+} (n = 1 - 5, *m* = 1, 2) liquid metal ion gun. The analysis chamber pressure was maintained below 5.0 x 10^{-9} mbar to avoid contamination of the surfaces. For high mass resolution spectra acquired in this study, a pulsed Bi_3^+ primary ion beam with a 45° incident of angle at 25 keV impact energy and a pulse with less than a 1 ns width was used. An electron gun was used to prevent charge buildup on the insulting sample surfaces. The total accumulated primary ion dose for data acquisition was less than 1 x 10^{13} ions/cm^2, which is within the static SIMS regime. For high mass resolution mass spectra acquisition, the mass resolution on Si wafer is about ~8000 m/Δm at 29 AMU. The negative secondary ion mass spectra obtained were calibrated using C^-, O^-, OH^-, C_n^-, respectively. The positive secondary ion mass spectra were calibrated using H^+, C^+, $C_2H_3^+$, $C_3H_5^+$, $C_4H_7^+$.

3.3 Results and Discussion

3.3.1 Degrafting proof of concept

To test the use of TBAF as a viable agent for degrafting polymer chains from silica substrates, we chose a model system of PMMA brushes grown by SI-ATRP from eBMPUS initiator centers chemisorbed to native silica layers (thickness ~1.5 nm) of silicon wafers. The dry thickness of layers on the substrate (h_P) was measured using ellipsometry, the chemical composition was characterized by X-ray photoelectron spectroscopy (XPS), and time-of-flight secondary ion mass spectrometry (TOF-SIMS), and the wettability of the substrate was

determined by contact angle measurements using deionized water (θ_{DIW}) as the probe. **Figure 3.1** shows the results of XPS analysis along with h_P and θ_{DIW} for samples at various stages of preparation, *i.e.*, the bare silica surface (black), after initiator deposition (red), after PMMA brush growth (blue), and after PMMA brush degrafting from the substrate using TBAF (green). The cartoons on the left of the figure illustrate the sample configurations. The UVO-treated silicon wafer (black) has a very

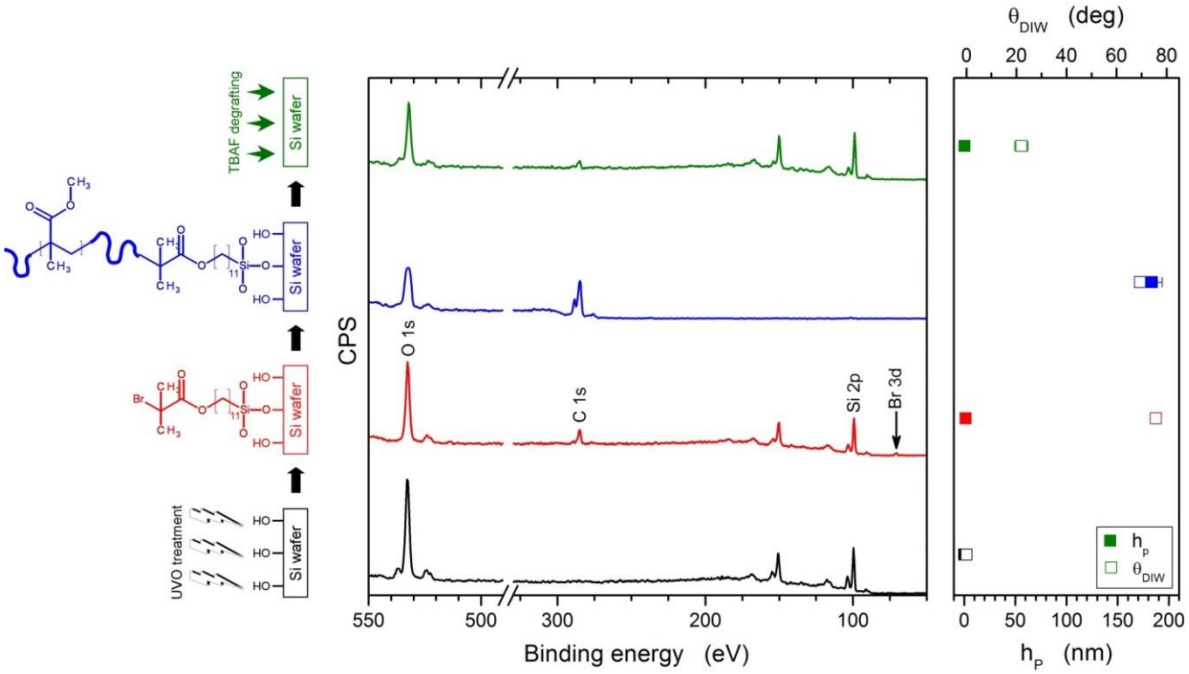

Figure 3.1. XPS scans for four different samples, color coded with the cartoons on the left. The thickness and contact angle are plotted on the right-side for the same 4 samples.

small amount of adventitious carbon (binding energy [BE] ~285 eV) before deposition; this is further demonstrated by the low intensity carbon high resolution spectrum in **Figure 3.2**. This surface is hydrophilic as indicated by the low value of θ_{DIW}; UVO is therefore an efficient

method to remove organic impurities from the surface in addition to generating active –OH for attachment of the initiator. The substrate cleaning step is followed by deposition of the eBMPUS (red) initiator monolayer (thickness 1.5 ± 0.2 nm), which shows an increase in carbon peak intensity and the appearance of a bromine peak (BE ~70 eV). For both of these surfaces, we detect peaks for silicon (BE ~99 eV) and oxygen (BE ~533 eV) from the underlying silica layer (thickness ~1.5 nm). When the 184 ± 10 nm thick PMMA brush layer (blue) is grown from the eBMPUS initiator centers, the escape electrons from silicon cannot reach the surface and cannot be detected. Here we only observe carbon and oxygen signals in PMMA. In addition to a thickness increase, there is a concurrent increase in θ_{DIW} for the substrate, corresponding to PMMA. The PMMA brush layer was incubated in 0.1 M TBAF at 50°C for 6 hours in order to degraft the polymer from the substrate. After degrafting the PMMA layer with TBAF, the thickness of the top layer (green) reduces dramatically to 0.4 ± 0.1 nm. Concurrently, the θ_{DIW} drops significantly but it remains higher than that of the corresponding bare silica. XPS detects the reduction of the layer because the signals corresponding to silica can now be resolved. However, there are small carbonaceous residues present on the substrate that may originate from remaining grafted polymer chains, unactivated eBMPUS molecules, or can be simply present due to adventitious carbon.

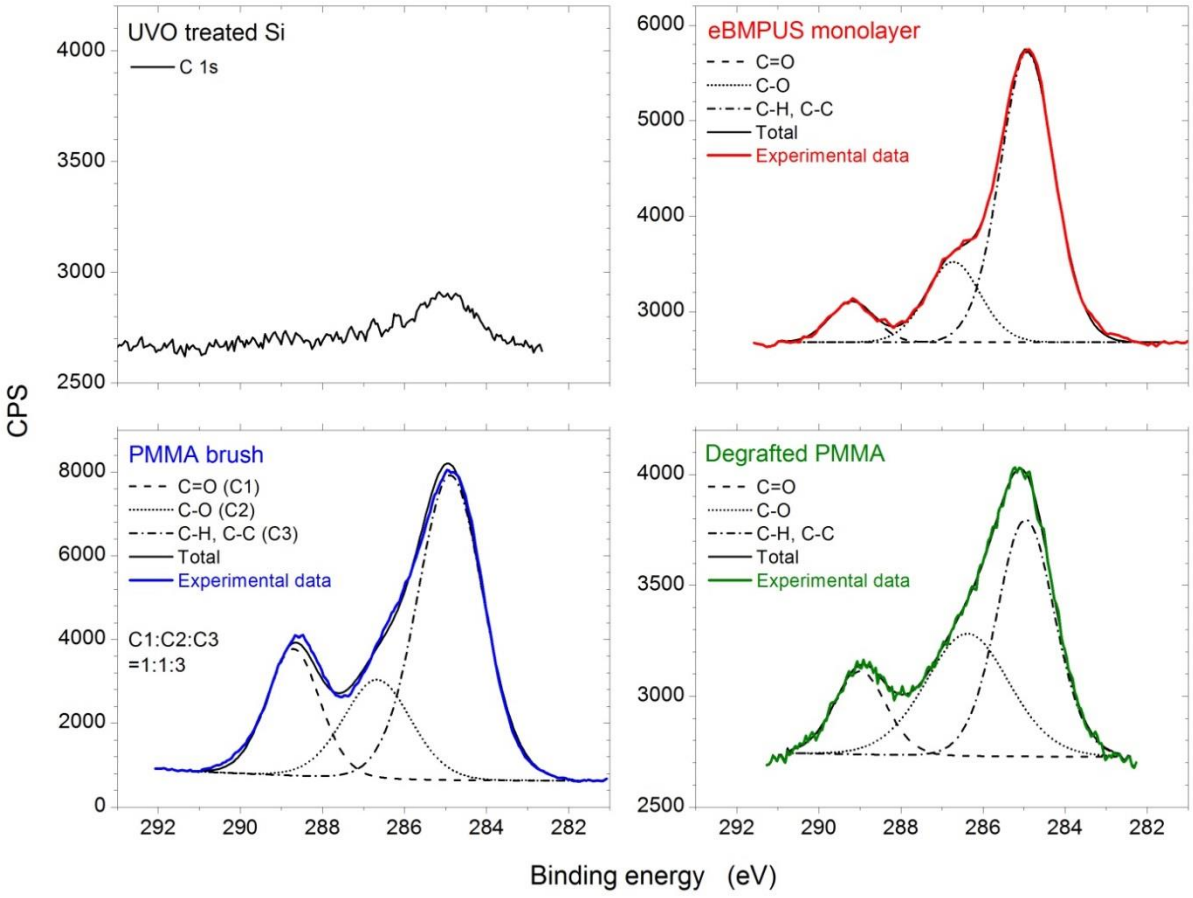

Figure 3.2. High resolution XPS spectra of the C 1s peak for the four substrates shown in Figure 3.1. The various types of bonds are depicted in dashed, dotted and dash-dotted lines. For the PMMA brush, the ratio of the areas of the peaks corresponds to the atomic ratios of the different bonded carbons.

In **Figure 3.2** we plot high resolution C 1s XPS spectra for the four substrates discussed previously. The XPS spectra were de-convoluted by fitting individual peaks corresponding to various carbon bonds. Those are shown by the dashed (C=O), dotted (C-O), and dash-dotted (C-H and C-C) lines. The solid black line is the sum of all the individual peaks. For the PMMA brush layer, the peak areas of C=O, C–O and all other carbon atoms give the ratio of

1:1:3 which corresponds to the PMMA atomic composition. The synthetic components of O 1s for PMMA also match the atomic composition of PMMA (see Appendix A) confirming its presence. The absolute intensity of C 1s peaks for the eBMPUS monolayer and degrafted substrate is relatively weak as compared to the PMMA layer. The ratio of areas in the degrafted substrate is visibly different from that of the PMMA layer, indicating that a minuscule amount of PMMA could remain to be present on the surface after degrafting. TOF SIMS experiments, however, provide indisputable evidence that all PMMA was removed from the substrate and that the carbon signal detected on the surface of the degrafted wafer originates likely from adventitious carbon-based impurities. In **Figure 3.3** we plot the TOS SIMS spectra collected from silica substrates exposed to 0.1 M solution of TBAF (black), the eBMPUS initiator layer (red), the PMMA brush layer (blue), and the substrate after degrafting PMMA with TBAF (green). The characteristic fragments for PMMA *i.e.* $C_4H_5O_2^{-1}$ (m/z=85) and $C_3H_3O^{-1}$ (m/z=56) are not prominent in the TBAF treated and degrafted substrate, while $SiHO_3^{-1}$ (m/z=77) is seen for the degrafted substrate. In addition, the presence of Br (m/z=79) is detected in only in the eBMPUS sample. The TOF SIMS spectrum of the degrafted substrate resembles that of the TBAF-treated silica and is very different from that of the PMMA brush layer.

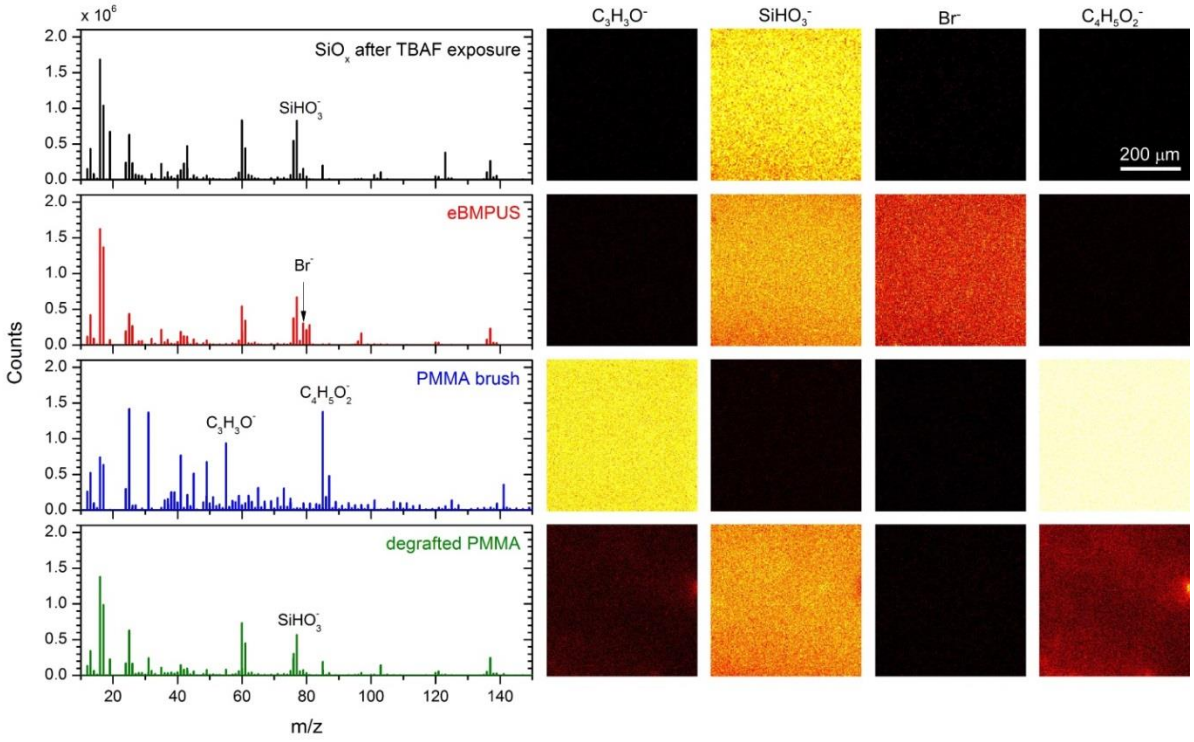

Figure 3.3. TOF SIMS spectra collected from (top to bottom): an SiO_x substrate treated with TBAF (black), SiOx substrate coated with eBMPUS ATRP initiator (red), after PMMA brush growth (blue), and after degrafting the PMMA brush with TBAF (green). The images on the right depict 0.5 x 0.5 mm^2 areas on the sample corresponding to various mass signals marked in the spectra. The color scale depicts the counts/second. It ranges from 0 (black) to C_{max} (white), where C_{max} = 30 for $C_3H_3O^-$, $SiHO_3^-$, and $C_4H_5O_2^-$, and C_{max} = 18 for Br^-.

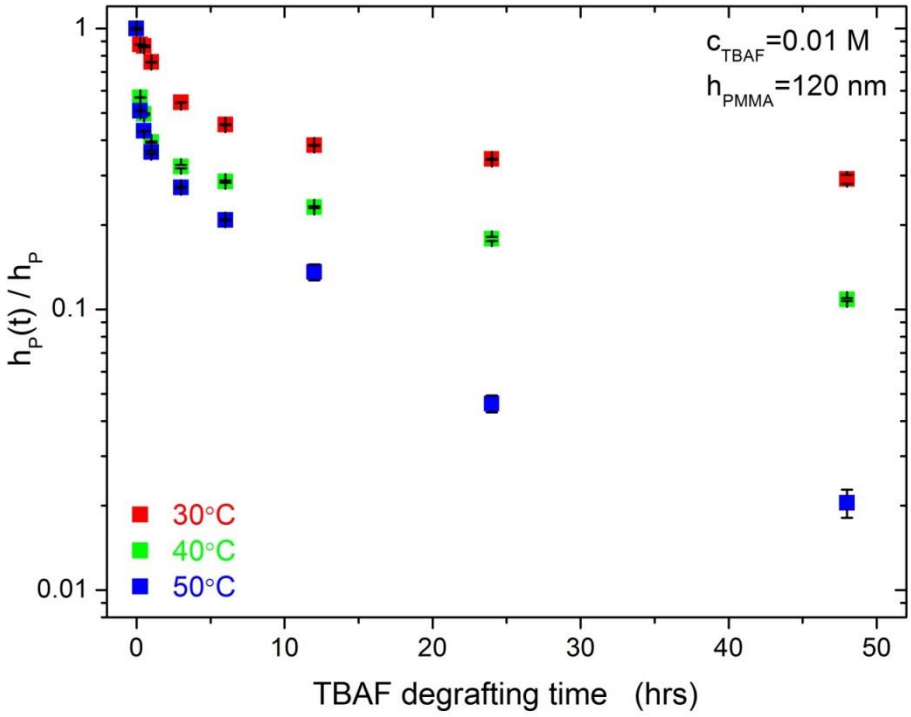

Figure 3.4. Relative brush thickness (i.e., time-dependent thickness normalized by the initial thickness) of a PMMA brush as a function of TBAF degrafting time at three different temperatures. The original dry thickness of the PMMA brush was ~120 nm and the concentration of the TBAF solution was 0.01 M.

3.3.2 Kinetics of degrafting

We studied the PMMA brush degrafting process by varying the initial thickness of the PMMA brush, the concentration of TBAF, the temperature, and the exposure time to TBAF. A detailed study reporting on the kinetics of degrafting is provided in chapter 4. Here we offer only a brief discussion. **Figure 3.4** shows the variation of thickness normalized with the initial PMMA dry thickness (h_P~120 nm in this case) as a function of incubation time in TBAF at a concentration of 0.01 M. The dry thickness represents the amount of material present on the

surface as a function of time. This data provides a measure of the extent of degrafting. The normalized PMMA brush thickness decreased exponentially with incubation time and the rate of degrafting increased with increasing temperature of the TBAF solution. Based on the data, TBAF degrafting appears to follow double exponential behavior indicating two distinct regimes, which are an initial fast rate and a later slow degrafting rate. As will be discussed elsewhere, assuming Arrhenius type kinetics for the decay, we get a low average initial activation energy of ~101 kJ/mol and a final activation energy of ~52 kJ/mol. The kinetic experiments offer a way to precisely control the thickness of the brush layer by varying the incubation time, the temperature or the concentration of the TBAF solution.

3.3.3 Molecular weight distribution

Distribution of molecular weights of the degrafted PMMA chains was assessed via size exclusion chromatography (see experimental section for details). The black lines in **Figure 3.5** correspond to PMMA chains grown from substrates via ATRP at $Cu^{(II)}/Cu^{(I)}$ =0.01 for a) 6, b) 9, c) 12, d) 16, e) 20, and f) 24 hrs. With increasing polymerization time the elution curves shift towards higher molecular weights and broaden, as expected. To quantify the SEC data and gain insight into the mechanism of surface-initiated polymerization, we fit the experimental data to several molecular weight distribution models. The calculated MWD curves are plotted in **Figure 3.5** for the Schulz-Zimm (SZ, red lines), ATRP (green line), Wesslau (W, blue lines), Schulz-Flory (SF, cyan lines), and Smith *et al.* (S, magenta lines)

models. Detailed description of the various models and the method of fitting are provided in the Appendix A.

From the fits in **Figure 3.5**, it is visually evident that only the first three models provide a suitable description of the experimental MWDs. The Schulz-Flory and Smith *et al.* distributions capture the general shape of the experimental data but fail to provide a good fit. In order to probe the quality of the fits of the various models to the experimental molecular weight distributions, in **Figure 3.6** we plot PDI as a function of the number degree of polymerization, N_n, as determined by experiment (black star) and obtained from modeling the experimental data using the aforementioned models (other symbols). The fit of the data was obtained by minimizing the distance between the distributions and the model as measured by the Kolmogorov-Smirnov statistic (K-S, see Appendix A).[45] The sections a)-f) in **Figure 3.6** correspond to the same sections in **Figure 3.5**. The insets in **Figure 3.6** show the K-S statistic between the fitted model and experimental distributions, verifying our observation that the Schulz-Flory and Smith *et al.* distributions are inadequate in describing the experimental data. In general, the SZ, ATRP, and W distributions capture the properties of the experimental MWDs well as indicated by low values of the K-S parameter and a good match between the PDI and N_n obtained from experiment and those obtained from the three respective models. The Appendix A contains a detailed analysis of samples prepared with other $Cu^{(II)}/Cu^{(I)}$ ratios and polymerization times. The fits obtained by the various models exhibit the same trends as those described here for $Cu^{(II)}/Cu^{(I)}=0.01$.

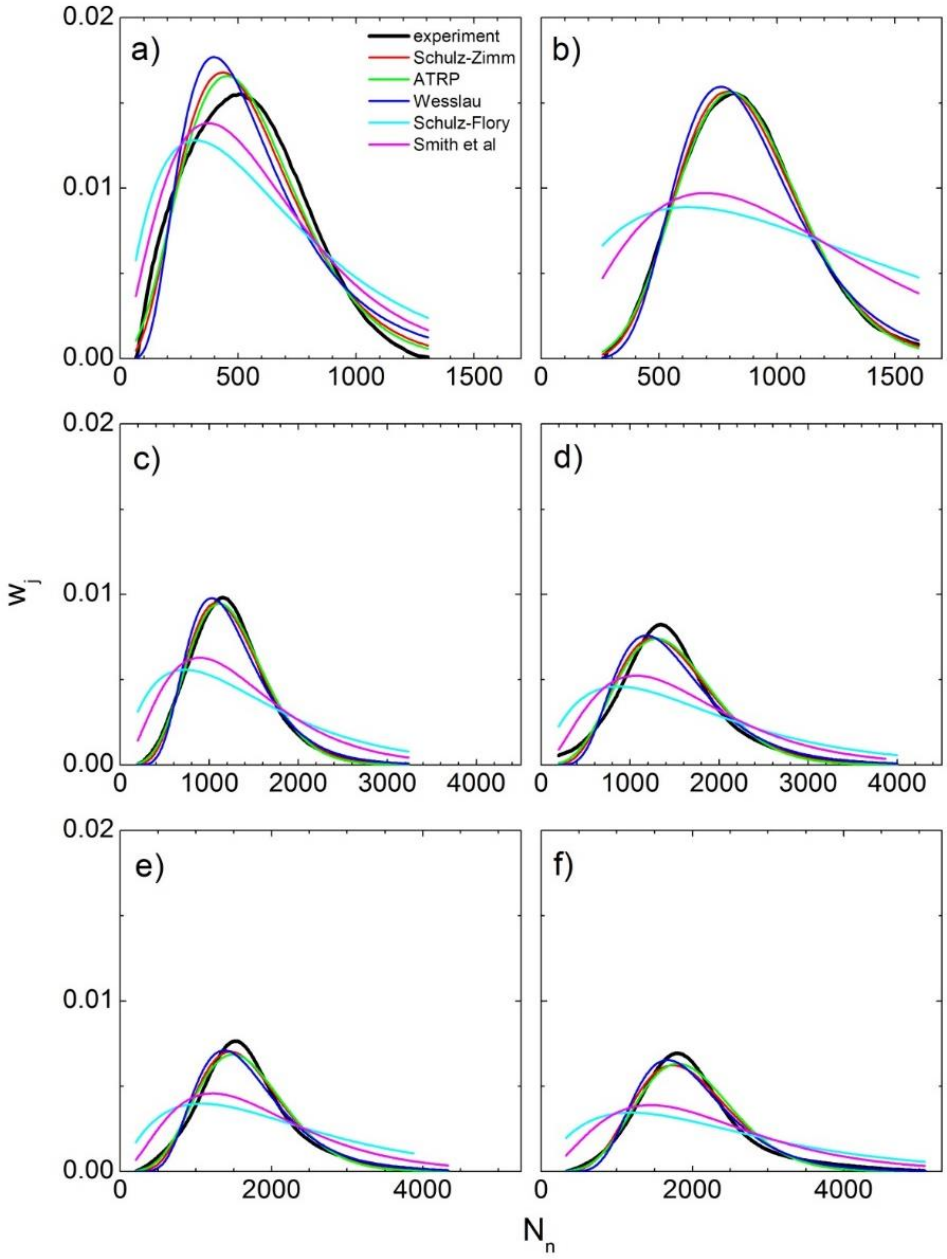

Figure 3.5. Weight fraction of PMMA chains (w_j) degrafted from flat surfaces (black lines) as a function of number average degree of polymerization (N_n) for PMMA brushes grown for a) 6, b) 9, c) 12, d) 16, e) 20, and f) 24 hrs with $Cu^{(II)}/Cu^{(I)}$=0.010 (see experimental section for details). The experimental data were fit by minimizing the distance between the model and data as measured by the Kolmogorov-Smirnov (K-S) statistic. The distributions tested were Schulz-Zimm (SZ, red lines), ATRP (green line), Wesslau (W, blue lines), Schulz-Flory (SF, cyan lines), and Smith *et al.* (S, magenta lines).

From the data in **Figure 3.6,** it is challenging to determine which of the three models is the best; however, the ATRP model seems to fit the data consistently better than the SZ and W models for the majority of the samples. Turgman Cohen and Genzer previously reported that the MWD of polymer brushes prepared by "living" surface-initiated polymerization can be described by the SZ distribution[46]. Although Mastan *et al.* developed an ATRP model for continuously stirred tank reactors with no termination[47], we argue that it is also applicable for these results since the SGPAs discussed here were grown with a large excess of monomer and relatively low monomer conversions. This assured that monomer concentration around the brush remained approximately constant as long as effects due to the monomer diffusion to the surface are negligible. Importantly, one can conclude that the PMMA brushes do not exhibit excessive terminations due to the high quality of the fits to the ATRP model, which does not take termination into account.

3.3.4 Grafting density of polymeric grafts on the substrate

M_n and σ_P play a critical role in defining the conformation of SGPAs. It is known that controlled polymerization techniques like ATRP generate a narrow MWD and a PDI<1.2 for bulk polymers. Here we aim to understand the effect of ATRP catalyst ratio (*i.e.*, concentration of deactivation/activation $Cu^{(II)}/Cu^{(I)}$) and polymerization time on the molecular weight distribution for surface-initiated ATRP. Equation (1) describes the relationship between σ_P and M_n for polymer brushes via h_P. To determine σ_P we need to measure M_n of polymers degrafted from the silica substrates. We have tested the sensitivity of the differential refractive

index (DRI) detector of the SEC and found that a minimum polymer sample concentration of 0.1 mg/ml is needed to get a reasonable signal without any significant loss in fidelity of the data. This critical value was determined by analyzing monodisperse and polydisperse polymer samples of known molecular weight at different concentrations and studying the shape of the eluograms (see Appendix A). Based on this threshold concentration, the minimum dry thickness of PMMA required on a 4.2 cm x 4.2 cm substrate is ~48 nm. For thicknesses less than 48 nm but greater than 24 nm we have combined the degrafted solution from two identical substrates such that the mass of polymer remains above the threshold amount.

The ATRP catalyst ratio (*i.e.*, $Cu^{(II)}/Cu^{(I)}$) controls both the rate of polymerization in the bulk and the monodispersity of the product. Based on bulk data a higher $Cu^{(II)}/Cu^{(I)}$ catalyst ratio is expected to lead to a slower growth rate leading to more control of the polymer distribution resulting in lower PDIs.[48] **Figure 3.7** shows h_P, M_n, and PDI as a function of polymerization time for different values of $Cu^{(II)}/Cu^{(I)}$. The h_P and M_n increase nearly linearly with increasing polymerization time in agreement with standard ATRP results. The dry thickness growth rate increases from 4.4 to 6.6 nm/hr when the ATRP catalyst ratio decreases from 0.015 to 0, respectively. The initial polymerization rate for <6 hr is likely higher but cannot be determined due to limitations in the sensitivity of our SEC set up. After 24 hours of polymerization the living nature of polymer growth is no longer sustained and the thickness starts to plateau.[49,50]

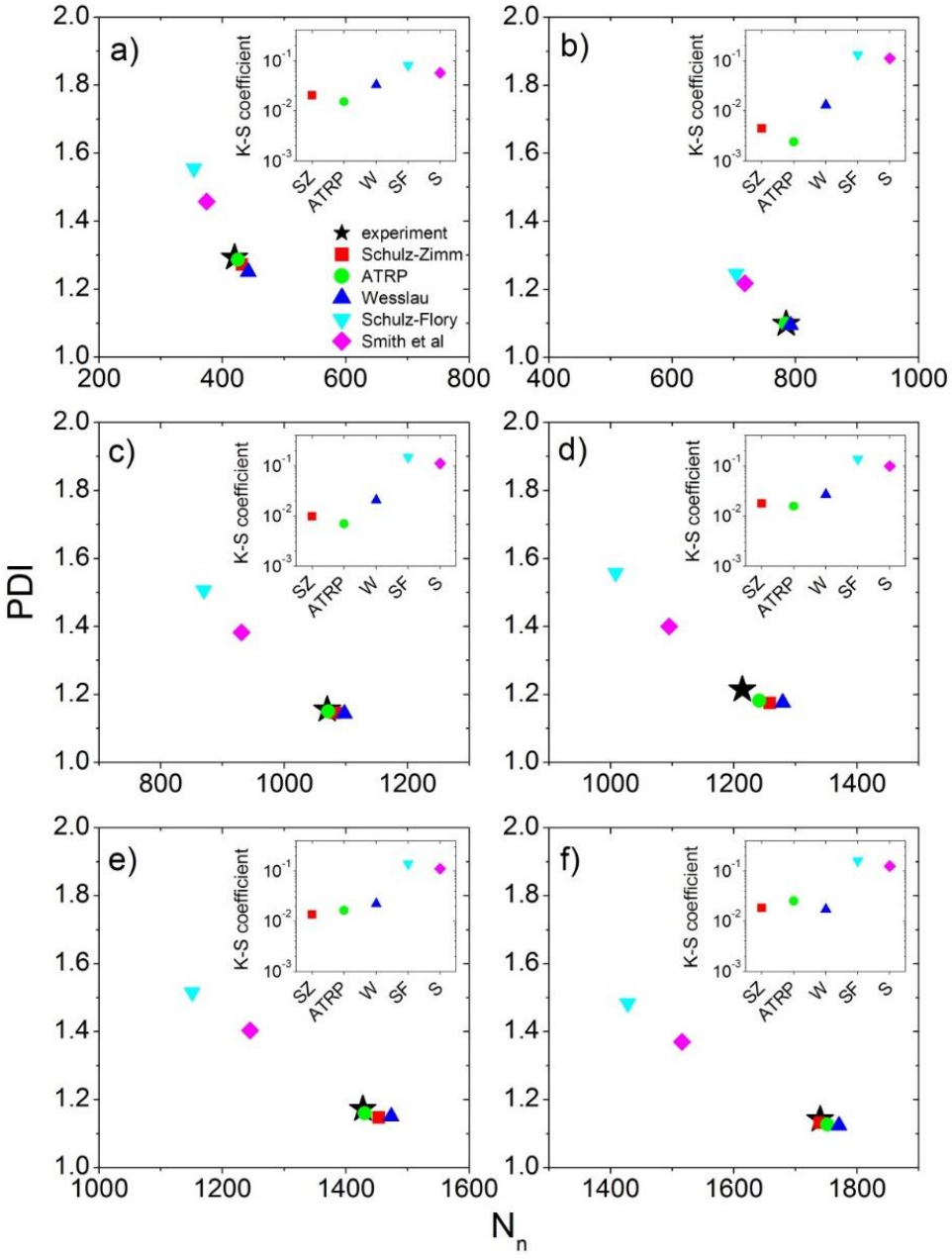

Figure 3.6. Polydispersity index (PDI) vs. number average degree of polymerization (N_n) for PMMA chains degrafted from flat surfaces (black star) grown for a) 6, b) 9, c) 12, d) 16, e) 20, and f) 24 hrs with $Cu^{(II)}/Cu^{(I)}$=0.010 (see experimental section for details). The experimental data were fit by minimizing the distance between the model and data as measured by the Kolmogorov-Smirnov (K-S) statistic. The distributions tested were Schulz-Zimm (SZ, red lines), ATRP (green line), Wesslau (W, blue lines), Schulz-Flory (SF, cyan lines), and Smith *et al.* (S, magenta lines).

The bottom of **Figure 3.7** depicts the values of PDI for the various $Cu^{(II)}/Cu^{(I)}$ ratios as a function of polymerization time. Generally, the PDI values for all samples are higher than those grown in bulk using ATRP under identical polymerization conditions (typically <1.2). Because of the large scatter in the data (1.05 ~ 1.35) it is difficult to identify clear trends. The average values (and their standard deviation) shown by the dashed lines split the data into two groups. Specifically, for $Cu^{(II)}/Cu^{(I)}$ =0 we obtain PDI=1.188±0.015. This value is somewhat larger than the PDIs determined for polymerizations with $Cu^{(II)}/Cu^{(I)}$>0, where PDI equals 1.147±0.020, 1.139±0.028, and 1.146±0.028 for $Cu^{(II)}/Cu^{(I)}$ equal to 0.005, 0.010, and 0.015, respectively). This trend, if real, is consistent with the notion that polymers grown under controlled conditions (*i.e.*, $Cu^{(II)}/Cu^{(I)}$>0) exhibit lower PDI. These findings are in line with previous computer simulations, which revealed that altering the life time of active growing polymers in surface-initiated polymerizations at constant grafting density of the initiators exhibits only minor changes in the PDI of the growing brushes.[30]

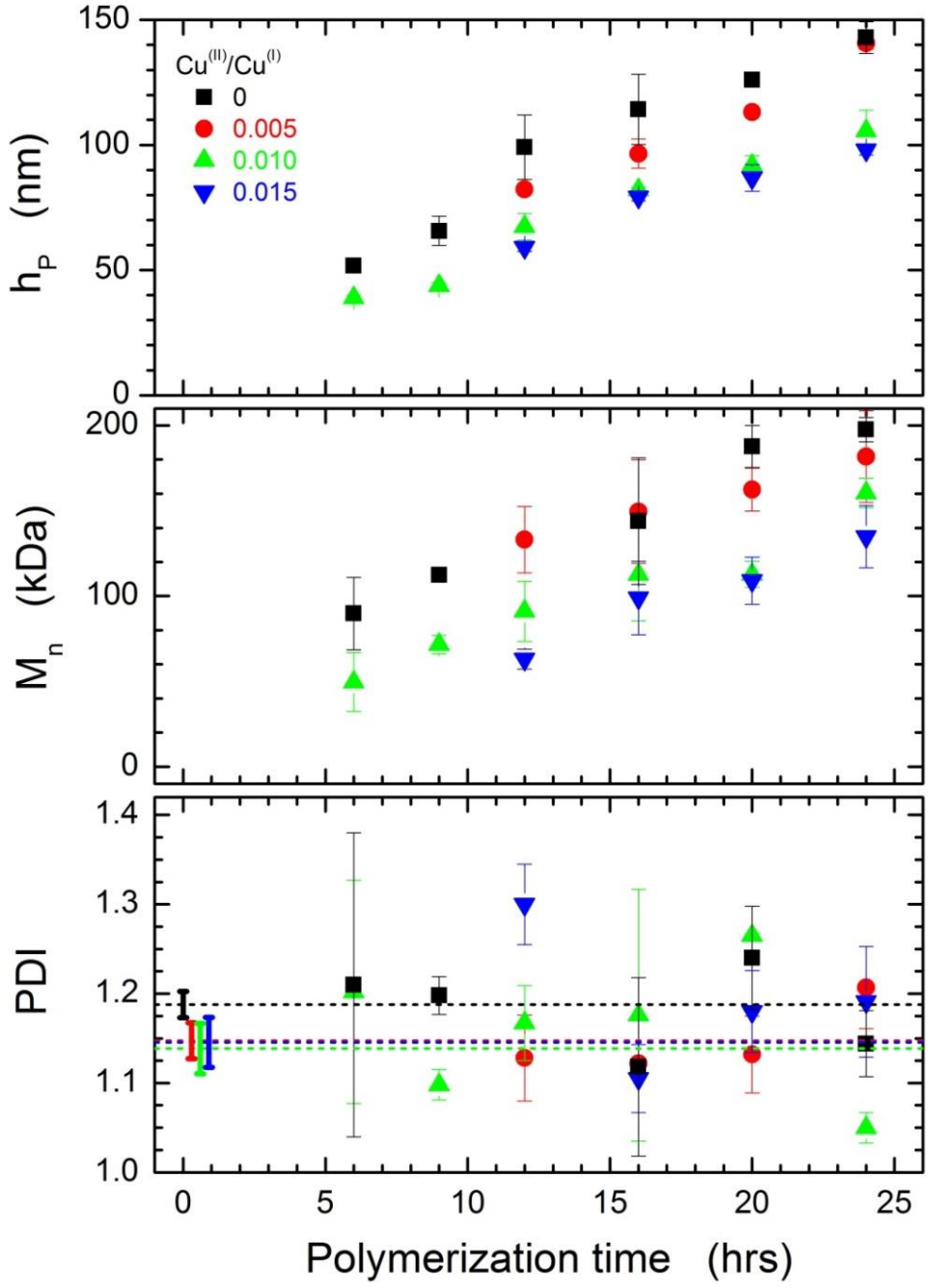

Figure 3.7. Number average molecular weight (M_n), dry PMMA brush thickness (h_P), and polydispersity index (PDI) plotted as a function of polymerization time for 4 different ATRP catalyst ratios. The dotted lines in the bottom plot denote the average values of the PDIs; the line colors correspond to those in the legend.

In **Figure 3.8** we plot M_n as a function of h_P (data from **Figure 3.7**). The slope of this graph is proportional to the inverse of σ_p based on Equation (1). Regressing the data for all catalyst ratios and setting the intercept to zero gives $\sigma_p = 0.517 \pm 0.012$ chain/nm^2. In **Figure 3.9** we plot the σ_p for the individual values of $Cu^{(II)}/Cu^{(I)}$ and we observe a slight increase in the σ_p with increasing $Cu^{(II)}/Cu^{(I)}$. We attribute this apparent change in σ_p to a combination of the effect of fast initiation and a detection limit of the SEC. The ATRP initiation takes place nearly instantaneously based on results for bulk initiation.[51] This is further supported by the fact that we use a hybrid initiator/catalyst halide system with Br-based initiator (eBMPUS) and Cl-based transition metal ion, chloride being the more stable bond tends to form early.[52]

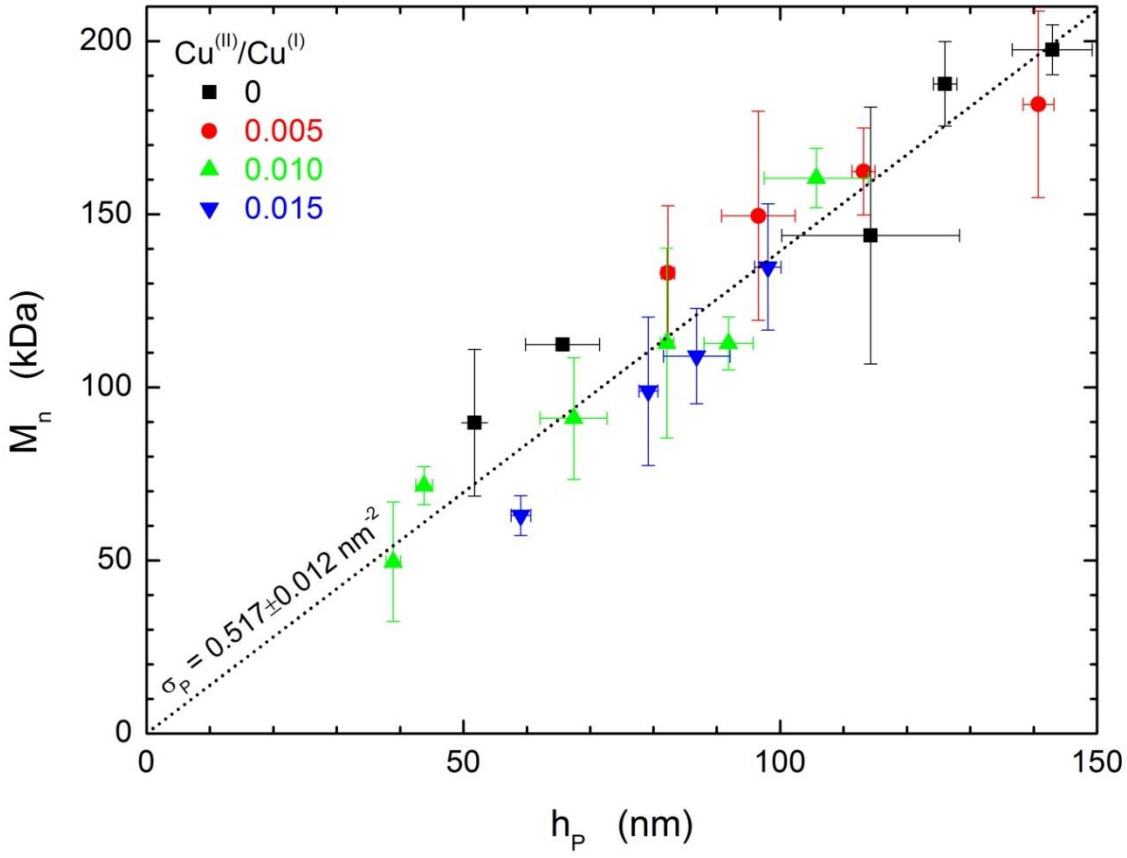

Figure 3.8. Number average molecular weight (M_n) as a function of dry PMMA brush thickness (h_P) for four ATRP catalyst ratios. The dotted line is a linear fit passing through the origin.

We consider our calculated σ_p a lower bound because of the characteristics of our measurement methods, discussed hereafter. The dry brush thickness measured by ellipsometry accounts for every (macro)molecule attached to the substrate regardless of its length. This, in principle, also includes all the unreacted initiators on the substrate. On the contrary, the measurement of the MWD by means of SEC is not likely to detect every single polymer chain on the surface. In fact, it is likely that the MWD in our samples has low- and high- molecular weight tails that

our instrument fails to detect due to lack of sensitivity. By necessity, we expect and assume that the effects of these two tails will largely cancel out when computing the M_n shown in **Figure 3.8**.

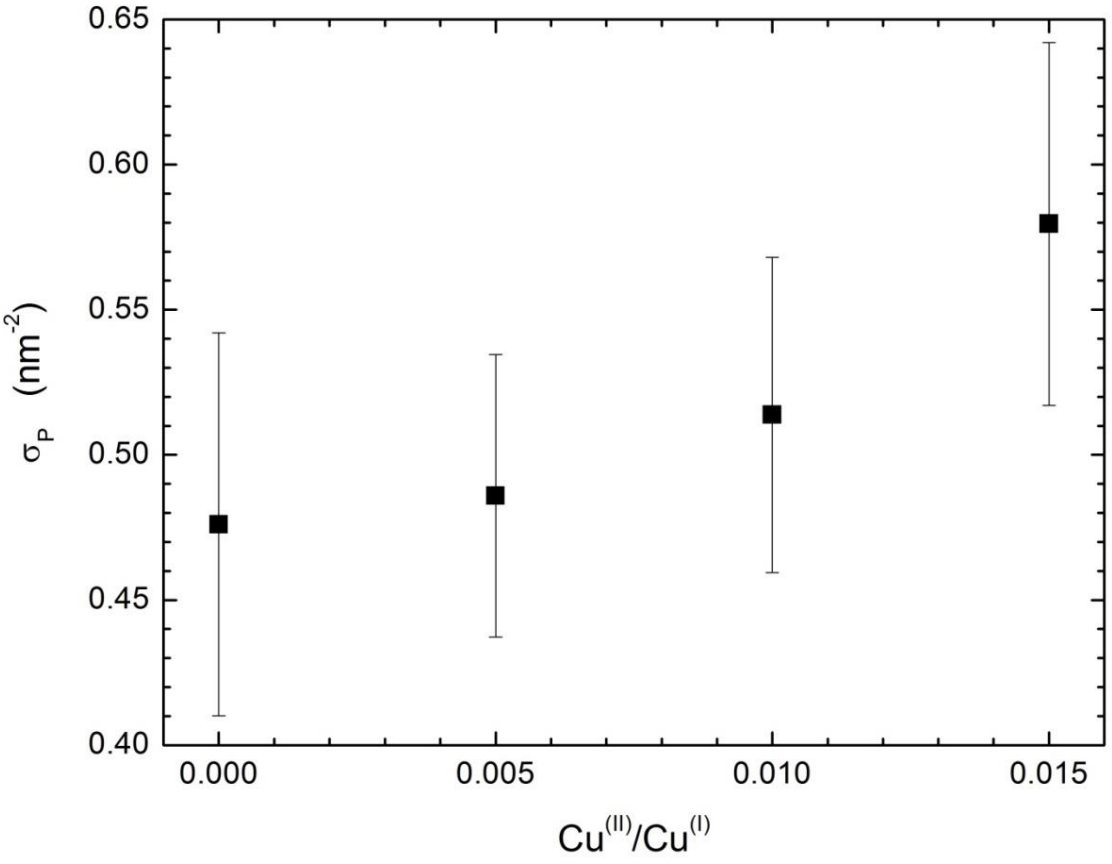

Figure 3.9. Polymer grafting density (σ_p) as a function of ATRP catalyst ratio.

However, it is possible that the low molecular weight tail of the distribution is larger than the high molecular weight one, including short polymers that only grow at the onset of polymerization and any initiators that never polymerized. If this is the case, then the value of M_n calculated herein with SEC is an overestimate and the slope shown in **Figure 3.8** is larger

than the true value making the grafting density smaller. This can be explained as follows. At a lower $Cu^{(II)}/Cu^{(I)}$ ratio the chains grow rapidly and suffer from a higher rate of early terminations, thus creating short chains, which are below the detection limit of the SEC. Thus the measured M_n for low $Cu^{(II)}/Cu^{(I)}$ ratio is skewed towards a higher value resulting in a lower σ_p (*cf.* Equation 1). In contrast, for higher $Cu^{(II)}/Cu^{(I)}$ ratio the reaction will be more controlled; as a result, the formation of shorter grafts due to early termination will be suppressed. Even if additional chains initiate after the first polymerization commences, their growth will very likely be hindered by stearic hindrance to delivery of the catalyst and monomer. The polymerization is carried out in methanol/water system which is a poor solvent for PMMA chains.[53] This will lead to limited swelling of the polymer chains causing them to adopt a collapsed state further hindering the growth of any short chains.

It is worthwhile to compare our findings with those of Kang *et al.*[39] who performed similar measurements for brushes comprising either poly(lauryl methacrylate) or polystyrene. Although the authors of that study did not explore the effects of $Cu^{(II)}/Cu^{(I)}$ ratio, they reported that the σ_p was independent of the polymerization time, which is in agreement with our study. Furthermore, the σ_p Kang *et al.* reported for polystyrene was very close to the one calculated for PMMA in this study.

3.4 Conclusions

We have demonstrated a viable technique for degrafting PMMA brushes from flat silica-based substrates using TBAF, and we determined their molecular weight distribution using SEC. The degrafting rate for chains on the substrate can be controlled readily by varying the concentration of TBAF, the temperature, and sample incubation time in TBAF solution. The grafting density for all PMMA brushes was found to be 0.517 ± 0.012 chains/nm^2 for polymerization times in the range 6 and 24 hours irrespective of the ATRP deactivator/activator ratio (*i.e.*, $Cu^{(II)}/Cu^{(I)}$). The thickness and M_n showed the expected trends for an ATRP mechanism but the PDI did not reveal any significant dependence on the deactivator/activator ratio. The values of PDI were marginally higher than those typically observed in bulk polymer grown under similar conditions. We attribute growth under confinement as the major cause of the deviation from the living nature of the polymer. This is what makes a grafted polymer system unique, *i.e.*, a higher grafting density. A higher $Cu^{(II)}/Cu^{(I)}$ does result into an apparent increase in the grafting density, which is an outcome of low early termination combined with detect limits of SEC for very short and sparsely populated chains.

3.5 Acknowledgements

The work was supported by the National Science Foundation (Grant no. DMR-0906572) and the Army Research Office and (Grant no. W911NF-04-D-0003-0016).

3.6 References

(1) de Gennes, P. G. *J. Phys.* **1976**, *37* (12), 1445–1452.

(2) Alexander, S. *J. Phys.* **1977**, *38*, 977–981.

(3) Milner, S. T. *Science* **1991**, *251* (4996), 905–914.

(4) Zhao, B.; Brittain, W. J. *Prog. Polym. Sci.* **2000**, *25*, 677–710.

(5) Luzinov, I.; Minko, S.; Tsukruk, V. V. *Prog. Polym. Sci.* **2004**, *29* (7), 635–698.

(6) Uhlmann, P.; Merlitz, H.; Sommer, J.-U.; Stamm, M. *Macromol. Rapid Commun.* **2009**, *30* (9-10), 732–740.

(7) Cohen Stuart, M. A.; Huck, W. T. S.; Genzer, J.; Müller, M.; Ober, C.; Stamm, M.; Sukhorukov, G. B.; Szleifer, I.; Tsukruk, V. V; Urban, M.; Winnik, F.; Zauscher, S.; Luzinov, I.; Minko, S. *Nat. Mater.* **2010**, *9* (2), 101–113.

(8) Chen, J.-K.; Hsieh, C.-Y.; Huang, C.-F.; Li, P.-M.; Kuo, S.-W.; Chang, F.-C. *Macromolecules* **2008**, *41* (22), 8729–8736.

(9) Chen, T.; Amin, I.; Jordan, R. *Chem. Soc. Rev.* **2012**, *41* (8), 3280–3296.

(10) Yandi, W.; Mieszkin, S.; Martin-Tanchereau, P.; Callow, M. E.; Callow, J. A.; Tyson, L.; Liedberg, B.; Ederth, T. *ACS Appl. Mater. Interfaces* **2014**, *6* (14), 11448–11458.

(11) Suriyanarayanan, S.; Lee, H.-H.; Liedberg, B.; Aastrup, T.; Nicholls, I. A. *J. Colloid Interface Sci.* **2013**, *396*, 307–315.

(12) Hoshi, Y.; Xu, Y.; Ober, C. K. *Polymer*. **2013**, *54* (7), 1762–1767.

(13) Klein, J. *Annu. Rev. Mater. Sci.* **1996**, *26*, 581–612.

(14) Kobayashi, M.; Terayama, Y.; Hosaka, N.; Kaido, M.; Suzuki, A.; Yamada, N.; Torikai,

N.; Ishihara, K.; Takahara, A. *Soft Matter* **2007**, *3* (6), 740–746.

(15) Bielecki, R. M.; Crobu, M.; Spencer, N. D. *Tribol. Lett.* **2012**, *49* (1), 263–272.

(16) Bhairamadgi, N. S.; Pujari, S. P.; Leermakers, F. A. M.; Rijn, C. J. M. Van; Zuilhof, H. *Langmuir* **2014**, *30*, 2068–2076.

(17) Kobayashi, M.; Terada, M.; Takahara, A. *Soft Matter* **2011**, *7* (12), 5717–5722.

(18) Shah, R. R.; Merreceyes, D.; Husemann, M.; Rees, I.; Abbott, N. L.; Hawker, C. J.; Hedrick, J. L. *Macromolecules* **2000**, *33* (2), 597–605.

(19) Huang, X.; Wirth, M. J. *Anal. Chem.* **1997**, *69* (22), 4577–4580.

(20) Ejaz, M.; Yamamoto, S.; Ohno, K.; Tsujii, Y.; Fukuda, T. *Macromolecules* **1998**, *31*, 5934–5936.

(21) Barbey, R.; Lavanant, L.; Paripovic, D.; Schüwer, N.; Sugnaux, C.; Tugulu, S.; Klok, H.-A. *Chem. Rev.* **2009**, *109* (11), 5437–5527.

(22) Sedjo, R. A.; Mirous, B. K.; Brittain, W. J. *Macromolecules* **2000**, *33*, 1492–1493.

(23) Baum, M.; Brittain, W. J. *Macromolecules* **2002**, *35* (3), 610–615.

(24) Husseman, M.; Malmstrom, E. E.; McNamara, M.; Mate, M.; Mecerreyes, D.; Benoit, D. G.; Hedrick, J. L.; Mansky, P.; Huang, E.; Russell, T. P.; Hawker, C. J. *Macromolecules* **1999**, *32*, 1424–1431.

(25) Bain, E. D.; Turgman-Cohen, S.; Genzer, J. *Macromol. Theory Simulations* **2013**, *22* (1), 8–30.

(26) Elliott, L. C. C.; Jing, B.; Akgun, B.; Zhu, Y.; Bohn, P. W.; Fullerton-Shirey, S. K. *Langmuir* **2013**, *29* (10), 3259–3268.

(27) Laurent, P.; Souharce, G.; Duchet-Rumeau, J.; Portinha, D.; Charlot, A. *Soft Matter* **2012**, *8* (3), 715–725.

(28) Audouin, F.; Larragy, R.; Fox, M.; O'Connor, B.; Heise, A. *Biomacromolecules* **2012**, *13* (11), 3787–3794.

(29) He, X.; Yang, W.; Pei, X. *Macromolecules* **2008**, *41* (13), 4615–4621.

(30) Genzer, J. *Macromolecules* **2006**, *39*, 7157–7169.

(31) von Werne, T.; Patten, T. E. *J. Am. Chem. Soc.* **1999**, *121*, 7409–7410.

(32) von Werne, T.; Patten, T. E. *J. Am. Chem. Soc.* **2001**, *123*, 7497–7505.

(33) Ejaz, M.; Tsujii, Y.; Fukuda, T. *Polymer.* **2001**, *42*, 6811–6815.

(34) Gorman, C. B.; Petrie, R. J.; Genzer, J. *Macromolecules* **2008**, *41*, 4856–4865.

(35) Wu, T.; Efimenko, K.; Genzer, J. *J. Am. Chem. Soc.* **2002**, *124* (32), 9394–9395.

(36) Prucker, O.; Rühe, J. *Macromolecules* **1998**, *31* (3), 592–601.

(37) Kobayashi, M.; Terada, M.; Terayama, Y.; Kikuchi, M.; Takahara, A. *Macromolecules* **2010**, *43* (20), 8409–8415.

(38) Jia, X.; Zhang, G.; Li, W.; Sheng, W.; Li, C. *J. Polym. Sci. Part A Polym. Chem.* **2014**, *52* (13), 1807–1814.

(39) Kang, C.; Crockett, R. M.; Spencer, N. D. *Macromolecules* **2014**, *47* (1), 269–275.

(40) Schuh, C.; Lomadze, N.; Rühe, J.; Kopyshev, A.; Santer, S. *J. Phys. Chem. B* **2011**, *115* (35), 10431–10438.

(41) Cox, P.; Terpinski, J.; Lawrynowicz, W. *J. Org. Chem.* **1984**, *49* (27), 3216–3219.

(42) DePuy, C. H.; Bierbaum, V. M.; Flippin, L. A.; Grabowski, J. J.; King, G. K.; Schmitt,

R. J.; Sullivan, S. A. *J. Am. Chem. Soc.* **1980**, *102* (15), 5012–5015.

(43) Kirsch, P. In *Modern Fluoroorganic Chemistry: Synthesis, Reactivity, Applications*; Wiley-VCH Verlag GmbH & Co. KGaA: Weinheim, Germany, 2013; p 8.

(44) Matyjaszewski, K.; Miller, P. J.; Shukla, N.; Immaraporn, B.; Gelman, A.; Luokala, B. B.; Siclovan, T. M.; Kickelbick, G.; Vallant, T.; Hoffmann, H.; Pakula, T. *Macromolecules* **1999**, *32* (26), 8716–8724.

(45) Clauset, A.; Shalizi, C. R.; Newman, M. E. J. *SIAM Rev.* **2009**, *51* (4), 661–703.

(46) Turgman-Cohen, S.; Genzer, J. *Macromolecules* **2010**, *43* (22), 9567–9577.

(47) Mastan, E.; Zhou, D.; Zhu, S. *J. Polym. Sci. Part A Polym. Chem.* **2014**, *52* (5), 639–651.

(48) Wang, J.; Matyjaszewski, K. *Macromolecules* **1995**, *28*, 7572–7573.

(49) Jeyaprakash, J. D.; Samuel, S.; Dhamodharan, R.; Rühe, J. *Macromol. Rapid Commun.* **2002**, *23* (4), 277–281.

(50) Liu, Y.; Klep, V.; Zdyrko, B.; Luzinov, I. *Langmuir* **2004**, *20* (16), 6710–6718.

(51) Braunecker, W. A.; Matyjaszewski, K. *Prog. Polym. Sci.* **2007**, *32* (1), 93–146.

(52) Schellekens, M. A. J.; de Wit, F.; Klumperman, B. *Macromolecules* **2001**, *34* (23), 7961–7966.

(53) Cowie, J. M. G.; Mohsin, M. A.; McEwen, I. J. *Polymer* . **1987**, *28* (February), 1569–1572.

(54) Brandrup, J.; Immergut, E. H.; Grulke, E. A. *Polymer handbook*, 4th ed.; New York, 2003.

(55) Sigma Aldrich http://www.sigmaaldrich.com/chemistry/solvents/tetrahydrofuran-center.html (accessed Oct 9, 2014).

(56) Sigma Aldrich http://www.sigmaaldrich.com/chemistry/solvents/toluene-center.html (accessed Oct 9, 2014).

(57) Hiemenz, P. C.; Lodge, T. P. *Polymer chemistry*, 2nd Editio.; Taylor & Francis: Boca Raton, FL, USA, 2007, 2007.

(58) Schulz–Zimm distribution http://goldbook.iupac.org/S05502.html (accessed Oct 9, 2014).

(59) Most probable distribution (in macromolecular assemblies) http://goldbook.iupac.org/M04035.html (accessed Oct 9, 2014).

(60) Grulke, E. A. *Polymer process engineering*; TPS Publishing Company: Lexington, KY, USA, 1994.

(61) Smith, W. B.; May, J. A.; Kim, C. W. *J. Polym. Sci. Part A-2* **1966**, *4*, 365–374.

(62) Odian, G. *Principles of polymerization*; John Wiley & Sons: Hoboken, NJ, USA, 2004.

(63) Painter, P. C.; Coleman, M. M. *Essentials of polymer science and engineering*; DEStec publications: Lancaster, PA, USA, 2009.

(64) Hollander, M.; Wolfe, D. A. *Nonparametric statistical methods*; Wiley-VCH Verlag GmbH & Co. KGaA: Chicester, UK, 1999.

(65) Greenwood, P. E.; Nikulin, M. S. *A guide to chi-squared testing*; Wiley-VCH Verlag GmbH & Co. KGaA: New York, 1996.

4. Studying the Kinetics of Degrafting Polymer Brushes

4.1 Introduction

Surface tethered (or grafted) polymer chains form an important class of materials for surface modification. Visually, they appear like polymer films but the chemical attachment to the underlying substrate imparts novel behavior such as swelling/deswelling or stability in various solvents.[1,2] The distance between the attachments points of the chains on the surface, which is a measure of the surface grafting density, dictates the conformation of polymeric grafts. When the distance between neighboring chains is sufficiently small the chains interact, stretch, and form structures referred to as "brush", as opposed to "mushroom" where the distance between the chains on the surface is larger than the dimension of the polymer and there are no inter-chain contacts (**Figure 4.1**). The unique properties of grafted polymer systems are utilized in applications such as creating stimuli responsive surfaces[3–5], anti-biofouling coatings[6–8], controlled lubrication/adhesion[9–13] and patterned surfaces[14–17].

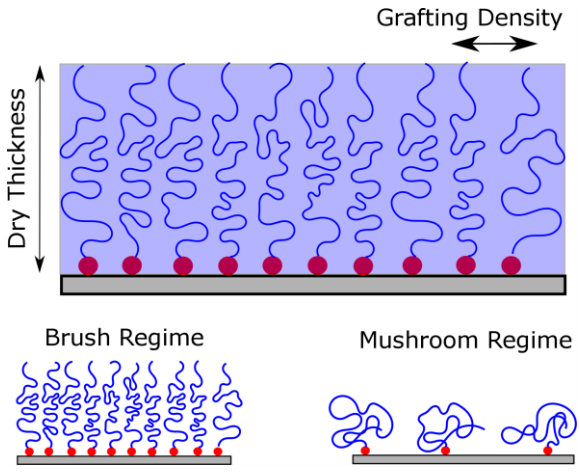

Figure 4.1. Schematic of a polymer brush indicating the key parameters - dry thickness and grafting density. The difference between "brush" and "mushroom" regime is also displayed.

Determination of the properties of a grafted polymer system by "degrafting" is crucial and forms the basis of this PhD Thesis. We have demonstrated in Chapter 3, that tetrabutyl ammonium fluoride (TBAF) is a versatile and effective reagent for degrafting and further study of polymer brush properties.[18,19] However, the process of degrafting polymer chains from the substrate is not yet completely understood. We endeavor to understand the mechanism of degrafting polymeric grafts by studying how the rate of degrafting is affected by the initial grafting density of the grafted system on the substrate, TBAF concentration in solution, and the temperature of the TBAF solution.

We have focused primarily on a simple model system of grafted poly(methyl methacrylate) (PMMA) in the brush regime. These brushes are grown on flat silicon substrates with a thin layer of silica present on top of the silicon support using a well-established atom transfer radical polymerization (ATRP) protocol.[20–23] The idea behind this study is that the dry thickness of the brush, which is related to the grafting density, is representative of the "amount" *i.e.* concentration in a chemical reaction. For a typical chemical reaction, we monitor the concentration of species as a function of time. Using this, we can deduce information such as the rate constants and the order of the reaction. In a similar manner, we intend to study the degrafting process by observing the change in grafting density as a function of time. The effect of concentration of TBAF and the initial grafting density of the system is varied systematically. The various rate constants derived for such an analysis are put forward to explain the degrafting of PMMA brushes from silica surfaces.

We first study the effect of the initial grafting density and TBAF concentration (C_{TBAF}) on the rate of degrafting. In that respect, we utilize an orthogonal gradient approach, to carry out the experiments in an effective manner, and to study a wide range of parameters on a single sample. In the orthogonal approach, we first form a uniform layer of PMMA brush on the substrate. We then immerse the sample vertically into the TBAF solution at a steady rate to form a grafting density gradient of PMMA brushes in one direction. The same is then rotated 90 degrees so that a second degrafting in TBAF solution takes place in solutions on various TBAF concentrations. The set up enables determining the effect of the initial grafting density of PMMA brushes on degrafting kinetics. The degrafting is monitored by measuring grafting density, which is inferred from the dry thickness measured by ellipsometry. Using Equation (4.1) and assuming an initial grafting density of 0.5 chains/nm^2 for dense brushes,[19] the grafting density for every dry thickness is calculated:

$$\sigma_P = \frac{h_P \rho N_A}{M_n} \tag{4.1}$$

where σ_P is the grafting density of the polymer chains, h_P is the dry thickness, N_A is the Avogadro's number, ρ is the bulk density and M_n is the number average molecular weight. While carrying out this study, in most cases we will keep the initial h_P and hence the M_n constant for consistency and vary σ_P by degrafting.

In an attempt to investigate the mechanism of brush degrafting, at the base of the polymer/initiator region, the change in the grafting density is modeled using a *series reaction*. The reason for considering a series reaction is the nature of the attachment of the organosilane bonds present at the base of the polymer brush. TBAF has a tendency to form Si-F bonds which

will occur by breaking the Si-O links. As shown in **Figure 4.2** the chlorosilane based initiator could attach by all three points to the surface (at the extreme), or it can form an in-plane network featuring Si-O-Si silanes that further stabilizes the attachment of the silanes to the substrate. The latter may be formed by condensation reaction among neighboring silane molecules once they attach to the surface (or even before they attach to the substrate). Generally, the degrafting characteristics depends on the type of attachment of the initiator to the substrate. Investigating stability of the brushes on surface (or model silane compounds) may provide additional information about the nature of tri-functional silane attachment to the substrate, which is not known. When degrafting takes place, up to three bonds break; there are possibly multiple steps involved in degrafting the chains, depending on the original structure of the silane self-assembled layer. We model this complex set of reactions as a two-step process. In the first step, we consider breaking all but one bonds that hold the silane to the substrate. In the second step, we consider the breakage of the last remaining bond that liberates the chain from the substrate. For orthogonal gradient experiments, we keep the temperature constant at 40 °C, vary C_{TBAF} and study *shorter* incubation times (~100 mins).

We further take into account the effect of temperature by carrying out the degrafting at three different temperatures of TBAF solutions. We carry out these experiments on discrete but uniform samples of PMMA brush layer to obtain the dependence of the brush thickness as a function of time, degrafting reaction temperature, and the concentration of TBAF in solution. For discrete degrafting experiments, we vary C_{TBAF} and temperatures with *longer* incubation times (~24 hours).

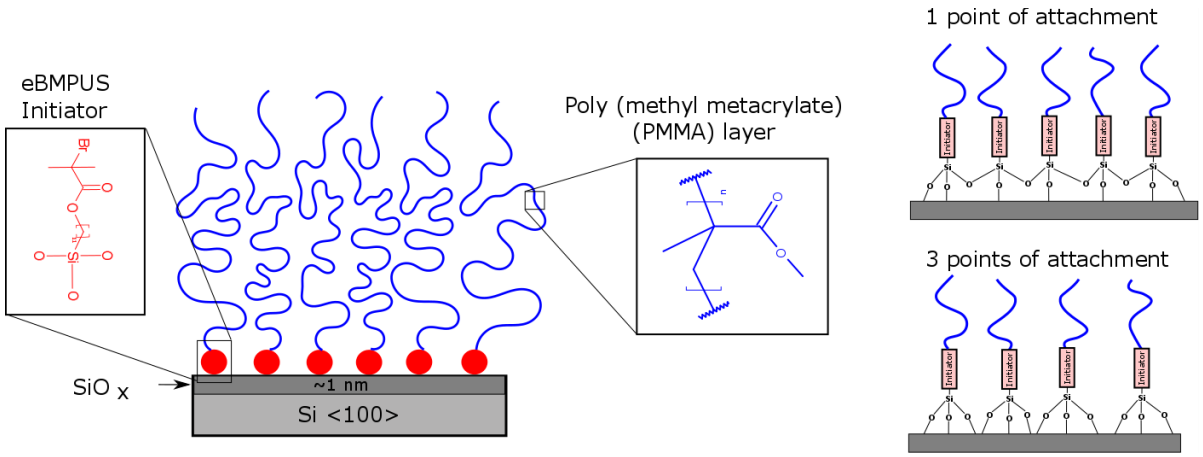

Figure 4.2. A schematic of the system under study. The polymer brush used is poly(methyl methacrylate) (PMMA), which is grown from eBMPUS initiator centers using ATRP. The right portion shows two of the possible extremes of how the chlorosilane based initiator is attached to the silica substrate by either 1 point or 3 points (at the extreme) to the surface.

4.2 Experimental details

All chemicals were purchased from Sigma Aldrich and used unless specified otherwise. Methyl methacrylate (MMA) was passed through a column of inhibitor remover to remove monomethyl ether hydroquinone. Copper (II) chloride was further purified by dissolution in ethanol followed by precipitation in hexanes. Silicon wafers (p-doped, orientation <100>) obtained from Silicon Valley Microelectronics (SVM) were used as flat substrates for all experiments. TBAF was purchased as a 1 M solution in THF but was diluted using ACS grade THF (Sigma-Aldrich) to obtain the solution of a desired concentration.

Initiator deposition and polymer brush growth

The procedure established earlier[24] was used to deposit surface initiator, (11-(2-bromo-2-methyl)propionyloxy undecyltrichlorosilane (eBMPUS). The surfaces were cleaned and activated using ultraviolet-ozone (UVO) treatment prior to initiator deposition. For large substrates (4.2 cm x 4.2 cm) the deposition was carried out in the custom setup[19] where two samples were placed back-to-back in eBMPUS solution, capped with argon, sealed, and placed in freezer at -18°C for 24 hours. PMMA brushes were synthesized using ATRP for a catalyst ratios, $CuCl_2$/CuCl ($Cu^{(II)}/Cu^{(I)}$) = 0.05 by grafting from polymerization following earlier procedure.[19] The polymerization time was 24 hours which gave a dry (ellipsometric) thickness of ~100 nm.

TBAF degrafting and making gradients by dipping method

For the initial kinetics experiments, uniform samples of PMMA brush layer from a mother sample (1 cm x 8 cm) were divided into 8 equal parts (1 cm x 1 cm). The samples were incubated individually for different times in the TBAF solution of a given concentration. This gave us discrete but uniformly degrafted samples of various grafting densities. A continuous gradient in grafting density was prepared by the dipping method. It was carried out in a custom Plexiglass box that was saturated with THF vapors, with the dipping and heating setup placed inside the box. For the orthogonal gradient samples, the conditions for the first dipping were kept consistent across all samples. These condition used were 0.1 M TBAF solution at 40 °C; the dipping rate was 0.4 mm/min with a total dipping time of 100 mins and a total length dipped

of 40 mm. The second degrafting was carried by rotating the sample 90 degrees relative to the first dipping direction to get an orthogonal gradient. TBAF concentrations of 0.01, 0.05, 0.1 and 0.3 M were used.

Characterization

The dry thickness of the polymer layer on the surface was measured using spectroscopic ellipsometry (VASE, J.A. Woollam Co. Inc.) with 3 angles of incidence (65, 70, and 75°) and measurements at 5 spots for each large sample (4.2 cm x 4.2 cm) before degrafting. After degrafting and making the gradient, the measurement was carried out in a grid fashion with measurement points spaced at 3-5 mm in each *x* and *y* direction. The ellipsometric data obtained for the polymer brush film were modeled using a 3-layer model with silicon substrate at the bottom, intermediate silica (SiO_x) layer in the middle, and a polymer 'Cauchy' layer on the top, to obtain dry film thickness of the polymer film. Since the geometry of the sample and the dipping rate is known, the incubation time can be related to the position on the sample.

4.3 Results and Discussion

4.3.1 Relation between grafting density and dry thickness

The removal of polymer chain from the substrate during the degrafting process is a result of a chemical reaction, which takes place in the vicinity of the polymer chain attachment to the silicon substrate at the Si-O bond. We know from Chapter 3, that the majority of the grafted polymeric material is removed during the degrafting process, which exposes the degrafted silica substrate.[19] The σ_P refers to the number of chains attached per unit area. As mentioned earlier, we think of σ_P as an analogue to concentration of a reactant in a chemical reaction. If we keep the initial thickness of the brush constant for a given experiment, we can then assume, based on Equation (4.1), that the dry thickness (h_P) is directly proportional to the grafting density (σ_P). This means that a gradient in h_P would result in a gradient in σ_P with constant M_n. Based on earlier results we can assume that the grafting density for PMMA brushes synthesized by ATRP on eBMPUS initiator is a constant value of 0.5 chains/nm^2.[18,19] Assuming that σ_P is the same for all our samples, the $\sigma_P(t)$, *i.e.*, σ_P as a function of time, can be obtained from the time dependence of h_P, *i.e.*, $h_P(t)$. In the subsequent sections we will look at $\sigma_P(t)$ to explore the degrafting process.

4.3.2 Orthogonal gradient experiments

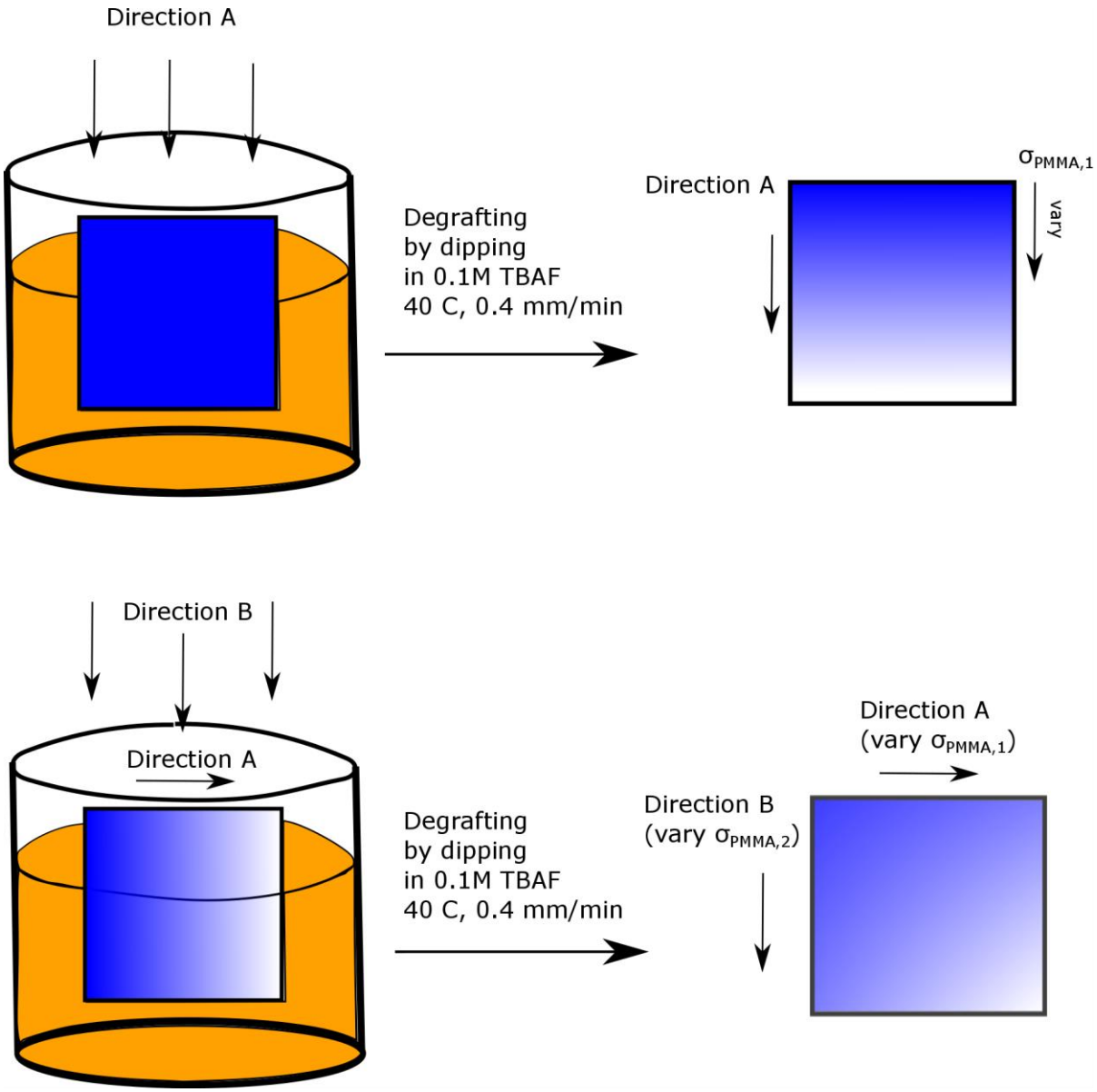

Figure 4.3. Schematic for making an orthogonal gradient in grafting density (σ_P). Directions A and B corresponds to variation in $\sigma_{PMMA,1}$ and $\sigma_{PMMA,2}$ respectively.

Figure 4.3 depicts a scheme detailing the steps leading to the formation of a sample for studying degrafting using the orthogonal gradient approach. The sample was created in two steps by the dipping method. In the first step, we take a sample featuring a homogeneous PMMA brush and dip it vertically into the TBAF solution. In the second step the sample was rotated by 90 deg (*cf.* **Figure 4.3**) and the dipping was carried out into solutions of various TBAF concentrations. For all the orthogonal gradient experiments, we kept the incubation temperature in TBAF constant at 40 °C, and the dipping rate was 0.4 mm/min. The total dipping time was 100 mins, which translates to a distance of 40 mm along the substrate. We refer to this length of time as *short*, in comparison to later described discrete degrafting data, wherein the incubation time is much longer (~24 hours). The C_{TBAF} for the first dipping step was kept constant at 0.1 M in THF, while it was varied from 0.01 M to 0.3 M for the second dipping step. We denote the initial value of grafting density as $\sigma_{PMMA,0}$ (=0.5 chains/nm^2). The grafting density for gradient obtained after the first dipping process (direction A) is denoted as $\sigma_{PMMA,1}$ while that for the second degrafting (direction B) is denoted as $\sigma_{PMMA,2}$.

The effect of grafting density on degrafting can be seen in **Figure 4.4** where the final grafting density ($\sigma_{PMMA,2}$) is plotted as a function of initial (after 1st dipping) grafting density ($\sigma_{PMMA,1}$). This particular data set refers to the second gradient by dipping into a solution having C_{TBAF} = 0.1 M. The dotted line ($\sigma_{PMMA,2} = \sigma_{PMMA,1}$) indicates the hypothetical case when 'no degrafting' takes place (zero incubation time). The farther we go below this dotted line, the more degrafting has taken place in absolute amount since $\sigma_{PMMA,2}$ will be lower. The colors indicate five different incubation times ranging from 0.5 to 70 minutes. The extent of

degrafting increases with increasing the incubation time. For a given incubation time, the extent of degrafting increases with increasing $\sigma_{PMMA,1}$. This is denoted, for the 70 mins incubation time (olive), by the difference between the dotted line (no degrafting) and the actual data, represented as red arrows. We concur that the rate of degrafting is greater at higher initial grafting density ($\sigma_{PMMA,1}$). Here the inter-chain interactions that cause the chain to stretch outwards cause bond tension that is higher at high $\sigma_{PMMA,1}$.

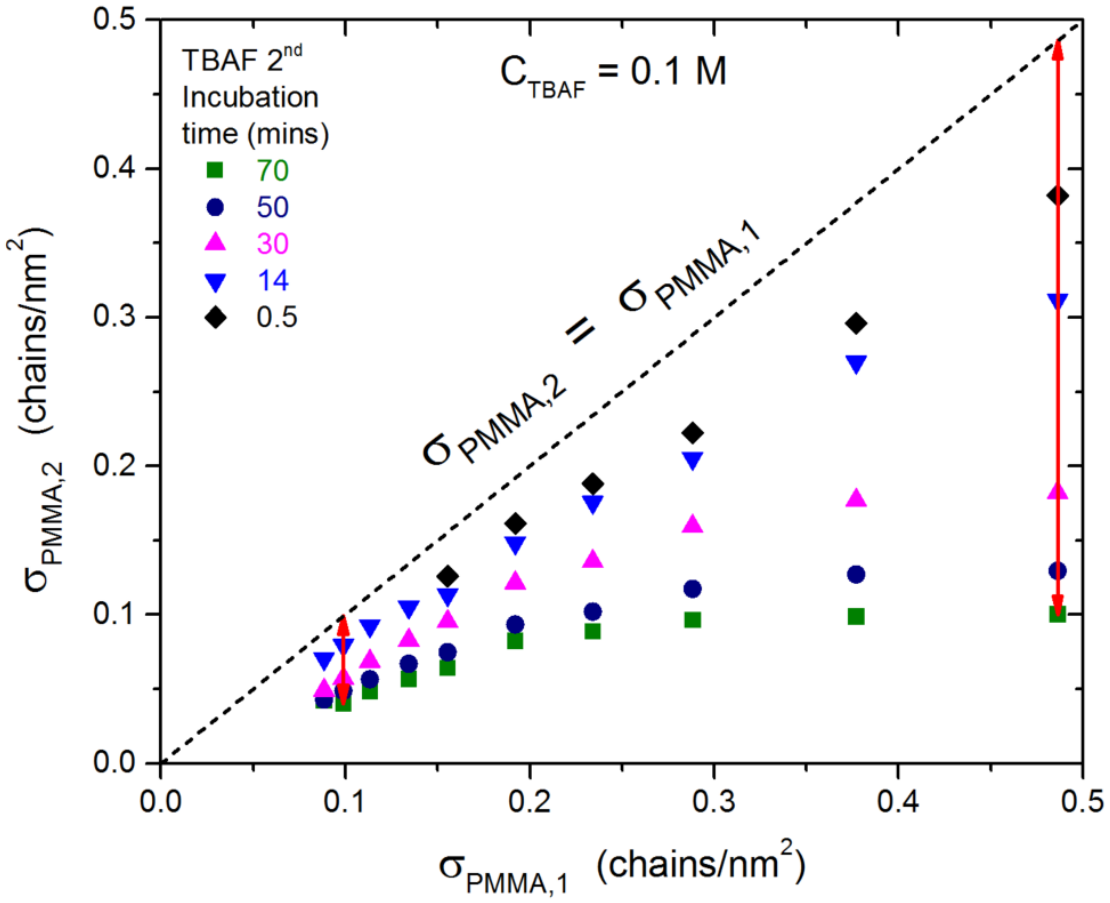

Figure 4.4. Final grafting density ($\sigma_{PMMA,2}$) as a function of initial grafting density ($\sigma_{PMMA,1}$) on an orthogonal gradient sample for 5 different incubation times ranging from 0.5 to 70 minutes. Both the first and second dipping were carried out in C_{TBAF} = 0.1 M. The length of the vertical red arrows is a measure of the extent of degrafting for incubation time of 70 mins (olive) at $\sigma_{PMMA,1}$ = 0.099 and 0.486 chains/nm^2.

4.3.3 Series reaction hypothesis

We hypothesize that the degrafting process of PMMA brushes can be explained by a *series reaction* represented in **Figure 4.5**. The various species in the reaction are denoted simply as A, A* and B. Here species A represents an ensemble of species comprising the initial state of the system and partially degrafted polymer chains. It essentially denotes all the polymer chains which are attached by more than one Si-O bond either directly to the substrate or to the substrate and the neighboring chains on the surface (*i.e.*, Si-O-Si in plane network). The species A* represents a moiety that is attached to the substrate by only one attachment point. Species B represents fully degrafted polymer chains with no attachment to the surface. The units for A, A* and B are same as that of the grafting density (*i.e.*, chains/nm^2).

We assume that the individual reactions are first order in nature. Moreover, we do not account for the effect of C_{TBAF} on the reaction. For a given orthogonal gradient sample, C_{TBAF} is kept constant; hence we assume a pseudo-first order reaction in C_{TBAF}. The effect of C_{TBAF} may be included in the rate constants as discussed later. We want to emphasize that individual values of A and A* cannot be measured separately because we do not know that number of Si-O linkages in the as prepared samples. However, the sum $A + A^*$ is represented by the instantaneous value of grafting density (σ_P) which is obtained by measuring dry ellipsometric thickness. The σ_P does not change when A is converted to A* (*i.e.*, no material removal from the substrate); this results in an initial slow decrease in the σ_P, and latter exponential-like decay.

$$A + T \xrightarrow{k_1} A^* + X$$

$$A^* + T \xrightarrow{k_2} B + X$$

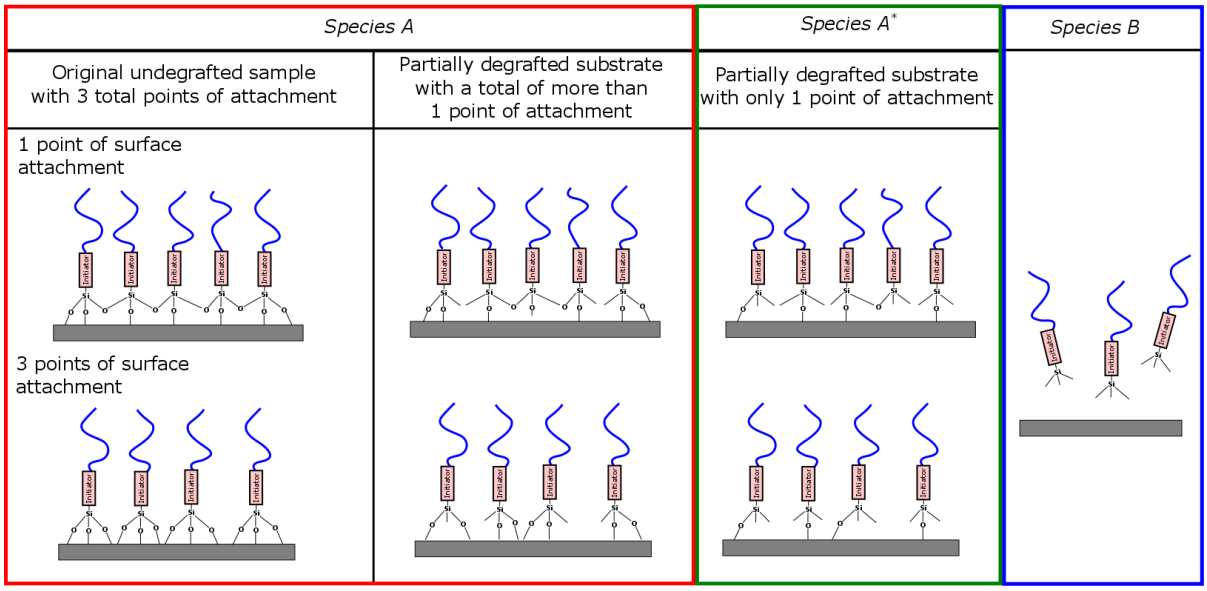

Figure 4.5. Degrafting mechanism represented as a series reaction. The species A, A* and B are color coded and represented in the below the reaction. T represents TBAF and X is an intermediate reactant that is formed during the reaction.

The rate of consumption of species *A* can be represented as follows

$$\frac{dA}{dt} = -k_1 A \tag{4.2}$$

In Eq. (4.2) t represents time in minutes and k_1 is the rate constant (min^{-1}). The rate equation for A* can be written as

$$\frac{dA^*}{dt} = k_1 A - k_2 A^* \tag{4.3}$$

Where k_2 is the rate constant for A* going to B. The equations can be solved analytically to obtain the following expressions

$$A = A_0 e^{-k_1 t} \tag{4.4}$$

$$A^* = A_0 \left(\frac{k_1}{k_2 - k_1}\right)[e^{-k_1 t} - e^{-k_2 t}] \tag{4.5}$$

Where A_0 = σ_0 = 0.5 chains/nm^2 is the initial concentrations of species A. The initial concentrations of A* and B are assumed to be zero. Here the conversion from A to A* does not cause any change in the thickness because the polymer does not leave the surface, hence there is no change in the apparent grafting density. The set of reactions leading to formation of A* can be called as *pre-degrafting reactions* since they do not result into the polymer chain leaving the substrate. The reaction going from A* to B, however, denotes the true degrafting process, where the change in σ_P can be observed experimentally. The measured σ_P accounts for the total of A and A* together. Hence we can write the following expression for σ_P.

$$\sigma_P = A + A^* \tag{4.6}$$

We now have an expression for σ_P as a function of time where σ_0 is initial grafting density shown as Equation (4.7).

$$\sigma_P = \sigma_0 \left[e^{-k_1 t} + \frac{k_1}{k_2 - k_1}[e^{-k_1 t} - e^{-k_2 t}]\right] \tag{4.7}$$

The series reaction is used to fit data for the orthogonal gradient data from Section 4.3.2. The $\sigma_{PMMA,2}$ data for 5 different initial grafting densities ($\sigma_{PMMA,1}$) and the corresponding fits (solid lines) to series reaction are shown in **Figure 4.6**. Here the set of data represents C_{TBAF} of 0.1 M for second dipping. In **Figure 4.6** we observe clearly two main regions, an initial plateau and a latter faster decay. The presence of this plateau denotes a *delay* in the degrafting process in the initial stages and it validates our *series reaction* approach.

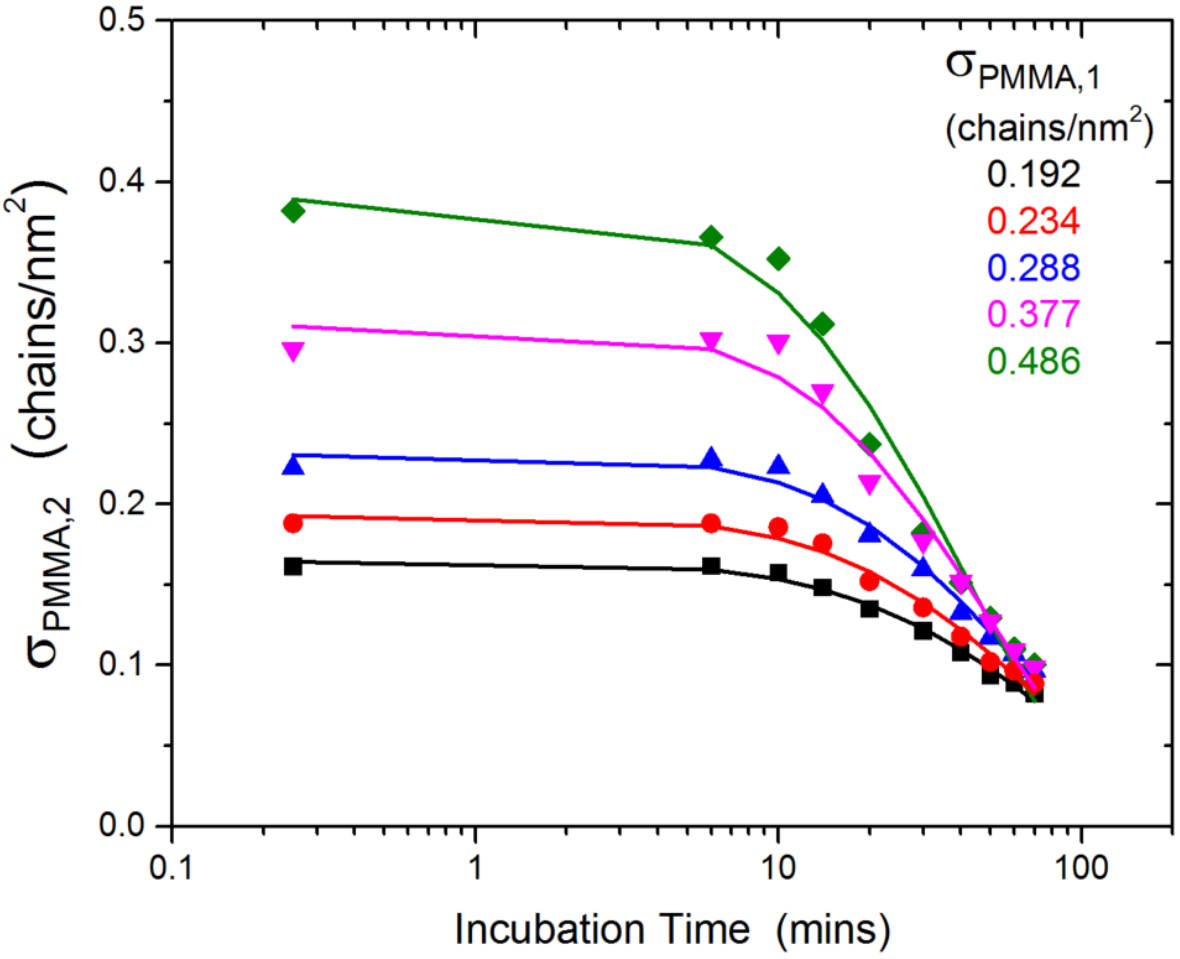

Figure 4.6. Final grafting density ($\sigma_{PMMA,2}$) as a function of incubation time for five different initial grafting density ($\sigma_{PMMA,1}$) in an orthogonal gradient sample. The corresponding series reaction fits are shown as solid lines.

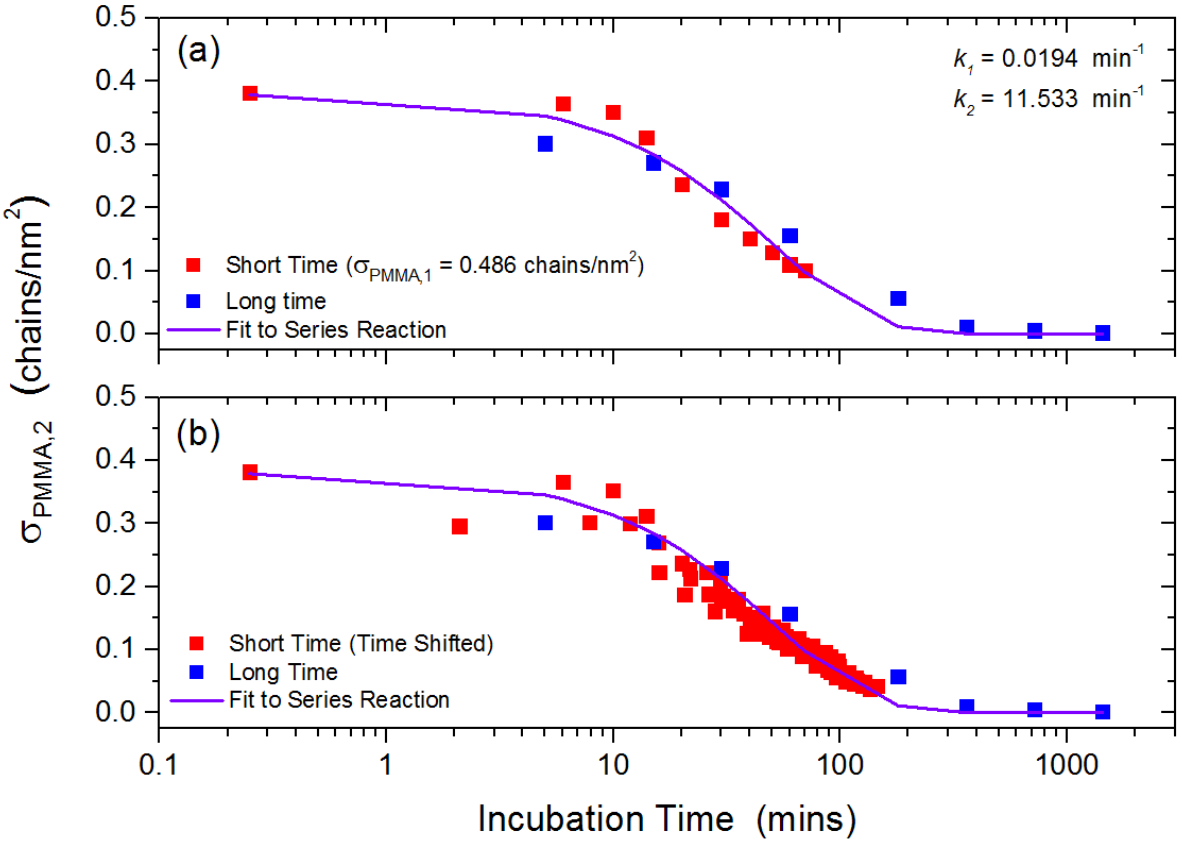

Figure 4.7. (a) Final grating density ($\sigma_{PMMA,2}$) data from the short time data (red) of highest initial grafting density ($\sigma_{PMMA,1}$ = 0.486 chains/nm^2) from **Figure 4.6**, long time data (blue) obtained by degrafting discrete samples and corresponding series reaction fit (violet, solid line). (b) The time shifted data for the orthogonal gradient sample for various $\sigma_{PMMA,1}$ is overlaid on the data in the above plot.

In the **Figure 4.7(a)**, we plot $\sigma_{PMMA,2}$ from the short time degrafting data (red) of highest initial grafting density ($\sigma_{PMMA,1}$ = 0.486 chains/nm^2) from **Figure 4.6** and the long time degrafting data (blue) obtained by degrafting discrete samples. The corresponding fit to the series of two reactions is also displayed (violet) along with the reaction constants k_1 and k_2. In **Figure 4.7** we observe the initial plateau region, followed by the exponential-like decay behavior. We assume that $k_2 >> k_1$, *i.e.*, the first reaction (A converting to A*) is slower than the conversion of A* into B. Thus the former reaction is the rate limiting/controlling step in this overall process. In **Figure 4.7b** we plot the *time-shifted data* for different $\sigma_{PMMA,1}$. When a PMMA brush is subjected to TBAF for a given amount of time ($t = t_1 + t_2$), there is a corresponding decrease in the thickness and grafting density. This decrease is the same as when the sample is incubated for shorter times (t_1 and t_2), which independently add up to the same total time (t). The shift factors are derived by interpolation from the '$\sigma_{PMMA,2}$ vs time' data for the highest initial grafting density ($\sigma_{PMMA,1}$) hence the data collapse on the master curve.

Our initial hypothesis for the series reaction assumed first order dependence on the grafting density (in terms of species A and A*) did not take the effect of C_{TBAF} into account. In **Figure 4.8**, we look a k_1 as a function of initial grafting density ($\sigma_{PMMA,1}$) for 4 different C_{TBAF}. There is a weak dependence on both; here k_1 increases with increasing $\sigma_{PMMA,1}$ and C_{TBAF}. The solid horizontal lines in **Figure 4.8** denote the k_1 obtained by global fit, *i.e.*, a single value for the entire orthogonal gradient sample (single C_{TBAF}) and with no dependence on $\sigma_{PMMA,1}$. The global value of k_1 does increases systematically with the increase in C_{TBAF} which could indicate that it incorporates the effect of C_{TBAF}.

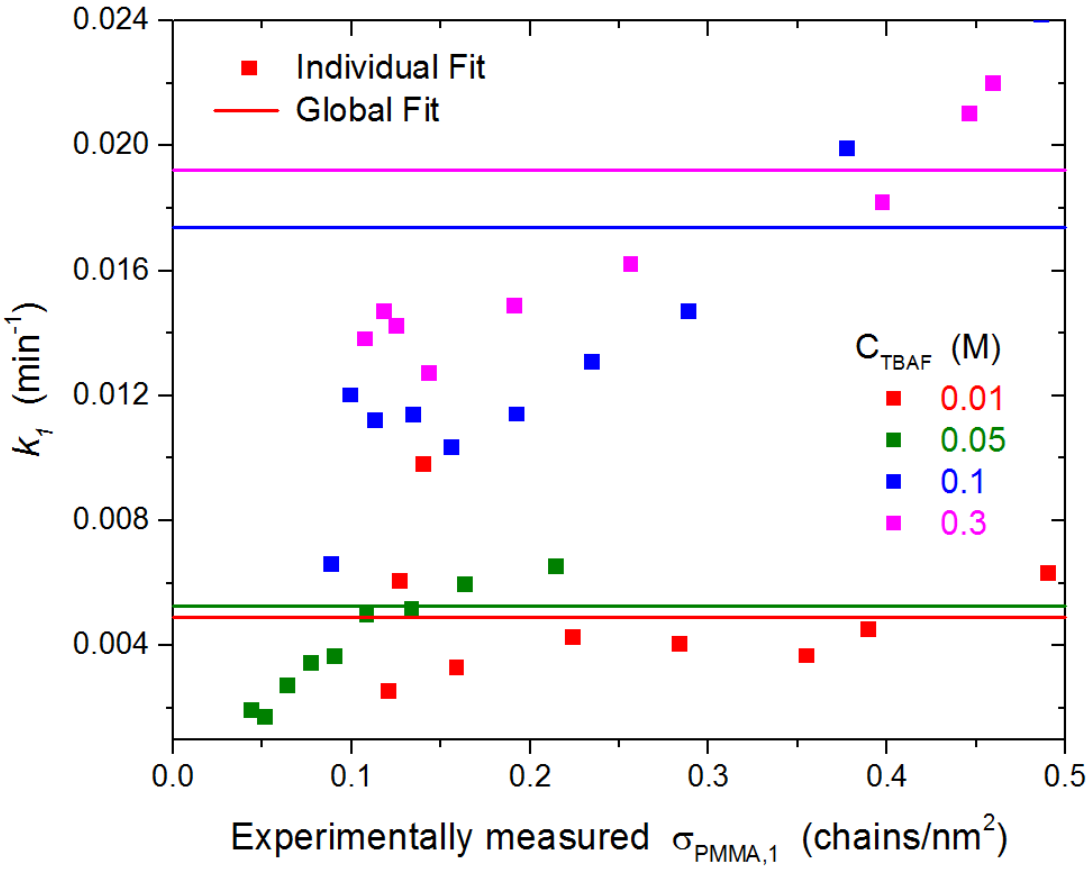

Figure 4.8. Series reaction rate constant k_1 as a function of initial grafting density ($\sigma_{PMMA,1}$) for four different C_{TBAF}. The solid horizontal lines show the k_1 obtained by global fit for each of the four C_{TBAF}.

The global fit values of k_1 and k_2 are plotted in **Figure 4.9**. The value k_2 does not show any trends with either C_{TBAF} or $\sigma_{PMMA,1}$ and we obtain an average value of 1.249±0.93 min^{-1}. If k_1 is plotted linearly as a function C_{TBAF}, the slope gives a value of 0.0762 min^{-1}, setting y-intercept to zero. Assuming first order dependence on C_{TBAF}, we can write the corrected equation for k_1 as

$$k_1 = 0.0762 C_{TBAF}\ min^{-1} \tag{4.8}$$

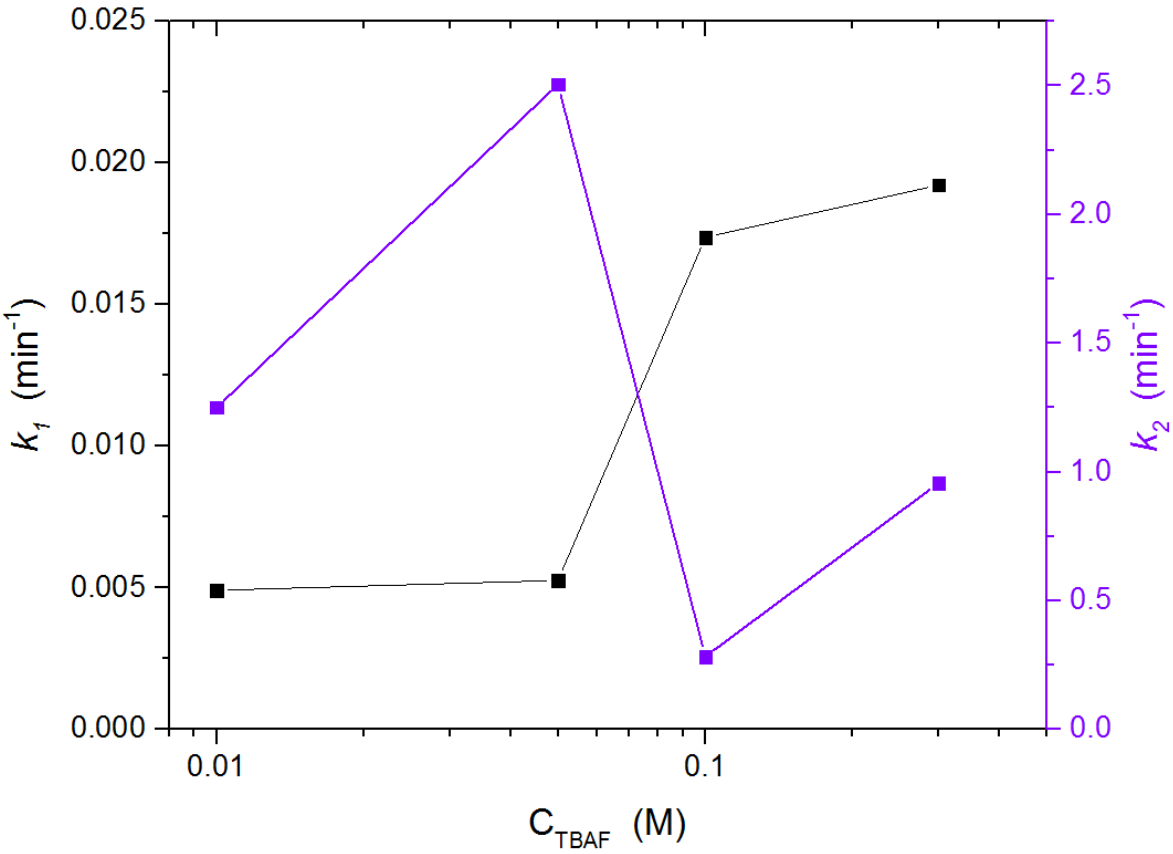

Figure 4.9. The series reaction rate constants k_1 and k_2, obtained by global fit, as a function of C_{TBAF}.

4.3.4 Effect of TBAF concentration and incubation temperature on degrafting

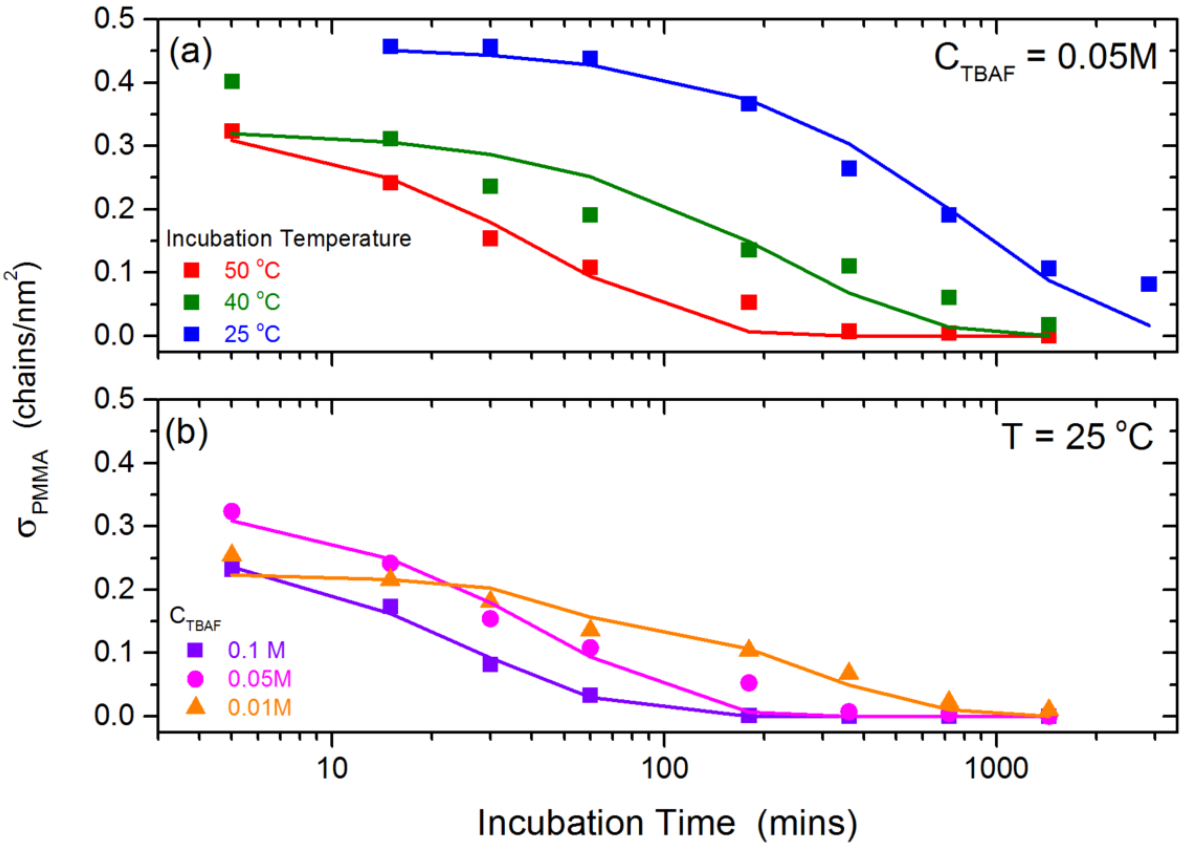

Figure 4.10. The grafting density as a function of incubation time for (a) three different incubation temperatures and (b) three C_{TBAF} for longer times, discrete degrafting, with initial h_P = 120 nm. The solid lines indicate corresponding fits to series reaction.

Figure 4.10 plots the discrete degrafting data for longer times carried out for PMMA brush layer with initial dry thickness of 120 nm. The incubation temperature has a noticeable effect on the rate of degrafting, as expected for a chemical reaction. The σ_{PMMA} decreases faster for higher temperatures. The effect of concentration, however, is weaker in comparison to that of temperature, and is observable only at longer incubation times. The decrease in σ_{PMMA} is slower

for small values of C_{TBAF} (orange). In all cases, we tend to converge at the asymptotic value on the time axis.

4.3.5 Degrafting of other systems

When PMMA or similar neutral polymer brush systems, *i.e.*, polystyrene (PS) or poly(tert-butyl methacrylate) (PtBMA), that are soluble in THF are subjected to TBAF, they exhibit an exponential-like decay in thickness; the rate of degrafting increases with increasing incubation temperature. However, some polymer brush systems, *i.e.*, poly(methacrylic acid) (PMAA), when subjected to TBAF solution exhibit an initial increase in the dry thickness followed by a decrease similar to an exponential-like decay (*cf.* **Figure 4.11**). Such an initial increase is not observed in PtBMA brushes (similar to PMMA), from which the PMAA brushes are made by hydrolysis. This could indicate that TBAF could associate and form a complex with the PMAA (a weak polyacid). Formation of this complex would increase the apparent thickness of the system due to association and increase in the sample volume. Concurrently, the degrafting also progresses since the thickness decreases eventually (albeit at a slower rate). The initial increase is prominent at a lower temperature of 25 °C since the rate of degrafting at this temperature is relatively slow. With increasing temperature, the rate of degrafting increases, while there is little or no increase in the association. The initial increase in thickness, due to association, becomes less significant as the incubation temperature is increased, because degrafting dominates with increasing temperature. The PMAA system represents an interesting example of the competing effects of complex formation (leading to increasing the thickness) and

degrafting (which reduces the thickness). The complex formation and the resulting thickness increase is a weaker function of temperature while the degrafting rate increases significantly with rise in temperature.

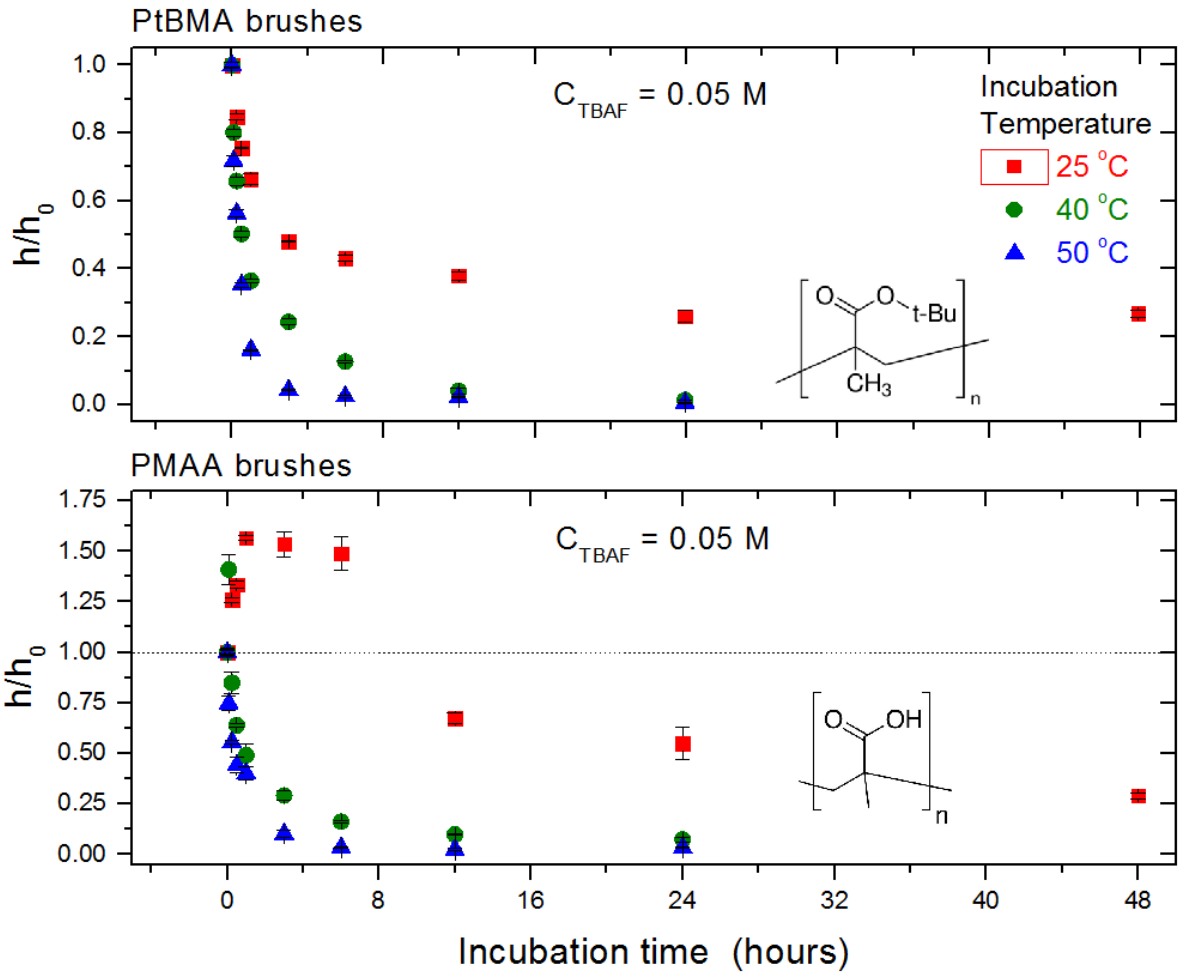

Figure 4.11. Normalized dry ellipsometric thickness as a function of incubation time for (a) poly(t-butyl methacrylate) (PtBMA) and (b) poly(methacrylic acid) (PMAA) when incubated in 0.05 M TBAF solution at 25, 40 and 50 °C.

4.4 Conclusions

We have presented a simple method aiming to comprehend the process of degrafting of polymer grafts from silica substrates using an analogy with conventional reaction kinetics. The rate of degrafting of PMMA brushes by TBAF is a strong function of the initial grafting density of the polymer brush; it also depends on the TBAF incubation time, TBAF concentration in solution, and temperature. The trends in the grafting density can be explained by invoking a simple model comprising a series reactions with first order dependence in the instantaneous grafting density. The dependence on concentration of TBAF is significantly weaker, and was deducted to be pseudo first order in nature. The pre-degrafting reactions, which break the initial set of bonds without degrafting represent the rate limiting process, while the actual degrafting of polymer chains (*i.e.*, cleaving the last existing Si-O bond) is relatively fast. Studying other polymer brush systems, like that of PMAA, could help us understand competing effects, such as complex formation *vs.* degrafting, on the thickness of polymer brushes.

4.5 Acknowledgement

We thank Dr. Balaji Rao (NC State) for his insights into understanding reaction kinetics and degrafting mechanisms. The work was supported by the National Science Foundation (Grant no. DMR-1404639) and the Army Research Office under their Staff Research Program (Grant no. W911NF-04-D- 0003-0016).

4.6 References

(1) Milner, S. T. *Science* **1991**, *251* (4996), 905–914.

(2) Zhao, B.; Brittain, W. J. *Prog. Polym. Sci.* **2000**, *25*, 677–710.

(3) Luzinov, I.; Minko, S.; Tsukruk, V. V. *Prog. Polym. Sci.* **2004**, *29* (7), 635–698.

(4) Uhlmann, P.; Merlitz, H.; Sommer, J.-U.; Stamm, M. *Macromol. Rapid Commun.* **2009**, *30* (9-10), 732–740.

(5) Cohen Stuart, M. A.; Huck, W. T. S.; Genzer, J.; Müller, M.; Ober, C.; Stamm, M.; Sukhorukov, G. B.; Szleifer, I.; Tsukruk, V. V; Urban, M.; Winnik, F.; Zauscher, S.; Luzinov, I.; Minko, S. *Nat. Mater.* **2010**, *9* (2), 101–113.

(6) Yandi, W.; Mieszkin, S.; Martin-Tanchereau, P.; Callow, M. E.; Callow, J. A.; Tyson, L.; Liedberg, B.; Ederth, T. *ACS Appl. Mater. Interfaces* **2014**, *6* (14), 11448–11458.

(7) Suriyanarayanan, S.; Lee, H.-H.; Liedberg, B.; Aastrup, T.; Nicholls, I. A. *J. Colloid Interface Sci.* **2013**, *396*, 307–315.

(8) Hoshi, Y.; Xu, Y.; Ober, C. K. *Polymer.* **2013**, *54* (7), 1762–1767.

(9) Klein, J. *Annu. Rev. Mater. Sci.* **1996**, *26*, 581–612.

(10) Kobayashi, M.; Terayama, Y.; Hosaka, N.; Kaido, M.; Suzuki, A.; Yamada, N.; Torikai, N.; Ishihara, K.; Takahara, A. *Soft Matter* **2007**, *3* (6), 740–746.

(11) Bielecki, R. M.; Crobu, M.; Spencer, N. D. *Tribol. Lett.* **2012**, *49* (1), 263–272.

(12) Bhairamadgi, N. S.; Pujari, S. P.; Trovela, F. G.; Debrassi, A.; Khamis, A. A.; Alonso, J. M.; Al Zahrani, A. a; Wennekes, T.; Al-Turaif, H. a; van Rijn, C.; Alhamed, Y. a; Zuilhof, H. *Langmuir* **2014**, *30* (20), 5829–5839.

(13) Kobayashi, M.; Terada, M.; Takahara, A. *Soft Matter* **2011**, *7* (12), 5717–5722.

(14) Chen, J.-K.; Hsieh, C.-Y.; Huang, C.-F.; Li, P.-M.; Kuo, S.-W.; Chang, F.-C. *Macromolecules* **2008**, *41* (22), 8729–8736.

(15) Chen, T.; Jordan, R.; Zauscher, S. *Soft Matter* **2011**, *7* (12), 5532–5535.

(16) Chen, T.; Amin, I.; Jordan, R. *Chem. Soc. Rev.* **2012**, *41* (8), 3280–3296.

(17) Patil, R.; Kiserow, D.; Genzer, J. *RSC Adv.* **2015**, *5* (105), 86120–86125.

(18) Patil, R. R.; Turgman-Cohen, S.; Šrogl, J.; Kiserow, D.; Genzer, J. *ACS Macro Lett.* **2015**, *4* (2), 251–254.

(19) Patil, R. R.; Turgman-Cohen, S.; Šrogl, J.; Kiserow, D.; Genzer, J. *Langmuir* **2015**, *31* (8), 2372–2381.

(20) Shah, R. R.; Merreceyes, D.; Husemann, M.; Rees, I.; Abbott, N. L.; Hawker, C. J.; Hedrick, J. L. *Macromolecules* **2000**, *33* (2), 597–605.

(21) Huang, X.; Wirth, M. J. *Anal. Chem.* **1997**, *69* (22), 4577–4580.

(22) Ejaz, M.; Yamamoto, S.; Ohno, K.; Tsujii, Y.; Fukuda, T. *Macromolecules* **1998**, *31*, 5934–5936.

(23) Barbey, R.; Lavanant, L.; Paripovic, D.; Schüwer, N.; Sugnaux, C.; Tugulu, S.; Klok, H.-A. *Chem. Rev.* **2009**, *109* (11), 5437–5527.

(24) Matyjaszewski, K.; Miller, P. J.; Shukla, N.; Immaraporn, B.; Gelman, A.; Luokala, B. B.; Siclovan, T. M.; Kickelbick, G.; Vallant, T.; Hoffmann, H.; Pakula, T. *Macromolecules* **1999**, *32* (26), 8716–8724.

5. Surface Patterning Using Degrafting of Polymer Brushes*

5.1 Introduction

Surface grafted polymer assemblies (SGPAs) comprise polymer chains tethered to a substrate or interface.[1–3] Such systems are colloquially referred to as "polymer brushes", although the term "brush" describes correctly only a particular conformation of polymeric grafts, in which the grafted macromolecules stretch away from the substrate due to close proximity of the grafting points and excluded volume interactions. The tethered nature of the SGPAs imparts additional stability and offers the ability to control polymer conformation by changing the grafting density (σ_P), *i.e.*, the number of grafted polymer chains per unit area on the substrate. Altering the molecular weight (MW), topology and chemical composition (including sequence distribution of monomers, for the case of copolymers) enable additional fine-tuning of the brush characteristics. In addition to varying chemical composition within the individual polymer chains, some applications demand generating structures with chemical composition variation in the plane of the substrate. Creating surface patterns on thin films, specifically in regard to polymer brushes, is of immense interest due to potential applications in studying polymer brush structure[4], protein patterning[5,6], protein adsorption[7], cell adhesion[8,9], or stimuli-responsive surfaces.[10,11]

*A part this chapter contains material published as "Creating surface patterns of polymer brushes by degrafting via tetrabutyl ammonium fluoride" in the journal RSC Advances, vol. 5, pp. 86120 - 86125, 2015, © Royal Society of Chemistry.

Patterned brush surfaces are generated typically by two general methodologies. The first approach involves creating patterns of initiators on the substrate and then growing polymer brushes directly from the substrate-bound initiator centers. A pattern of an initiator layer is formed typically by using photolithographic or soft lithographic methods, *i.e.*, micro-contact printing[12]. Alternatively, the initiator arrays may feature gradients in density[13,14] or mixed monolayers featuring two different initiators.[15] The polymer brush is grown by surface-initiated (SI) polymerization, for instance via atom transfer radical polymerization (ATRP). Previous efforts include the work of Chen *et al.* on depositing patterned thiol based surface initiator on a gold substrate and growing polymer on top using SI-ATRP.[16] The patterns of initiators were generated by employing PDMS stamps[17] and self-assembled microspheres.[18] The initiator patterns were later translated into polymer brush patterns after growing polymers using ATRP from the initiator sites on the substrate. A complimentary technique involves preparing a uniform layer of initiator and deactivating part of the layer using UV light incident across a mask.[8,9] The second approach starts with a homogeneous polymer brush layer, which is subsequently patterned by: 1) chemically or physically altering the existing brushes (*e.g.* irreversibly crosslinking a patterned area using UV light[10]), 2) growing new blocks onto predefined regions on the substrate, or by selectively removing chains from the substrate (*i.e.*, by photocleaving[19]). Micrometer scale chemical gradients of quaternized poly(2-dimethylaminoethyl methacrylate) (PDMAEMA) have been prepared by Koo *et al.* by controlling the diffusion of alkylating agent through a PDMS channel.[20] Schuh *et al.* created patterns on a azo functionalized poly(methacrylic acid) brush layer by photomechanical

degrafting using interference patterns of light.[21] Wei *et al.* used a hybrid approach where the initiator pattern was deposited on top of a polymer brush layer and then a second polymer brush layer was grown, which amplified the initiator pattern.[22]

We have demonstrated recently that poly(methyl methacrylate) (PMMA) brushes can be degrafted efficiently from silicon substrates by using tetrabutyl ammonium fluoride (TBAF).[23,24] TBAF is a mild degrafting reagent, in comparison to others, such as HF[25], acids[26], bases[27] or techniques which use UV light[28], which could damage either the substrate or the polymer backbone. The kinetics and extent of degrafting can be controlled with high fidelity by tuning the incubation time, temperature, and concentration of TBAF. TBAF reacts selectively with the Si–O bonds present exclusively at the base of the initiator without affecting the backbone of the polymer. In this chapter we demonstrate that various polymer patterns can be created on the substrate by controlling the position and time for delivery of TBAF solution. The substrate can be reused to grow brushes multiple times. We also show that polystyrene brushes can be degrafted using TBAF followed by regrowing PMMA brushes. Partial degrafting and regrowing of brushes allows us to create regions with diblock copolymer and homogeneous polymer brushes on the same substrate. This technique can be extended to make patterns of monolayers as well although their degrafting characteristics are different. Silane based monolayers on silicon substrates have similar chemical attachment and vulnerability to TBAF as earlier mentioned polymer brush layers, but there is no excess bond tension to accelerate the degrafting process. Monolayer patterns are a useful tool for further surface modification and they can be created by degrafting with ease and control.

5.2 Results and discussion

5.2.1 Creating gradients of polymer brush grafting density using degrafting

Degrafting of PMMA using TBAF can be controlled by 1) adjusting the incubation time of the sample in TBAF solution, 2) varying the concentration of TBAF in solution, and 3) altering the temperature of the TBAF solution. These attributes are employed in conjunction with gradual sample exposure to TBAF solution using the dipping method to create a gradient in grafting density of polymer brushes. **Figure 5.1** shows the thickness measured over the length of sample before (blue squares) and after (red circles) dipping vertically in a degrafting TBAF solution for 2 different specimens. The bottom most part of the substrate (*i.e.* position 5 mm) has the lowest grafting density since it is incubated for the longest time in the TBAF solution and hence has undergone the highest degree of degrafting.

The σ_P and hence the corresponding dry thickness of the brush vary gradually across the sample. Such a substrate represents a true gradient in σ_P with constant polymer MW since we begin with a uniform polymer brush layer. This technique is superior to creating σ_P gradients of brushes by a "conventional method"[29] based on depositing an inert silane layer using diffusion and then backfilling the substrate with an initiator. In the conventional method, the polymer brush at different locations on the substrate grows under different degree of confinement, which may cause differences in the MW and PDI of the chains.[30] The dipping method also offers creating a desired σ_P gradient profile of the grafted polymer on the substrate by simply programming the dipping rate that corresponds to the desired profile. The ease of control is the key to having precision over the degrafting rate by TBAF.

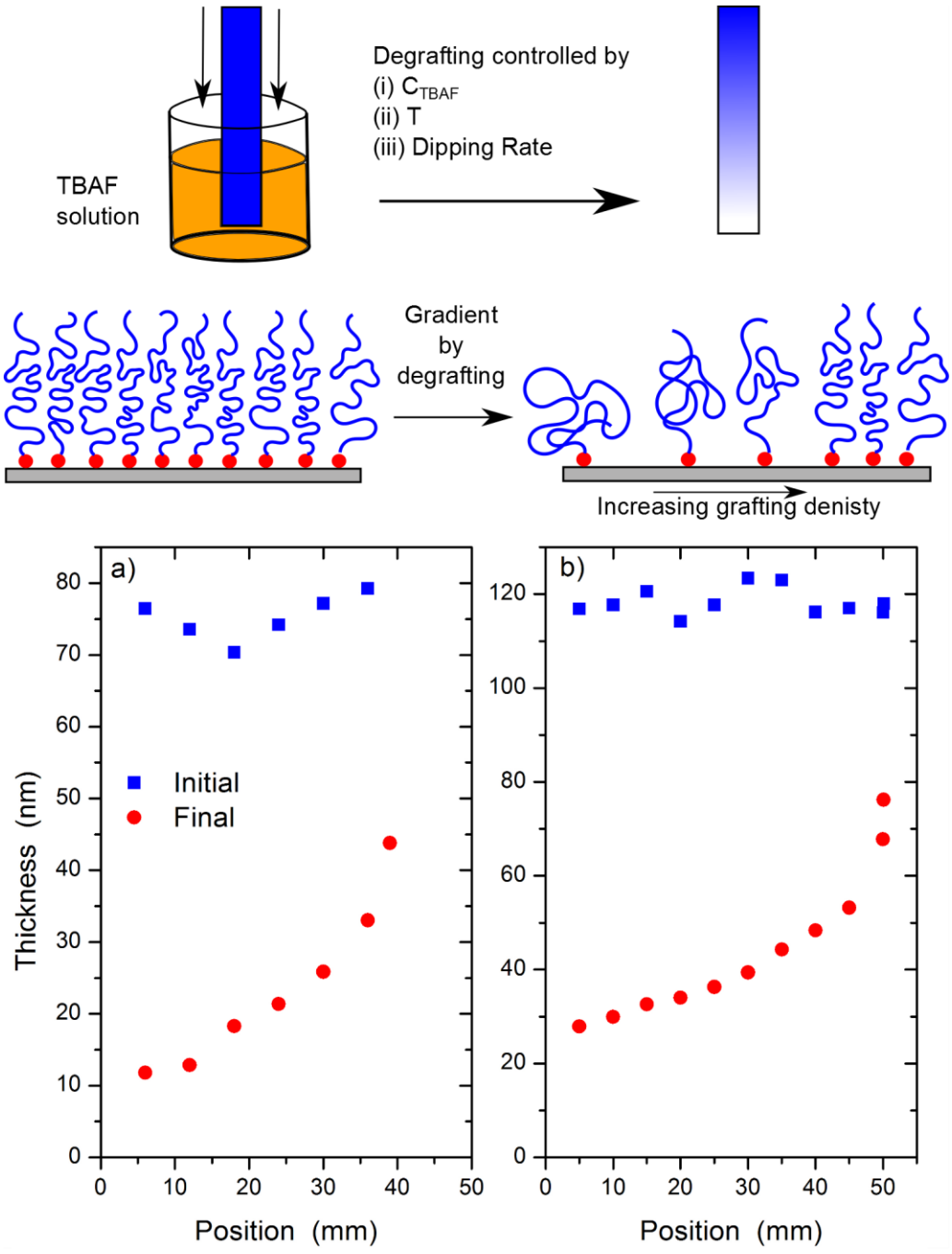

Figure 5.1. Dry thickness (h_P) of PMMA brushes plotted against the position on a substrate. Because the initial grafting density of PMMA was constant over the substrate the dry thickness change is a measure of the grafting density of PMMA brushes. Experimental conditions: a) C_{TBAF}=0.1 M, T=25°C, dipping rate=0.1 mm/min. b) C_{TBAF}=0.05 M, T=25°C, dipping rate=1.0 mm/min.

5.2.2 Creating other polymer brush patterns

While the dipping method creates a continuous variation in the thickness, surface patterns with various in-plane shapes of polymer brushes can be created by delivering the TBAF solution to specific regions on the substrate. Using micro-contact printing, TBAF solution can be exposed using a hydrogel stamp with a desired shape. Here we used agarose as the hydrogel stamp material because it is not degraded by TBAF. An agarose stamp was soaked in 0.1 M TBAF solution in THF for 1 hr. The stamp was then brought in contact with a PMMA brush layer surface for 1 hr. The resulting pattern (mm scale) is visible to eye since the change in thickness changes the color of the polymer film. **Figures 5.2a-5.2c** show the initial substrate with polymer brush, the hydrogel stamp, and the substrate after stamping, respectively. **Figure 5.2d** shows patterns created by drying drops of TBAF solution. Optical microscopy images (**Figure 5.2e**) reveal that distinct regions on the surface are formed due to changing evaporation rate of the drop. The inner circle evaporated the latest; hence it will have the lowest grafting density and hence lowest thickness. **Figure 5.2f** shows an optical micrograph of the near interface region of one of the gradient sample (*cf.* **Figure 5.1b**) created using the dipping method explained earlier. The region to the left of the dotted line shows the gradation in color due to gradient in grafting density (and hence thickness) while the region to the right of the dotted line shows un-degrafted polymer brush layer. In all these examples, the incubation time and TBAF concentration can be varied to achieve greater control over the grafting density of the resulting pattern.

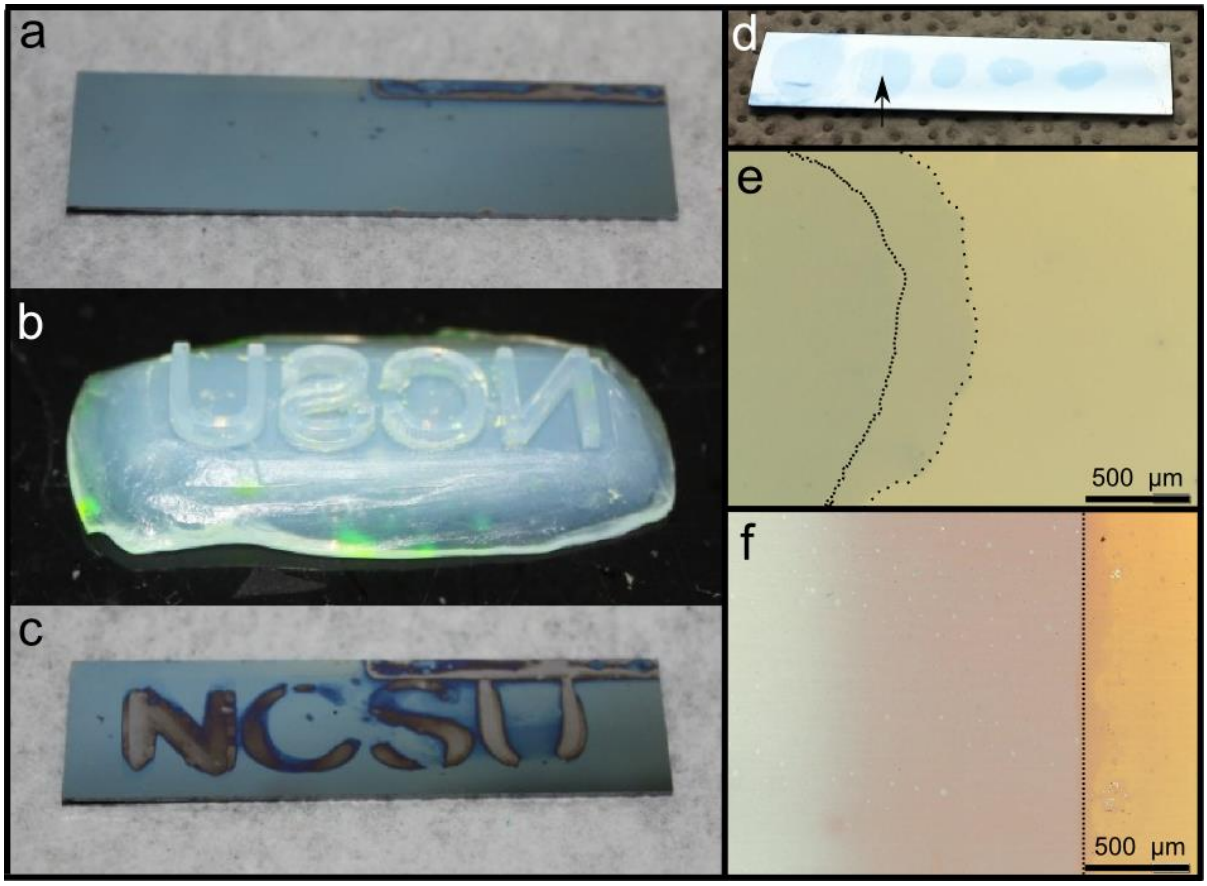

Figure 5.2. Surface pattern images on polymer brush containing substrate. a) Substrate coated with PMMA brush. b) Agarose hydrogel stamp with the desired pattern. c) Substrate after contact with TBAF-soaked agarose stamp; the grey regions have PMMA removed. d) Patterns of removed PMMA formed by depositing TBAF drops and letting them evaporate. e) Optical micrograph of the second drop from the left in d), the dotted line is drawn to guide the eyes and emphasize the different zones inside the drop. f) Optical micrograph of the region of the gradient sample where the gradient ends and un-degrafted polymer brush region begins. The dotted line is drawn to separate the two regions. The dimensions of the substrates in a), c) and d) are 1 cm x 4.3 cm.

5.2.3 Reusability of substrates

The low concentrations and incubation temperature during TBAF treatment ensure mild degrafting conditions so that the surface is not etched or damaged and is available for further and repeated modification. In **Figure 5.3** we plot thickness (h_P) and water contact angle (θ_{DIW}) for a sequence of initiator deposition and PMMA brush growth steps before and after degrafting. The first eBMPUS layer (E1) was deposited by conventional method, *i.e.*, by first treating the substrate with ultraviolet ozone (UVO) treatment prior to the solution deposition of eBMPUS. The second and third initiator layers (E2 and E3) were deposited after degrafting PMMA and without any UVO treatment. PMMA brush was grown using ATRP as described in the Experimental section. Control samples (Control 1 and Control 2) were grown in the same reaction vessels but had eBMPUS layers deposited by conventional method, *i.e.*, by using UVO treatment prior to the initiator deposition. The results show that the thickness of the samples grown without any UVO treatment is comparable with that on samples prepared by the UVO-based conventional substrate treatment method. This is an important observation as it indicates: 1) complete removal of the organic layer via eBMPUS, which has been eluted to earlier,[23,24] and 2) the ability of TBAF to activate the surface for attachment of organosilanes.

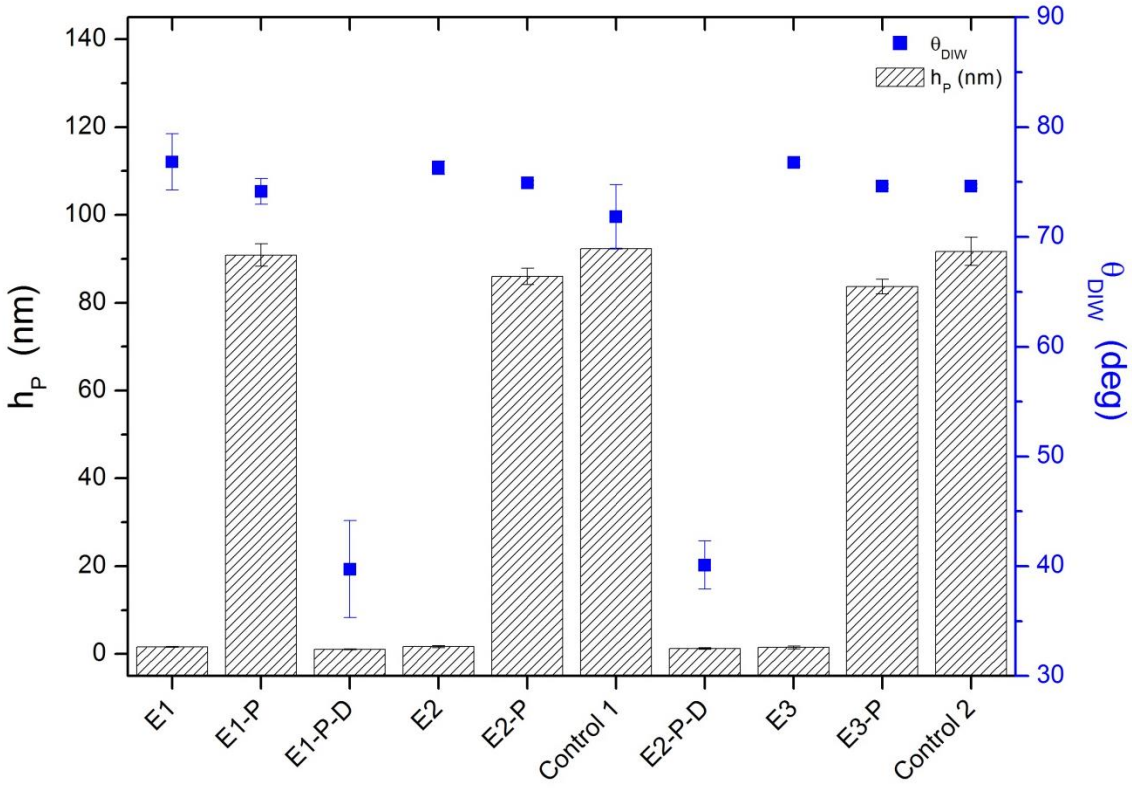

Figure 5.3. Dry ellipsometric thickness (h_P, bars) and water contact angle (θ_{DIW}, blue symbols) for repeated sequential deposition of eBMPUS (E) initiator and PMMA brush layer (P) grown after degrafting by ATRP. E1, E2, E3 refer to the first, second and third initiator deposition, respectively.

5.2.4 Re-growing polymer brushes without using UVO

We have shown previously that PMMA brushes can be degrafted from SiO_x substrates without any degradation and the collected PMMA can be analyzed using SEC to obtain molecular weight of the polymer.[23,24] Here we demonstrate that the degrafted surface can be reused to deposit a second initiator layer which can then be employed to grow a different polymer brush layer. The second layer could be any polymer that can be grown by ATRP; here we first grow a polystyrene (PS) brush first followed by a PMMA brush. The X-ray photoelectron

spectroscopy (XPS) data shown in **Figure 4** provide insight into chemical changes on the substrate during the technological steps involved in grafting/degrafting/regrafting. In addition, for each step we monitor the dry film thickness (h_p, solid symbols) and water contact angle (θ_{DIW}, open symbols). The starting substrate is a silicon wafer subjected to UVO treatment (data not shown), which cleans the surface from organic impurities and creates free hydroxyl groups needed for the attachment of the eBMPUS initiator molecules. The substrate is then covered with a monolayer of the eBMPUS initiator (black data). The silicon (Si 2p) and oxygen (O 1s) peaks (binding energies, BE, ~99 and ~534 eV, respectively) represent the underlying silica layer (~1 nm in thickness). The carbon (C 1s, BE ~285 eV) and bromine (Br 3d, BE ~70 eV) signals in the monolayer with $h_P=1.6 \pm 0.1$ nm and $\theta_{DIW}=77 \pm 2$ deg further confirm the presence of eBMPUS on the surface. A polystyrene (PS) brush (red data) with $h_P=49 \pm 3$ nm is then grown from the initiator sites via ATRP. A strong carbon peak (BE ~285 eV) is detected in XPS but no silicon and oxygen peaks are observed since the escape electrons from the underlying silica cannot reach the detector. The θ_{DIW} measured is 93 ± 2 deg, which is typical for PS. The high resolution XPS spectra show a characteristic aromatic peak in the C 1s peak at BE ~292 eV (see Appendix A). This PS polymer brush layer is then degrafted using 0.1 M TBAF at 50°C for 4 hrs. The green data in **Figure 5.4** correspond to the sample after TBAF degrafting. The Si 2p and O 1s peaks in the XPS data are visible again and the surface is hydrophilic with $\theta_{DIW}=43 \pm 3$ deg. A monolayer of the eBMPUS ATRP initiator is subsequently deposited (blue) on this substrate but this time without exposing the substrate to UVO treatment. The C 1s and Br 3d peaks are detected in the XPS spectra and the θ_{DIW}

increases to 73 ± 3 deg, close to the original eBMPUS monolayer (black data). PMMA layer of thickness 81 ± 2 nm (θ_{DIW}=60 ± 3 deg) is then grown using ATRP (magenta). The high resolution C 1s peak in XPS for PMMA layer can be resolved into its synthetic components; the ratio of their areas matches the stoichiometric ratio in PMMA (see Appendix A).

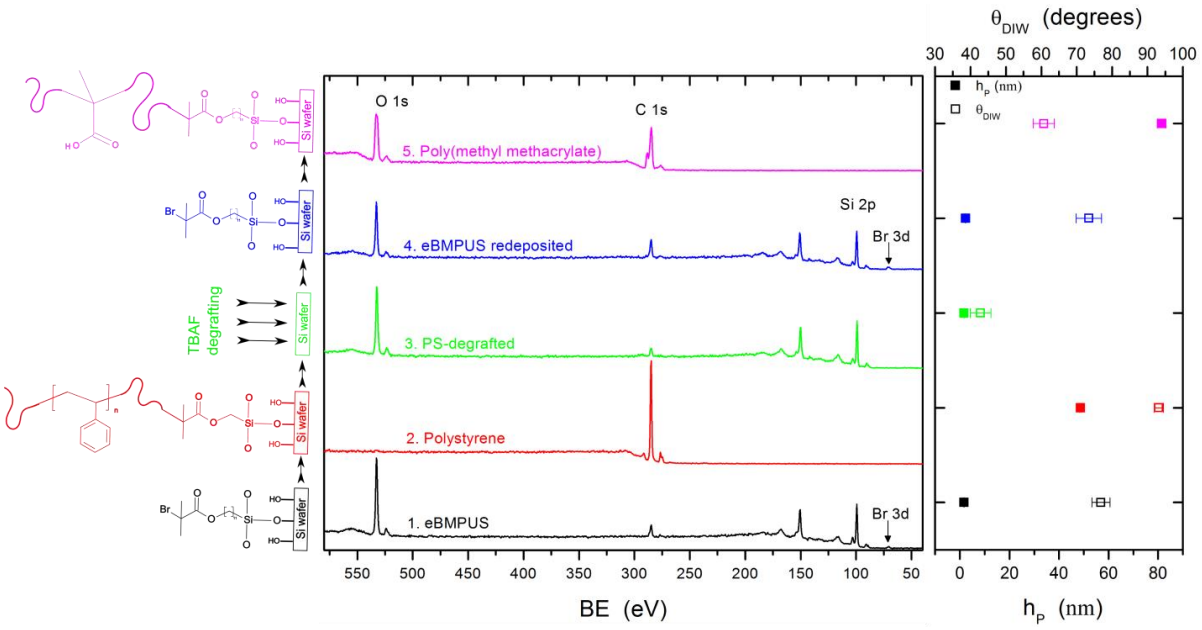

Figure 5.4. XPS scans for 5 different substrates, color coded with the cartoons on the left at different stages. The dry thickness (h_P, solid symbols) and water contact angle (θ_{DIW}, open symbols) are plotted on the right-side for the same 5 samples.

5.2.5 Degrafting of half substrate and growing di-block copolymer on other half

One can degraft the polymer from selected sections on the substrate and re-growing a layer of a new polymer brush over the entire substrate. This procedure will lead to the formation of block copolymers (growth initiated from the remaining polymer brushes, which act as macroinitiators) and homopolymer brushes that grow from the degrafted regions of the

substrate. To demonstrate this concept we first grow a PS brush (shown in red in **Figure 5**) from eBMPUS initiators by ATRP (h_P=104.9 ± 0.1 nm and θ_{DIW}=95 ± 2 deg). A half of this substrate is then degrafted by incubating it in 0.1 M TBAF in THF at 50°C for 4 hrs resulting into half area available for new initiator deposition. This substrate is then incubated in eBMPUS solution followed by PMMA brush grown by ATRP for 24 hrs. Since there are ATRP active ends on the PS chains, a PS-b-PMMA diblock copolymer is grown on the PS covered area while the degrafted region is only decorated with PMMA hompolymer brushes. The thickness of diblock region was 158.9 ± 4 nm (θ_{DIW}=61 ± 1 deg) and the PMMA only region was measured as 124.8 ± 1.2 nm (θ_{DIW}=59 ± 2 deg). The substrate areas were characterized using FTIR. A carbonyl peak, characteristic for PMMA, observed at 1730 cm^{-1}, is detected in PMMA homopolymer and PS-PMMA diblock region while peaks corresponding to CH_2 deformation (~1460 cm^{-1}), aromatic ring vibration (~1493 cm^{-1}) and CH_2 rocking (~700 cm^{-1}) for PS[31] are observed in the PS homopolymer and PS-PMMA diblock copolymer region. The contact angle (θ_{DIW}=61 ± 2 deg) of the diblock region indicates that the PMMA block is present on the top of the PS brush.

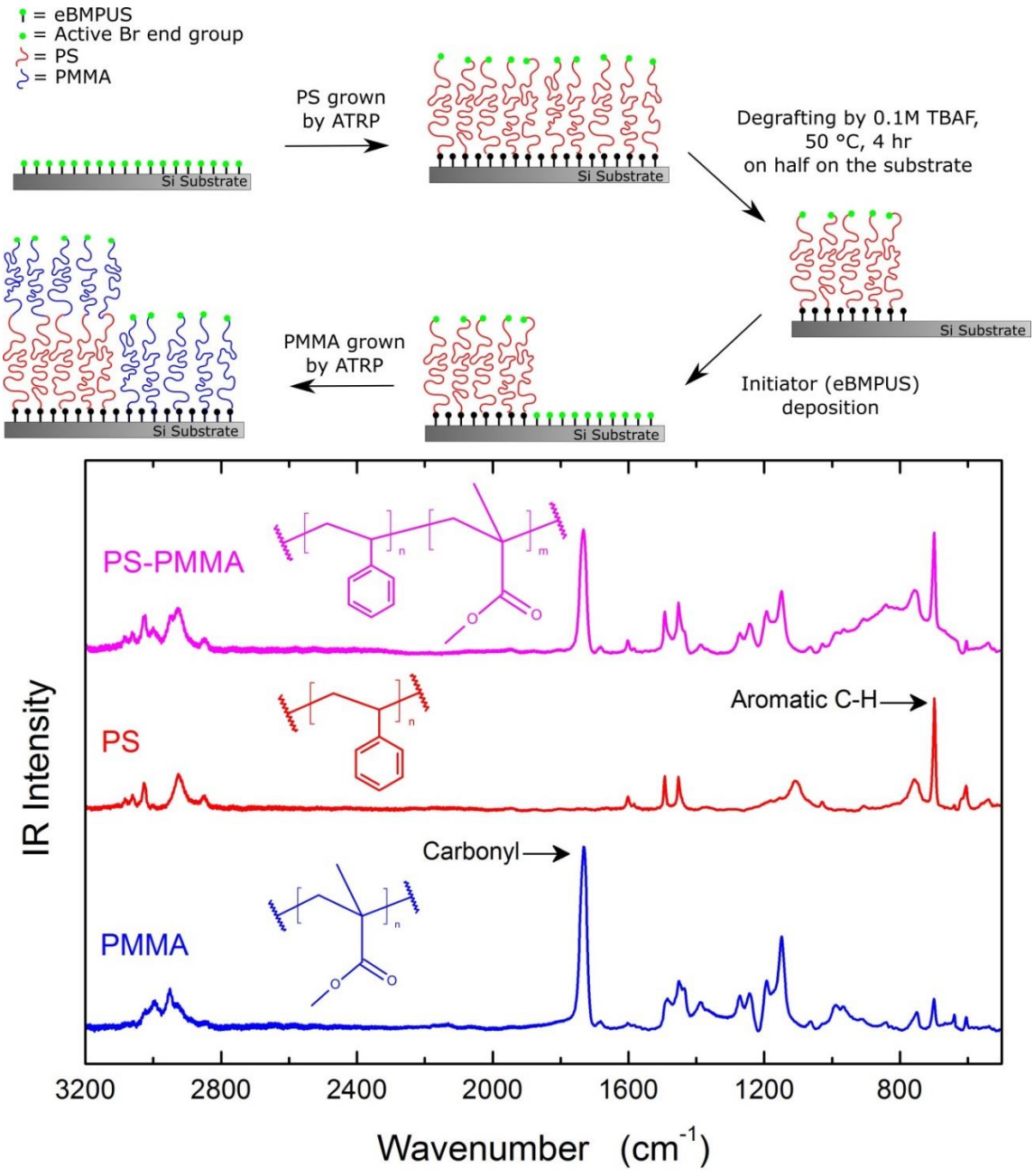

Figure 5.5. (Top) Scheme of creating a PMMA-PS diblock polymer brush on half of substrate while having PMMA only brush on the other half. (bottom) FTIR-spectra for PMMA region (blue), polystyrene only (red, control sample) and PS-PMMA diblock region (magenta).

5.3 Monolayer Degrafting and Gradients

The principle of creating degrafted patterns of polymer brushes using the TBAF degrafting method can be extended to self-assembled monolayers (SAMs) in a similar way. Creating density gradients of chemisorbed monolayers is of immense interest because they serve as a platform for further modification, for example, a pattern of initiator monolayer can be amplified by growing a polymer brush layer on top.[17,18] One would expect the degrafting of monolayers to be faster compared to polymer brushes since it is conceivably easier for the TBAF to access the silicon containing bonds. But in fact relatively harsher conditions (higher T and C_{TBAF}) are required to create monolayer density gradients. This indicates that the degrafting in case of polymer brushes is perhaps accelerated due to the bond tension at the base of polymer chain created due to the interaction from surrounding polymer chains in brush regime. The excess tension at the point of attachment could be acting as a catalyst, we will discussed this further in Chapter 4. As a proof of concept we have created a gradient of a monolayer for a fluorinated, very hydrophobic compound trichloro(1H,1H,2H,2H-perfluorooctyl)silane (F8H2). This compound can be degrafted and redeposited without using UVO on a Si substrate. The stability of such an F8H2 monolayer will depend on the number of points of attachment to the surface. The gradient itself can then be backfilled with other molecules such as ATRP initiators (eBMPUS), which can be further amplified by growing polymer brushes. We can extend this principle for use with any chlorosilane or alkoxy based attaching molecule because the point of attachment is through silicon atom which is vulnerable to TBAF.

5.3.1 Monolayer degrafting and re-deposition

The concept of degrafting a polymer brush layer and reusing the substrate for further deposition can be extended to monolayers themselves, but the attachment and stability of a monolayer is a strong function of the number of attachment points. To get an understanding of this parameter we consider two versions of a fluorinated monolayer, a monochloro (M) and trichloro (T) version of (1H,1H,2H,2H-perfluorooctyl)silane (F8H2) mentioned earlier. The main difference is that M can only attach to the surface at one point but T may attach to as many as 3 points; T could also form an in-plane network. The resulting molecular orientation in the M and T versions of F8H2 is significantly different.[32] The monolayers themselves were deposited by vapor deposition in a closed Petri dish exposing the UVO activated silicon substrate to a solution of silane and perfluorodecalin (volumetric ratio 1:4) for 1 minute. We subjected each of these monolayer coated substrates to TBAF solution (0.1 M in THF at 50°C for 4 hours). This resulted into degrafting and reactivation of the surface for further attachment. The substrate was then used to deposit, without using UVO, a new monolayer of either M or T. **Figure 4.6** examines the degrafting characteristics for each homogeneous monolayer of M and T type along with re-deposition of either M or T on each of them. The first monolayer in each case was deposited after UVO activation of the underlying substrate while the second layer was deposited without any UVO treatment. The dry thickness and water contact angle data indicate that T is more difficult to degraft; h_P and θ_{DIW} are higher in comparison to M for the same degrafting conditions. The monolayer of T is resistant to degrafting (1) because there are more bonds that need to be severed (attachment to the substrate as well as in-plane network

linking neighboring molecules) in order to degraft them, and (2) there are prone to forming in plane networks and multilayers which could provide extra stability to the monolayer.[33] The deposition times, relative humidity and length of the chains also affect the deposition.[33] The TOF-SIMS data for characteristic peak ion counts of F^-, HF_2^- and CF_3^-, normalized to the SiO_2^- ions, also support the above result qualitatively. It should be noted that the T version both originally deposited and re-deposited after degrafting gives a higher value of h_P and θ_{DIW} as well as ion count in each case. This is another indication of a possible multilayer and/or a close-packed network formation. This experiment at the very least proves that the re-deposition of monolayers is possible without using UVO treatment, and, that trichlorosilane are in general more stable and harder to degraft than their monochloro versions.

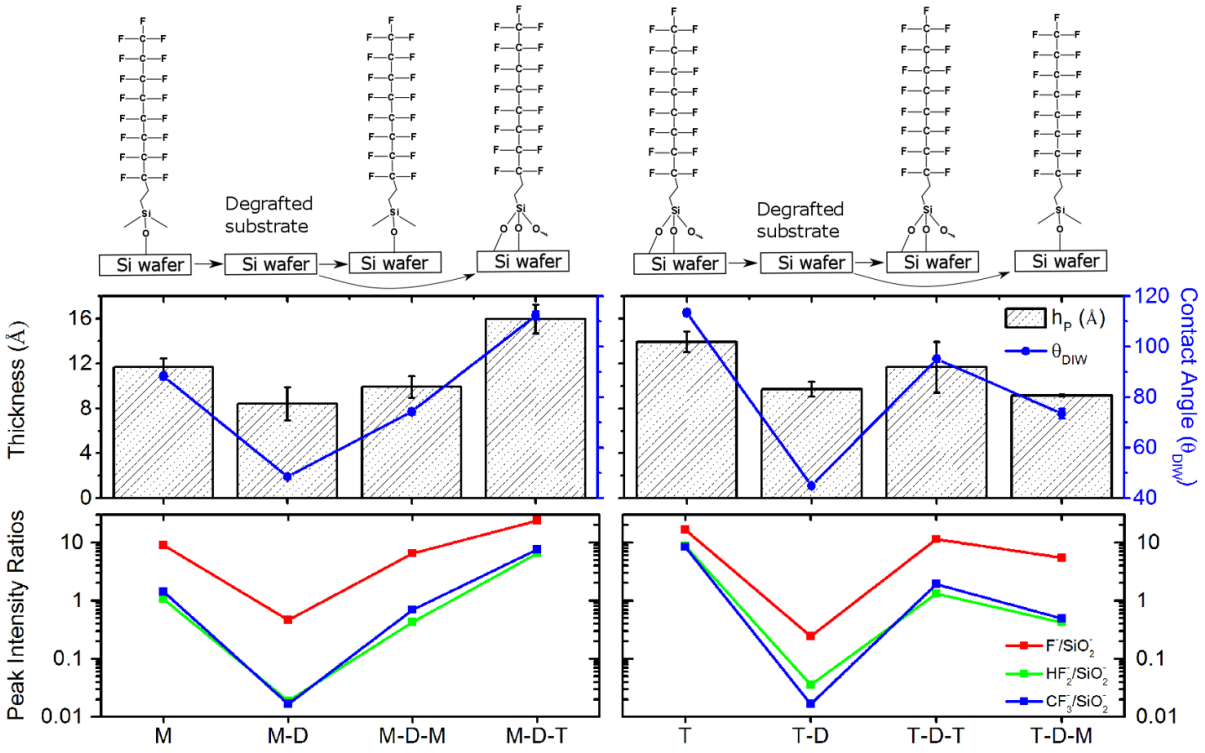

Figure 5.6. The dry thickness (h_P), water contact angle (θ_{DIW}) and selected peak ratios of ion count from TOF-SIMS for various stages of degrafting and re-deposition of monochloro (M) and trichloro (T) version of the fluorinated monolayer (F6H2).

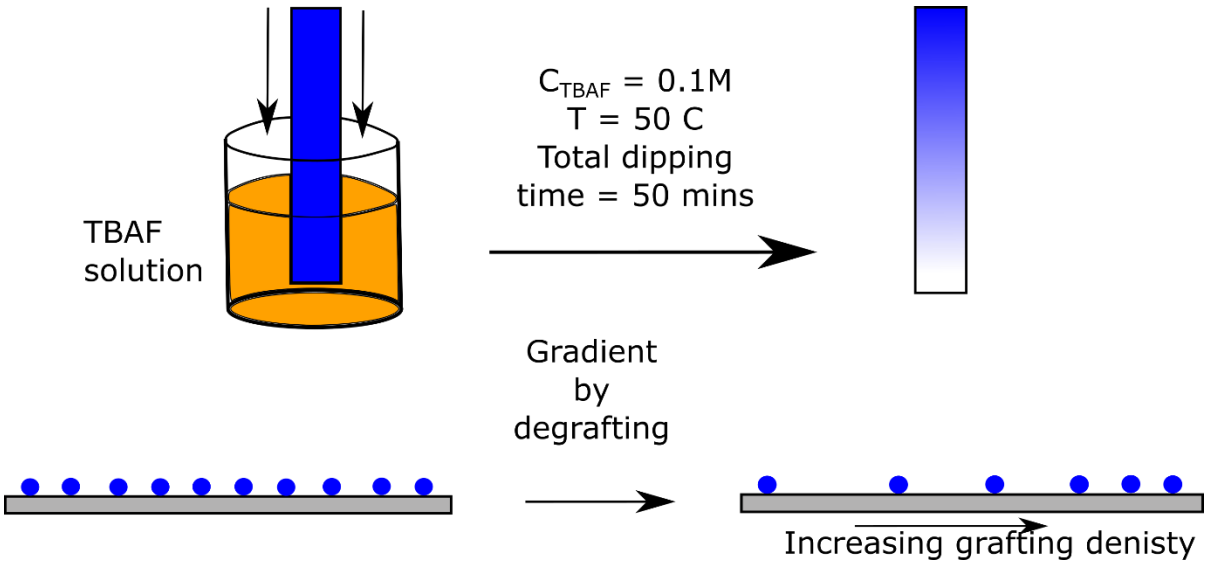

Figure 5.7. Scheme for creating gradient of monolayer by the dipping method using TBAF as the degrafting agent.

5.3.2 Gradient of a fluorinated monolayer

Figure 5.7 shows a schematic depicting the procedure for creating a density gradient in grafting density of organosilane SAMs, a method similar to that used for polymer brushes. We will demonstrate here that we can create a density gradient of trichloro(1H,1H,2H,2H-perfluorooctyl)silane (T). The silicon substrate in this case was about 30 mm long, the initial uniform monolayer of T was created by vapor deposition process described earlier. The degrafting gradient was created by dipping 25 mm of the substrate vertically (using a programmable dipper machine) in a 0.1 M TBAF solution in TBAF held at 50°C at the rate of 0.5 mm/min with a total dipping time of 50 mins. Advancing and receding water contact angles were measured using the 'drag the drop' method to ascertain the contact angle hysteresis of the surface. Our experiments reveal that the average value of the advancing and receding θ_{DIW}

lines closely with the static θ_{DIW}. We would like the reader to focus on the qualitative trends in θ_{DIW}. The trend shows that there is a systematic change in the θ_{DIW} from one side of the substrate to the other. The static θ_{DIW} for a uniform monolayer of T is 110±3°; the static θ_{DIW} and the average θ_{DIW} of advancing and receding are close to 70° on the end with the highest degrafting as seen in **Figure 5.8**. The hysteresis indicated by the difference between the advancing and receding θ_{DIW} increases with more degrafting.

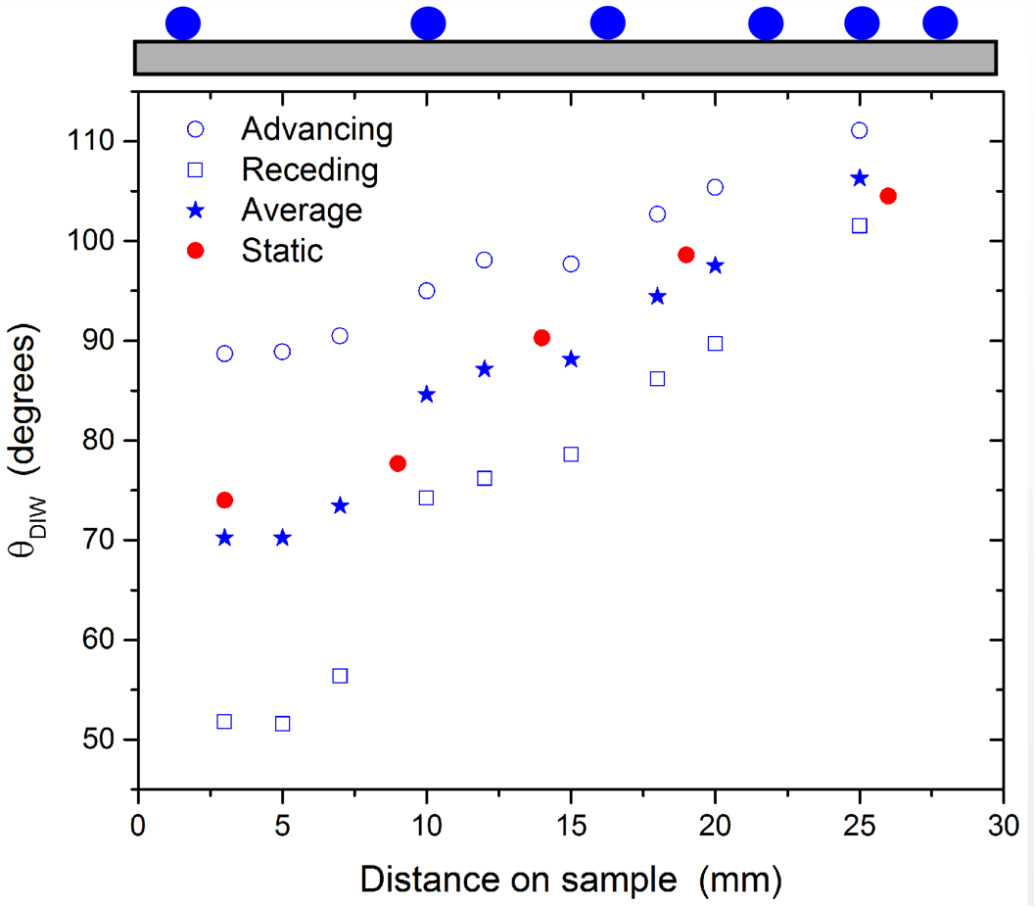

Figure 5.8. Static θ_{DIW}, advancing and receding θ_{DIW} on the gradient of trichloro(1H,1H,2H,2H-perfluorooctyl)silane on silicon substrate created by degrafting.

We further use this gradient surface as a platform to create a new gradient in another monolayer. Here we use eBMPUS, which is the ATRP initiator. The exposed regions on a gradient of T are activated for a deposition of a new chlorosilane based molecule. We amplified this backfilled gradient of eBMPUS by growing PMMA brush layer using ATRP. The surfaces are characterized using θ_{DIW}, dry ellipsometric thickness (PMMA layer only), and TOF-SIMS, the data for which is shown in **Figure 5.9**. The top two graphs indicate the θ_{DIW} where minimal hysteresis is observed for eBMPUS gradient (top left) because the non-uniformity is partially reduced owing to covering of the exposed silica surface. The chemical composition of this gradient substrate is revealed by exploring TOF-SIMS data, shown by the bottom two graphs, collected along various portion of the sample. The characteristic ion for eBMPUS gradient is bromine ($^{79}Br^-$ and $^{81}Br^-$) and while for PMMA we use the $C_3H_3O^-$ and $C_4H_5O_2^-$ fragments. There is a gradual change in bromine signal in TOF-SIMS as a function of position on the substrate for the eBMPUS gradient. For PMMA, the gradient is sharp because we can only observe the top ~1 nm surface. The same factor affects the θ_{DIW} measurements and cause it to have a sharp change as a function of position on the sample. In case of PMMA gradient, the ellipsometric thickness is a clear indicator of the formation of a gradient in grafting density. This gradient in polymer brush is essentially an amplification of a gradient in the monolayer of eBMPUS. The point of this experiment is to show that the degrafting of a monolayer is a reliable way for surface modification and to further create patterns of polymer brushes.

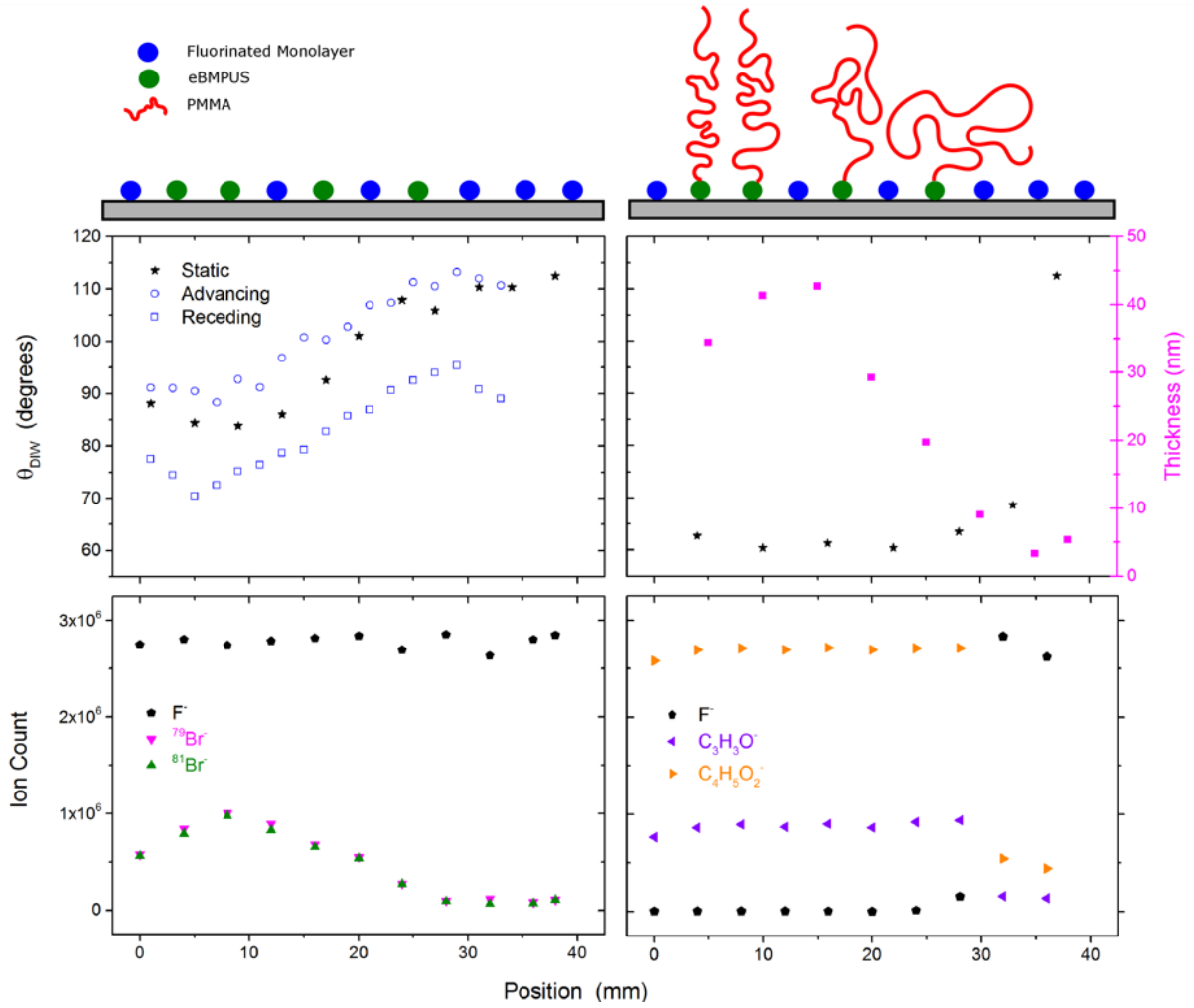

Figure 5.9. (Top) Schematic of a backfilled eBMPUS gradient and PMMA brush grafting density gradient. (Top Left Graph) Static, advancing and receding water contact angle (θ_{DIW}) for the eBMPUS gradient. (Top Right Graph) Dry ellipsometric thickness (h_P) and static water contact angle for PMMA gradient. (Bottom) TOF-SIMS data with absolute ion counts of (Left) F^-, $^{79}Br^-$ and $^{81}Br^-$ for eBMPUS gradient and (Right) F^-, $C_3H_3O^-$ and $C_4H_5O_2^-$ for PMMA gradient.

5.4 Conclusions

We have shown that polymer brushes grown from silica-based substrates can be removed selectively by TBAF. The degrafted substrate can then be employed to grow a new polymer brush. This process can be repeated multiple times, which makes this procedure attractive to create chemical patterns on surfaces. The properties of the regrown brush layers are comparable to those prepared by conventional deposition method which employs UVO for surface activation needed or initiator attachment. A true gradient of grafting density for PMMA brushes can be created with degrafting by dipping method in TBAF solution. Spatial patterns of polymer brushes can be prepared by stamping of molded agarose hydrogel by microcontact printing. We also created gradients of monolayer by the dipping method. The monolayer patterns by themselves are a great way to create surfaces with desired properties but they also serve as a platform for further modification. We use this fact to create a backfilled monolayer gradient which can then be used to create a gradient in grafting density of polymer brushes. Combining the knowledge of the kinetics of degrafting and soft lithographic techniques facilitates creation of a brush patterns with good in-plane and out-of-plane control of grafting density and brush chemical composition. The techniques mentioned in this chapter may serve as a good starting point for anyone who wants to use monolayers or polymer brushes for patterning applications.

5.5 Acknowledgements

We thank Dr. Jiří Šrogl for his contribution regarding understanding the chemistry of TBAF. The work was supported by the National Science Foundation (Grant no. DMR-1404639) and the Army Research Office under their Staff Research Program (Grant no. W911NF-04-D-0003-0016).

5.6 References

(1) Zhao, B.; Brittain, W. J. *Prog. Polym. Sci.* **2000**, *25*, 677–710.

(2) de Gennes, P. G. *J. Phys.* **1976**, *37* (12), 1445–1452.

(3) Milner, S. T. *Science* **1991**, *251* (4996), 905–914.

(4) Jones, D. M.; Smith, J. R.; Huck, W. T. S.; Alexander, C. *Adv. Mater.* **2002**, *14* (16), 1130–1134.

(5) Li, Y.; Zhang, J.; Fang, L.; Jiang, L.; Liu, W.; Wang, T.; Cui, L.; Sun, H.; Yang, B. *J. Mater. Chem.* **2012**, *22* (48), 25116–25122.

(6) Li, Y.; Zhang, J.; Liu, W.; Li, D.; Fang, L.; Sun, H.; Yang, B. *ACS Appl. Mater. Interfaces* **2013**, *5* (6), 2126–2132.

(7) Wang, X.; Berger, R.; Ramos, J. I.; Wang, T.; Koynov, K.; Liu, G.; Butt, H.-J.; Wu, S. *RSC Adv.* **2014**, *4* (85), 45059–45064.

(8) Hou, J.; Shi, Q.; Ye, W.; Fan, Q.; Shi, H.; Wong, S.; Xu, X.; Yin, J. *ACS Appl. Mater. Interfaces* **2014**, *6* (23), 20868–20879.

(9) Hou, J.; Shi, Q.; Ye, W.; Fan, Q.; Shi, H.; Wong, S.-C.; Xu, X.; Yin, J. *Chem. Commun.* **2015**, *51* (20), 4200–4203.

(10) Ionov, L.; Minko, S.; Stamm, M.; Gohy, J. F.; Jéróme, R.; Scholl, A. *J. Am. Chem. Soc.* **2003**, *125* (27), 8302–8306.

(11) Luzinov, I.; Minko, S.; Tsukruk, V. V. *Prog. Polym. Sci.* **2004**, *29* (7), 635–698.

(12) Kumar, A.; Whitesides, G. M. *Appl. Phys. Lett.* **1993**, *63* (14), 2002–2004.

(13) Genzer, J.; Bhat, R. R. *Langmuir* **2008**, *24* (6), 2294–2317.

(14) Genzer, J. *Annu. Rev. Mater. Res.* **2012**, *42* (1), 435–468.

(15) Zhao, B. *Langmuir* **2004**, *20* (26), 11748–11755.

(16) Chen, T.; Amin, I.; Jordan, R. *Chem. Soc. Rev.* **2012**, *41* (8), 3280–3296.

(17) Chen, T.; Jordan, R.; Zauscher, S. *Polymer.* **2011**, *52* (12), 2461–2467.

(18) Chen, T.; Jordan, R.; Zauscher, S. *Soft Matter* **2011**, *7* (12), 5532–5535.

(19) Kamada, T.; Yamazawa, Y.; Nakaji-Hirabayashi, T.; Kitano, H.; Usui, Y.; Hiroi, Y.; Kishioka, T. *Colloids Surfaces B Biointerfaces* **2014**, *123*, 878–886.

(20) Koo, H. J.; Waynant, K. V.; Zhang, C.; Haasch, R. T.; Braun, P. V. *Chem. Mater.* **2014**, *26* (8), 2678–2683.

(21) Schuh, C.; Lomadze, N.; Rühe, J.; Kopyshev, A.; Santer, S. *J. Phys. Chem. B* **2011**, *115* (35), 10431–10438.

(22) Wei, Q.; Yu, B.; Wang, X.; Zhou, F. *Macromol. Rapid Commun.* **2014**, *35* (11), 1046–1054.

(23) Patil, R. R.; Turgman-Cohen, S.; Šrogl, J.; Kiserow, D.; Genzer, J. *ACS Macro Lett.* **2015**, *4* (2), 251–254.

(24) Patil, R. R.; Turgman-Cohen, S.; Šrogl, J.; Kiserow, D.; Genzer, J. *Langmuir* **2015**, *31* (8), 2372–2381.

(25) von Werne, T.; Patten, T. E. *J. Am. Chem. Soc.* **1999**, *121*, 7409–7410.

(26) Kobayashi, M.; Terada, M.; Terayama, Y.; Kikuchi, M.; Takahara, A. *Macromolecules* **2010**, *43* (20), 8409–8415.

(27) Jia, X.; Zhang, G.; Li, W.; Sheng, W.; Li, C. *J. Polym. Sci. Part A Polym. Chem.* **2014**, *52* (13), 1807–1814.

(28) Kang, C.; Crockett, R. M.; Spencer, N. D. *Macromolecules* **2014**, *47* (1), 269–275.

(29) Chaudhury, M. K.; Whitesides, G. M. *Science* **1992**, *256* (5063), 1539–1541.

(30) Turgman-Cohen, S.; Genzer, J. *Macromolecules* **2010**, *43* (22), 9567–9577.

(31) Liang, C. Y.; Krimm, S. *J. Mol. Spectrosc.* **1959**, *3* (1-6), 554–574.

6. Outlook

This PhD Thesis delves into investigating viable techniques for studying the properties of polymer brushes by employing the degrafting approach. To this end, in Chapter 2, we discussed the plethora of techniques that are available to measure polymer brush properties published in literature. In Chapter 3 we presented a novel degrafting strategy that utilizes TBAF, which can be employed to cleave grafted polymer layers quantitatively from substrate. After collecting the degrafted polymer and passing it through the SEC we can determine the molecular weight distribution of surface grafted PMMA. Chapter 4 provides an attempt in understanding the mechanism of the TBAF-driven degrafting process by using its analogy to simple chemical reaction kinetics. The versatility of TBAF opens up new avenues for research work with potential use in degrafting other geometries and new grafted polymer systems. Creating surface patterns using degrafting by TBAF was put forward in Chapter 5. This can be extended to study the stability of organosilane-based monolayers on silica-like surfaces. In the following three sections of this Chapter, we present ideas about future work that builds upon our current understanding of the behavior of grafted polymer layers.

6.1 Future work for degrafting

We have established that TBAF acts as an effective reagent for degrafting neutral polymer brushes, such as PMMA, from silica substrates. This method can now be extended to other polymers, such as polymethacrylic acid (PMAA). The results presented in Chapter 5 provided a clue about competing effects arising during the TBAF-based degrafting process. The

association of tertrabutyl ammonium cation with the anionic part of the polymer causes an increase in the free volume and hence increases the thickness of the polymer brush layer. Degrafting, on the other hand, causes a decrease of the polymer brush thickness. Further information about counterion association can be inferred by studying degrafting of a strong polyelectrolyte, such as poly[(sulfopropyl methacrylate) potassium salt] (PSPMK), exposed to TBAF solutions. In this case, we surmise that there will be little or no association with the tertbutyl ammonium cation and hence the degrafting characteristics will be comparable to that of a neutral polymer brush. In other words, degrafting will be dominant. For neutral brushes, such as PMMA and PS, we only observe the effect of degrafting, causing a thickness decrease.

Polymers such as poly(dimethylaminoethyl methacrylate) (PDMAEMA) or poly(hydroxyethyl methacrylate) (PHEMA) do not degraft in TBAF solution at room temperature and high concentration (0.1 M) of TBAF. One should note that the preliminary experiments carried out for PDMAEMA and PHEMA used THF as the solvent for TBAF. The resistance to degrafting here could be a result of the tendency of these polymers to form physical networks by hydrogen bonding. It is possible that the degrafting conditions used were not optimized for these systems, and it may still be possible by use of co-solvents or higher temperatures since they have an upper critical solution temperature (UCST).[1,2] In any case, this requires further study and optimization.

Understanding the morphology of polymer brushes on particles is of great interest because it affects the mechanical properties of the system where these nanoparticles are utilized. For example, a given polymer chain attached to nanoparticles could exhibit two

regimes a concentrated polymer brush (CPB) and a semi-dilute polymer brush (SDPB).[3] TBAF can be utilized here for degrafting polymer brushes on convex surfaces such as that of silica nano- or micro particles; the M_n can be assessed with SEC. This was done in the past using hydrofluoric acid (HF)[4,5], strong acid[6] or strong base[7], but TBAF offers a far more milder and safer alternative as detailed in Chapter 3.

6.2 Study of polymer brush reactivity for block copolymerization

The use of living polymerization schemes is ubiquitous in creating surface grafted polymer assemblies.[8] In case of ATRP, the growing end possess a halogen atom which is capable of further undergoing polymerization when exposed to the right conditions.[8–10] Diblock, multiblock and gradient copolymer brush structures can be created by simply controlling the exposure of the substrate to the appropriate polymerization solution and by controlling the dipping rate in the ATRP solutions. The initiation of the second or latter block, however, is not the same as when initiated from a flat substrate decorated with initiator molecules. One reason is that, unlike monolayers, the active end could be buried inside the underlying polymer layer and it may be more difficult for a new monomer to access it. In addition, solvent quality could place limitations on the mobility of the chain ends, which could, in turn, affect its apparent reactivity for further polymerization.

These issues can be investigated by characterizing the reactivity of the end groups of a polymer brush layer. The active halogen group can be converted into an azide group by reaction with sodium azide which can then be attached by a fluorescent dye containing alkyne group

using click chemistry[11]. These reactions should be chosen such that they are relatively faster and easier than the polymerization itself, so that we ensure that it goes to completion. Polymer ends coated with a fluorescent dye can be visualized and quantified using a fluorescence microscopy due to its high sensitivity. This can be extended to the third block, and more if needed. This investigation will help us to quantify the reactivity ratio for grafted di-block and multi-block copolymer systems. Our degrafting approach can then be utilized in conjunction with fluorescence microscopy to determine change in the molecular weight distribution and any apparent change in grafting density when we grow diblock copolymer brushes.

6.3. Future work for monolayer degrafting

The technique to create monolayer gradients on Si substrate, as discussed in Chapter 5, can be applied to create degrafted regions of *any* organosilane molecule that features chloro- or alkoxy-silane head group. The attack target for TBAF is in the vicinity of the substrate-initiator region and it depends on the arrangements of the Si-O bonds. These bonds could be connected to other silane molecules thus forming a network-like structure or they may be attached only to the substrate (although this is unlikely due to high energy penalty associate with bending Si-O bonds). Since degrafting would be directly affected by these conditions, it stands to reason that studying the degrafting characteristics could provide us information about the monolayer structure.

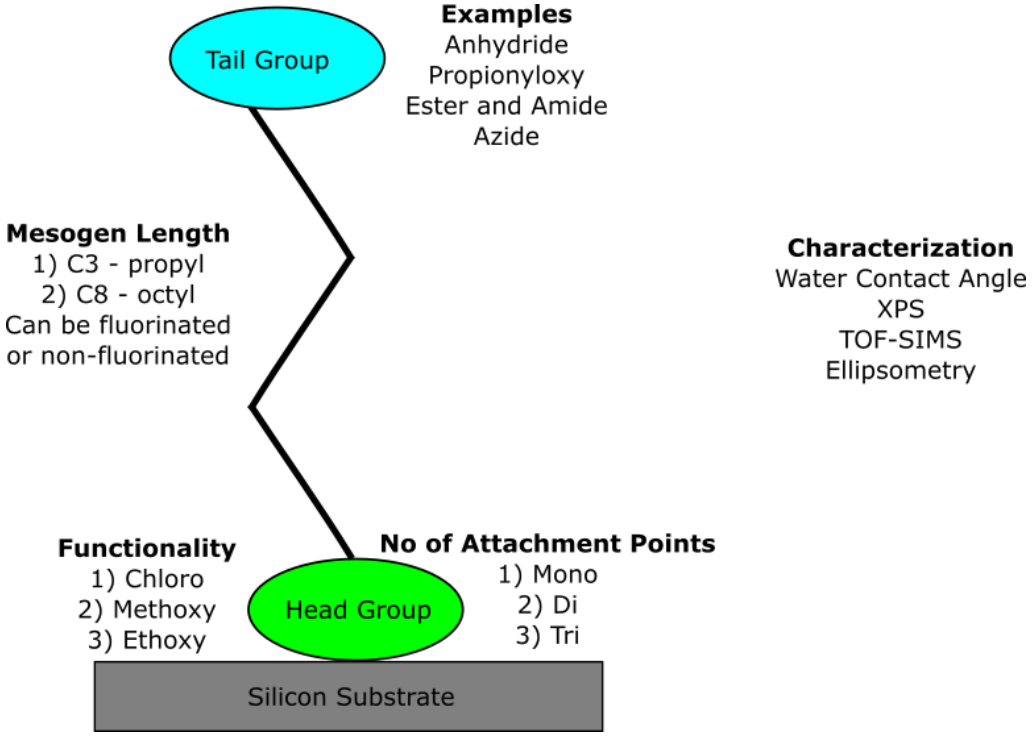

Figure 6.1. Schematic of a silane molecule attached to a silicon substrate and the variety of parameters that can be varied for a systematic study of its surface attachment.

These parameters can be studied in a systematic way as shown in **Figure 6.1** to obtain an exhaustive picture of the process of degrafting monolayers. First the number of the attachment points about the silicon head-group can be varied to range from one to three by using specialty silanes already available in the market. We can then vary the chemical functionality about the silicone tail-group, including chloro-, methoxy- or ethoxy- in this investigation. The connecting alkane group between the tail and the head group is referred to as mesogen and its length can be varied from C3 to C8. The tail group is present at the opposite end on the top surface, which in addition to dictating the surface chemistry, also provides opportunity for

further modification by chemical reaction. Both the mesogen and the tail group affect the ordering and deposition of a silane monolayer.

The reactivity of the tail group, such as maleic anhydride, can be studied as a function of grafting density, using the gradient approach. We can create a gradient of the inert monolayer n-octyltrichlorosilane (OTS) by first depositing it uniformly using vapor deposition followed by degrafting using dipping method. This can then be followed by backfilling with maleic anhydride-based silane. The anhydride groups can be further modified by reaction with primary amines bearing a fluorescent dye. This fluorescent dye can be subsequently visually observed and characterized using fluorescence microscopy, which would provide us an alternate way to TOF-SIMS for measuring the extent of degrafting. Studying the degrafting of silane monolayers will provide understanding of their stability on the surface as a function of the chemistry of attachment (chlorosilane *vs.* alkoxysilane) and the number of the attachment points. Such studies would aid in better design and use of monolayers in scientific studies and surface applications.

6.4 References

(1) Jung, S.-H.; Lee, H.-I. *Bull. Korean Chem. Soc.* **2014**, *35* (2), 501–504.

(2) Azzaroni, O.; Brown, A. A.; Huck, W. T. S. *Angew. Chemie Int. Ed.* **2006**, *45* (11), 1770–1774.

(3) Daoud, M.; Cotton, J. P. *J. Phys.* **1982**, *43* (3), 531–538.

(4) von Werne, T.; Patten, T. E. *J. Am. Chem. Soc.* **2001**, *123*, 7497–7505.

(5) Ejaz, M.; Tsujii, Y.; Fukuda, T. *Polymer.* **2001**, *42*, 6811–6815.

(6) Kobayashi, M.; Terada, M.; Terayama, Y.; Kikuchi, M.; Takahara, A. *Macromolecules* **2010**, *43* (20), 8409–8415.

(7) Jia, X.; Zhang, G.; Li, W.; Sheng, W.; Li, C. *J. Polym. Sci. Part A Polym. Chem.* **2014**, *52* (13), 1807–1814.

(8) Barbey, R.; Lavanant, L.; Paripovic, D.; Schüwer, N.; Sugnaux, C.; Tugulu, S.; Klok, H.-A. *Chem. Rev.* **2009**, *109* (11), 5437–5527.

(9) Huang, X.; Wirth, M. J. *Anal. Chem.* **1997**, *69* (22), 4577–4580.

(10) Matyjaszewski, K.; Miller, P. J.; Shukla, N.; Immaraporn, B.; Gelman, A.; Luokala, B. B.; Siclovan, T. M.; Kickelbick, G.; Vallant, T.; Hoffmann, H.; Pakula, T. *Macromolecules* **1999**, *32* (26), 8716–8724.

(11) Lee, B. S.; Lee, J. K.; Kim, W.-J.; Jung, Y. H.; Sim, S. J.; Lee, J.; Choi, I. S. *Biomacromolecules* **2007**, *8* (2), 744–749.

APPENDICES

APPENDIX A

Effect of TBAF on polymer molecular weight

We tested whether TBAF has an effect on the molecular weight of PMMA. To that end, we performed control SEC experiments using pure THF solvent, THF containing a high concentration of TBAF, and PMMA (standard synthesized by anionic polymerization; $M_n \approx 142$ kDa) solution containing various concentrations of TBAF at 50°C for 24 hours. The results (*cf.* **Figure A.1**) demonstrate that the elution time of PMMA is not affected by the presence of TBAF and that the molecular weight distribution of PMMA eluted from TBAF solutions of various concentrations is identical to that of PMMA in THF solvent only.

Determining the molecular weight distribution of polymers

We have performed size exclusion chromatography (SEC) experiments to test the lowest sensitivity of the DRI detector to determine unambiguously the molecular weight distribution (MWD) in our samples. In these tests, we used polystyrene (PS) standards (commercially available from Fluka) as well as PS and PMMA specimens prepared by free radical polymerization (FRP), atom transfer radical polymerization (ATRP) and reverse ATRP (RATRP).

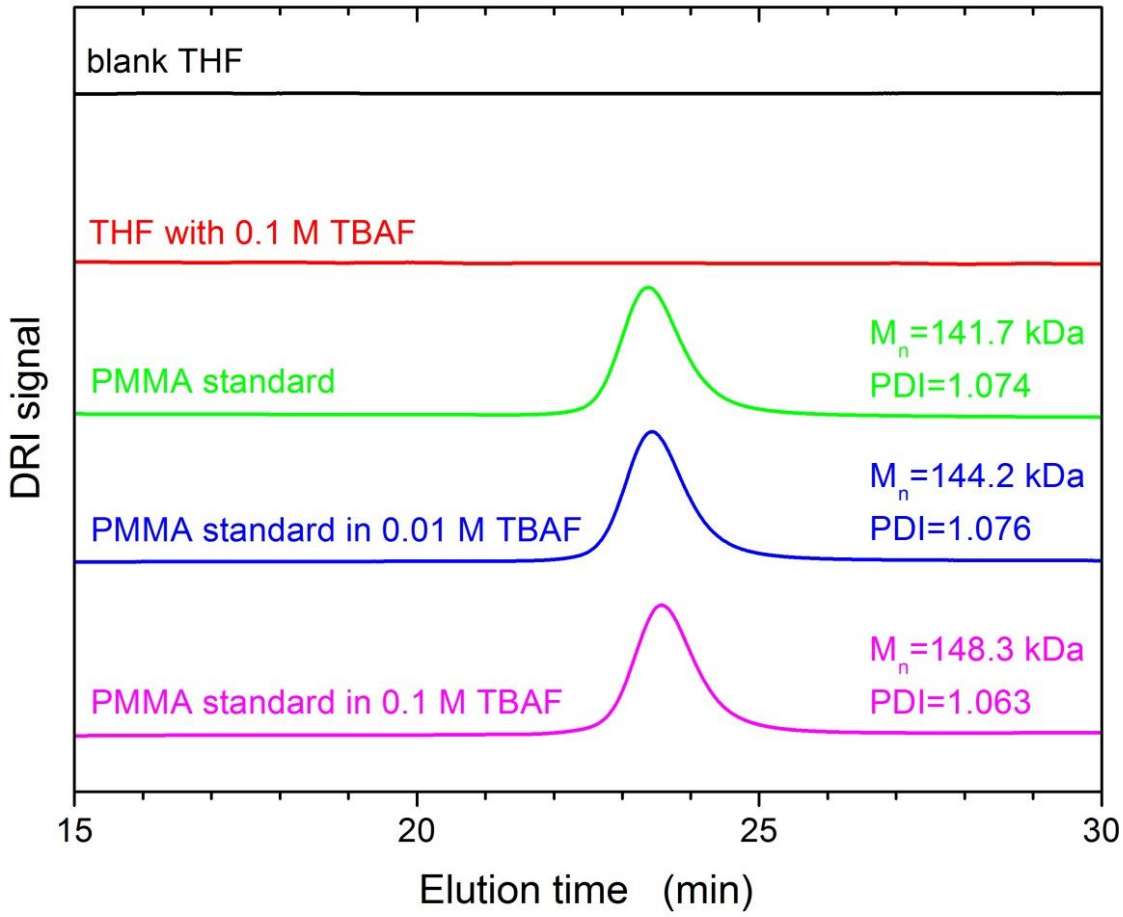

Figure A.1. DRI signal as a function of PS elution time in SEC collected from pure THF (black), THF with 0.1 M TBAF (red), PMMA standard (green), PMMA standard immersed in 0.01 M solution of TBAF (blue), and PMMA standard immersed in 0.1 M solution of TBAF (magenta).

The SEC experiments were carried out using polymer solutions in THF in order to maximize the refractive index contrast between the polymer and the solvent. For instance, the refractive indices of polystyrene (PS) and poly(methyl methacrylate) (PMMA) are 1.59[1] and 1.49[2], respectively. The refractive index of THF is 1.407[3] and that of toluene is 1.496.[4]

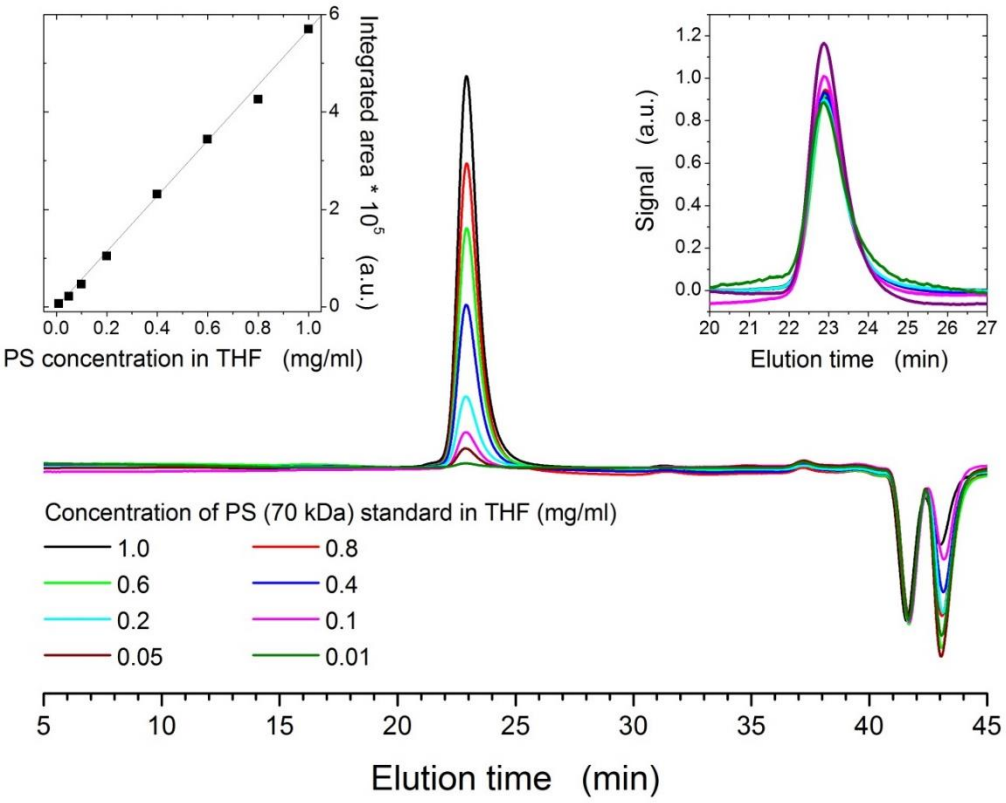

Figure A.2. (main) Elution curves as determined by the DRI detector for PS standards (synthesized by anionic polymerization and obtained from Fluka, with a nominal number average degree of polymerization of 70 kDa) as a function of polymer concentration in THF. (left inset) integrated area under the PS elution peak as a function of PS concentration in THF. (right inset) normalized DRI signal obtained by dividing the raw DRI signal by the PS peak integrated area (cf. inset on left) as a function of PS elution time.

We tested the sensitivity of the differential refractive index (DRI) detector by passing polystyrene solutions in THF of various concentrations through the SEC. The samples featured both PS standards (prepared by anionic polymerization and obtained from Fluka) as well as PS and PMMA specimens prepared by free radical polymerization, ATRP and reverse ATRP (RATRP). We determined that the minimum concentration of polymer solute in THF is 0.1 mg/ml. At this concentration the SEC elution peaks did not exhibit any distortion due to

sensitivity limit (see **Figure A.2** and **Figure A.3**) and provided consistently the same values of the first moment of the MWD, *i.e.*, the number average molecular weight, M_n, as well as the polydispersity index (PDI). For a substrate of dimensions 4.2 cm x 4.2 cm with PMMA layer (assuming bulk density of 1.18 g/cm^3)[2] the thickness of a film corresponding to 1 ml of 0.1 mg/ml solution is 48 nm. This is the minimum adequate thickness required for a measurement from a single sample.

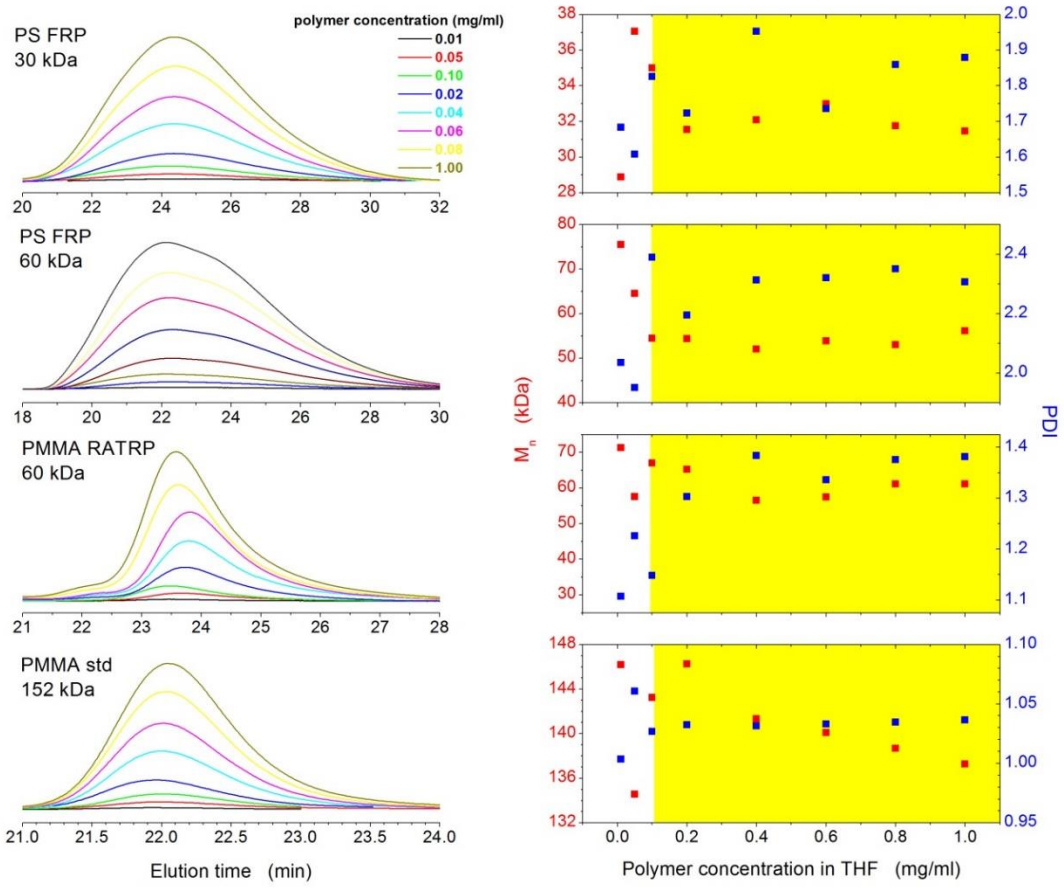

Figure A.3. (left column) Elution curves for various PS and PMMA samples as a function of the concentration in THF. (right column) The number average molecular weight (Mn, red symbols) and the polydispersity index (PDI, blue symbols) of the respective samples as a function of PS concentration in THF. The yellow area denotes the range of polymer concentrations that are safe to use for MWD analysis.

Molecular weight distribution determined from experiment

We use the MWDs measured experimentally by SEC to determine the number average degree of polymerization (N_n), *i.e.*, the 1st moment of the distribution, the weight average degree of polymerization (N_w), *i.e.*, the 2nd moment of the distribution, and the PDI. DRI SEC measures the weight fraction distribution of j-mers as a function of the number repeat units in each j-mer, *i.e.*, w_j=fxn(N_j). From this:

$$N_n = \frac{1}{\sum_{j=1}^{\infty} \frac{w_j}{N_j}} \quad , \tag{A3.1}$$

$$N_w = \sum_{j=1}^{\infty} w_j \cdot N_j \quad , \tag{A3.2}$$

$$PDI = \frac{N_w}{N_n} \quad , \tag{A3.3}$$

Note that PDI is related to the standard deviation of a distribution (σ) via[5]

$$\sigma = N_n \left(\frac{N_w}{N_n} - 1 \right)^{1/2} \tag{A3.4}$$

In the following section we provide mathematical description of several models that describe the molecular weight distributions in terms of weight fractions of an x-mer, $w_x(x)$.

Poisson distribution

The Poison (P) distribution describes the MWD in a truly living polymerization (*i.e.*, no termination or chain transfer). The general form of the P distribution is given by Equation (A3.5):

$$w_j = \frac{e^{-v} v^{N_j - 1}}{(N_j - 1)!} . \tag{A3.5}$$

In Equation (A3.5), v is defined as:

$$v = N_n . \tag{A3.6}$$

The PDI is defined as:

$$PDI = 1 + \frac{1}{v} . \tag{A3.7}$$

Note that because (x-1)!=Γ(x), Equation (A3.5) can also be written as:

$$w_j = \frac{e^{-v} v^{N_j - 1}}{\Gamma(N_j)} . \tag{A3.8}$$

Schulz-Zimm distribution

The Schulz-Zimm (SZ) distribution is based on a model for chain polymerization and is sometimes called the most probable distribution. As input, the SZ distribution function uses N_n, and either N_w or the PDI. Note that the aforementioned quantities are connected:

$$PDI = \frac{N_w}{N_n} = \frac{k+1}{k} . \tag{A3.9}$$

When one defines k and p as:

$$k = \frac{N_n}{N_w - N_n} = \frac{1}{PDI - 1}, \tag{A3.10}$$

$$p = \frac{1}{N_w - N_n} = \frac{k}{N_n} = \frac{1}{N_n} \cdot \frac{1}{PDI - 1}, \tag{A3.11}$$

one can show that:

$$N_n = \frac{k}{p}, \tag{A3.12}$$

$$N_w = \frac{k+1}{p}. \tag{A3.13}$$

The weight fraction of an x-mer, *i.e.*, $w_x(x)$, is given by:

$$w_j = \frac{N_j{}^k p^{k+1}}{\Gamma(k+1)} \cdot \exp(-p \cdot N_j) = \frac{N_j{}^k}{\Gamma(k+1)} \cdot \left(\frac{k}{N_n}\right)^{k+1} \cdot \exp\left(-\frac{k}{N_n} N_j\right). \tag{A3.14}$$

Equation (A3.14) is consistent with the IUPAC definition of the Schulz–Zimm distribution.[6]

ATRP distribution

Zhu and coworkers recently presented a theory for molecular weight distribution in ATRP.[7] While this model has been developed for bulk CSTR, we use it here as well assuming that conditions in the CSTR are roughly fulfilled (*i.e.*, the concentrations of the monomers and the reactive species are constant). In surface-initiated polymerization we work with a large excess of monomers; we further assume that the concentration of the active species is constant if no termination takes place. In this model, which assumes that no termination takes place, the probability that a radical will propagate is given by:

$$\phi_P = \frac{k_p[M]}{k_p[M] + k_d[XC]} \quad . \tag{A3.15}$$

In Equation (A3.15), [M] and [XC] are the concentrations of the monomer and the deactivator (*i.e.*, metal halide), respectively, and k_p and k_d are the reaction constants for propagation and deactivation, respectively.

When we define z as the number of activation cycles, we obtain:

$$N_n = \frac{z \cdot \phi_P}{1 - \phi_P} \quad . \tag{A3.16}$$

$$N_w = \frac{1 + \phi_P + z \cdot \phi_P}{1 - \phi_P} \quad . \tag{A3.17}$$

$$PDI = 1 + \frac{1}{N_n} + \frac{2}{z} \quad . \tag{A3.18}$$

The weight fraction of a j-mer is given by:

$$w_j = (1 - \phi_P)^2 (\phi_P)^{N_j - 1} e^{-z} \sum_{i=0}^{\infty} \left[\binom{N_j + i - 1}{i} \frac{z^{i-1}(1 - \phi_P)^{i-1}}{(i-1)!} \right] . \tag{A3.19}$$

where $z>0$ and $\phi_P<1$. Both z and ϕ_P are used as an input. Further expanding the sum in Equation (A3.19), one obtains:

$$\sum_{i=0}^{\infty} \left[\binom{N_j + i - 1}{i} \frac{z^{i-1}(1 - \phi_P)^{i-1}}{(i-1)!} \right] = \sum_{i=0}^{\infty} \left[\frac{(N_j + i - 1)!}{i!(N_j - 1)!} \frac{z^{i-1}(1 - \phi_P)^{i-1}}{(i-1)!} \right] \quad . \tag{A3.20}$$

The sum given by Equation (A3.20) can be expressed as:

$$\sum_{i=0}^{\infty}\left[\frac{(N_j+i-1)!}{i!(N_j-1)!}\frac{z^{i-1}(1-\phi_P)^{i-1}}{(i-1)!}\right]=-\frac{(\phi_P-1)N_j!}{(1-\phi_P)(N_j-1)!}\cdot{}_1F_1\left(N_j+1;2;-(\phi_P-1)z\right) \quad . \qquad \text{(A3.21)}$$

where ${}_1F_1(a;b;z)$ is (Kummer confluent) hypergeometric function.

Finally, by combining Equation (A3.19) with Equation (A3.21) one arrives at:

$$w_j=(1-\phi_P)(\phi_P)^{N_j-1}e^{-z}\frac{(1-\phi_P)N_j!}{\Gamma(N_j)}\cdot{}_1F_1\left(N_j+1;2;-(\phi_P-1)z\right) \quad . \qquad \text{(A3.22)}$$

Wesslau distribution

The Wesslau (W) distribution is a differential molecular weight distribution similar to Schulz-Zimm distribution, both of which are derived from a general form of most probable distribution:

$$w_j=\frac{1}{\beta\pi^{1/2}}\cdot\frac{1}{N_j}\cdot\exp\left(-\frac{1}{\beta^2}\cdot\ln^2\left(\frac{N_j}{N_0}\right)\right), \qquad \text{(A3.23)}$$

where

$$\beta^2=\ln\left(\frac{N_w}{N_n}\right)^2=\ln(PDI)^2, \qquad \text{(A3.24)}$$

$$N_0=N_n\cdot\exp\left(\frac{\beta^2}{4}\right). \qquad \text{(A3.25)}$$

The Wesslau distribution is referred to as log normal distribution. Another example of a log normal distribution is the so-called Lansing-Kraemer distribution.

Schulz-Flory distribution

The IUPAC definition of the Schulz–Flory (SF) distribution is:[8]

$$w_j = p^2 N_j (1-p)^{N_j - 1} . \quad \text{(A3.26)}$$

In Equation (A3.26) p is an empirically-determined adjustable parameter. One can write:[9]

$$(1-p)^{N_j - 1} = \exp(-p \cdot N_j) . \quad \text{(A3.27)}$$

Thus for k=1 and knowing that Γ(2)=1 one can recover (A3.26) from combining (A3.14) and (A3.27). This distribution implies is that shorter polymers are favored over longer ones.

Smith et al. distribution

Thee distribution due Smith *et al.* (S)[10] is used for "living polymerization" with propagation, termination and chain transfer, where:[11]

$$\beta = \frac{R_p}{R_p + R_t + R_{tr}} . \quad \text{(A3.28)}$$

In Equation (A3.28), the parameter β represents the probability that the chain will propagate rather than terminate.

Further:

$$PDI = \frac{2+\beta}{2} , \quad \text{(A3.29)}$$

or

$$\beta = 2(\mathrm{PDI} - 1) \quad . \tag{A3.30}$$

Then

$$w_j = A \cdot \left[N_j \cdot (1-\beta)^2 \cdot \beta^{N_j - 1} \right] + (1-A) \cdot \left[\frac{1}{2} \cdot N_j \cdot (N_j - 1) \cdot (1-\beta)^3 \beta^{N_j - 2} \right]. \tag{A3.31}$$

In Equation (3.S31), A is the fraction of polymer molecules formed by disproportionation and chain-transfer reactions. Thus for A=1 termination occurs only by disproportionation while for A=0 termination takes place by combination. The expression in the first bracket in Equation (A3.31) is mathematically identical to that obtained for w_j in condensation (*i.e.*, step growth) polymerization:[12]

$$w_j = N_j \cdot (1-p)^2 \cdot p^{N_j - 1} \quad , \tag{A3.32}$$

except now using p instead of β. In Equation (A3.32) p is defined as the extent of reaction (or the fraction of groups that have reacted or equivalently the probability of that a particular group has reacted).

Note also the similarity between the expression in the first bracket on in Equation (A3.31) and the definition of w_j given by the Schulz-Flory distribution, *i.e.*, Equation (A3.26). Specifically, when replacing β with 1-p in Equation (A3.32) one can recover Equation (A3.26). Recall in the definition of p for the Schulz-Flory distribution, p is assumed to be an empirically-determined adjustable parameter. This is different from the definition of p given by Equation (A3.32). Replacing p with 1-p in Equation (A3.32) also recovers Equation (A3.26). Hence, caution has to be taken with regard to the physical meaning and definition of p in all cases.

Modeling experimental MWD

We test how well are the MWD determined experimentally by SEC represented by each of the aforementioned models. In our analysis, we do not use the Poisson's distribution for true "living polymerization because the fits were of poor quality. To obtain the best fit to the experimental data, we employ two approaches. These feature fitting the data using the Kolmogorov-Smirnov distance statistic and the "chi-squared" approach.

The Kolmogorov-Smirnov (K-S) distance statistic is obtained by comparing the cumulative distributions functions of the experimental and model molecular weight distributions.[13] Once the two cumulative distributions are obtained, the K-S statistic is defined as the maximum absolute difference between the two:

$$K-S = \max\left\{D(1), D(2), D(3), \ldots D(N_{max})\right\}, \tag{A3.34}$$

where D(x) is given by:

$$D(x) = \left| \sum_{j=x}^{N_{max}} w_{j,experiment} - \sum_{j=x}^{N_{max}} w_{j,model} \right|. \tag{A3.35}$$

In Equation (A3.35), $w_{j,experiment}$ and $w_{j,model}$ represent the value of the cumulative distribution for the j-mer.

In addition, for each data set and each model we evaluate the standard "chi-squared" value, χ^2, defined as:[14]

$$\chi^2 = \sum_{j=1}^{N_{max}} \frac{\left[w_{j,experiment} - w_{j,model}\right]^2}{w_{j,experiment}}, \tag{A3.36}$$

Of the two methods, the "chi-squared" test is less preferred because binning the observations in this manner results in a loss of information. In contrast, the K-S method is more rigorous because it tends to find the best fit to the experimental data while maintaining the information about the functional form given by each respective model.

Dependence of grafting density on brush polydispersity

The grafting density of surface-anchored polymers is defined as:

$$\sigma_P = \frac{h_P \cdot \rho \cdot N_A}{M_n} \quad , \tag{A3.37}$$

where h_P is the dry film thickness, ρ is the bulk density, N_A is Avogadro's number, and M_n is the average molecular weight. M_n is given by:

$$M_n = N_n \cdot M_0 \, , \tag{A3.38}$$

where M_0 is the monomer molecular weight and N_n is the number average degree of polymerization, given by:

$$N_n = \frac{\sum_{j=1}^{\infty} X_j \cdot N_j}{\sum_{j=1}^{\infty} X_j} \quad , \tag{A3.39}$$

where X_j is number of polymers having a degree of polymerization of N_j.

From mass conservation it follows that h_P is obtained by dividing the total volume of polymer all units in the film ($V_{polymer}$) by the sample area (A):

$$h_P = \frac{V_{polymer}}{A} \quad . \tag{A3.40}$$

$V_{polymer}$ is a product of the volume of a monomer (V_0) and the total number of segments present:

$$V_{polymer} = V_0 \cdot \sum_{j=1}^{\infty} X_j \cdot N_j \quad . \tag{A3.41}$$

By inserting the expressions given by Equations (A3.38)-(A3.41) into Equation (A3.37), one obtains:

$$\sigma_P = \frac{\frac{V_0 \cdot \sum_{j=1}^{\infty} X_j \cdot N_j}{A}}{\frac{\sum_{j=1}^{\infty} X_j \cdot N_j}{\sum_{j=1}^{\infty} X_j}} \cdot \frac{\rho \cdot N_A}{M_0} \quad . \tag{A3.42}$$

Assuming that the density of a polymer is equal to the density of a monomer, one obtains:

$$M_0 = V_0 \cdot \rho \cdot N_A \quad . \tag{A3.43}$$

Finally, after some algebra one obtains:

$$\sigma_P = \frac{\sum_{j=1}^{\infty} X_j}{A} \quad . \tag{A3.44}$$

Equation (A3.44) recovers the definition of the grafting density as a total number of polymers, *i.e.*, the numerator in Equation (A3.44), per unit area. Equation (A3.44) demonstrates that the grafting density of polymer brushes does not depend on the molecular weight distribution (*i.e.*, polydispersity) of the polymer brushes as long as the number of polymer brushes initiated does not increase after the polymerization commenced.

Discussion of modeling the SEC curves

In the paper we presented the polymer weight fraction as a function of the number average degree of polymerization for PMMA brushes grown via surface-initiated ATRP with $Cu^{(II)}/Cu^{(I)}$=0.010 for various reaction times (*cf.* **Figure 3.5**). The experimental data were modeled using the Schulz-Zimm (SZ), ATRP, Wesslau (W), Schultz-Flory (SF), and Smith *et al.* (S) models. The fits were obtained by minimizing the K-S statistic and the value of the K-S statistic at the minimum was taken as a measure of the quality of the fit. The results of the fits were presented in **Figure 3.6**, where we plotted the PDI *vs.* N_n. The results obtained indicated that the SZ, ATRP, and W models performed very well; the values of N_n and PDI obtained from the models matched very closely the experimental values of the same quantities. In contrast, the SF and S models, while they did capture the general shape of the MWD profiles, failed to reproduce quantitatively the experimental values of N_n and PDI.

Here we present plots similar to those in **Figure 3.5** and **Figure 3.6** for the remaining $Cu^{(II)}/Cu^{(I)}$ ratios. Specifically, in **Figures A.4**, **A.6**, and **A.8** we plot the polymer weight fraction as a function of the number average degree of polymerization for PMMA brushes grown via surface-initiated ATRP with $Cu^{(II)}/Cu^{(I)}$=0, 0.005, and 0.015, respectively. Experimentally measured data as well as best fits to the aforementioned models are provided. **Figures A.5**, **A.7**, and **A.9** display the dependence of PDI on N_n for experimental data as well as the values obtained from the best fits. Just as for the case $Cu^{(II)}/Cu^{(I)}$=0.010, the fits to the remaining $Cu^{(II)}/Cu^{(I)}$ concentrations reveal that the SZ, ATRP, and W models fit the

experimental data quantitatively well. The SF and S models do not describe the experimental data well.

For completeness, we also include the fits using the "chi-squared" approach to MWDs from PMMA brushes grown from silica surfaces using ATRP with $Cu^{(II)}/Cu^{(I)}=0.010$ for various reaction times. Note that the fits obtained by the K-S method are plotted in **Figure 3.5** and **Figure 3.6**. The models due to SZ, ATRP, W, SF, and S approaches are plotted in **Figure A.10**. The PDI vs. N_n dependence is presented in **Figure A.11**. The trends seen in **Figure A.11** match those discussed earlier with regard to **Figure 3.6**. In spite of this agreement, the K-S method is preferred in fitting the data because if captures the functional form of the various models better than the "chi-squared" approach, as discussed earlier.

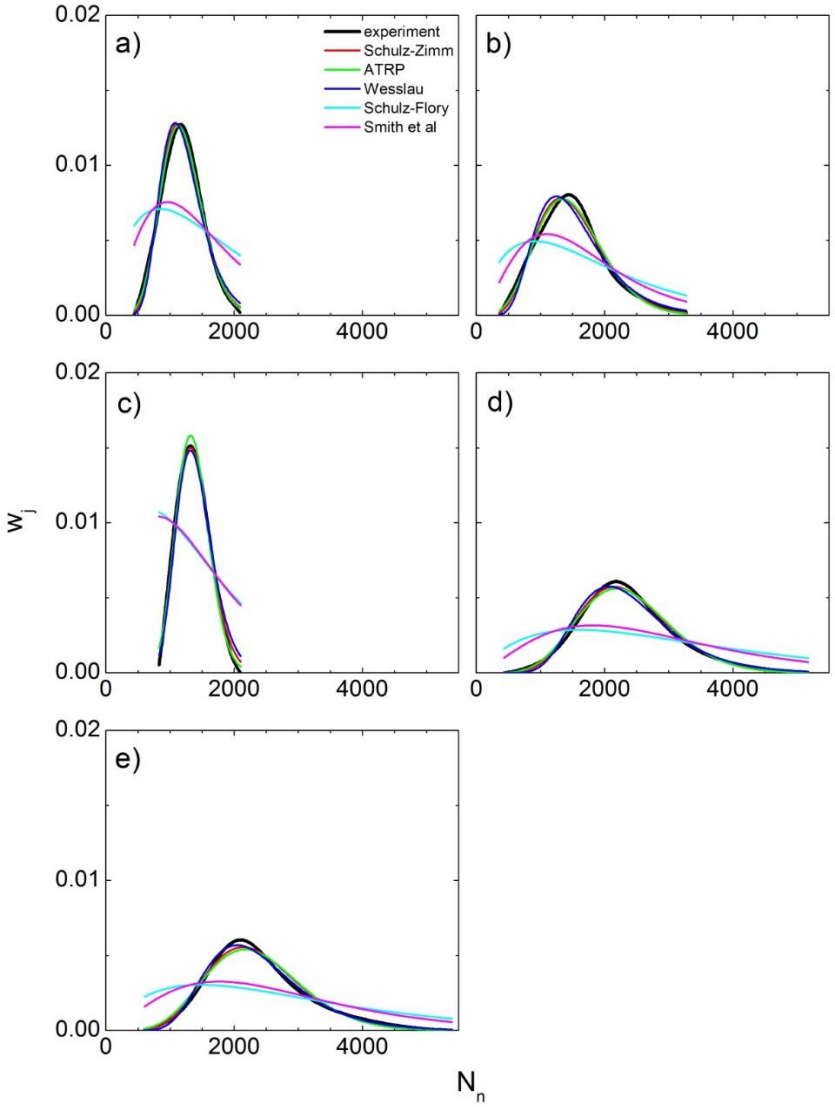

Figure A.4. Weight fraction of PMMA chains (w_j) degrafted from flat surfaces (black lines) as a function of number average degree of polymerization (N_n) for PMMA brushes grown for a) 6, b) 9, c) 16, d) 20, and e) 24 hrs with $Cu^{(II)}/Cu^{(I)}=0$ (see experimental section for details). The experimental data were fitted using the Kolmogorov-Smirnov (K-S) method to distributions featuring the models of Schulz-Zimm (red), ATRP (green), Wesslau (blue), Schulz-Flory (cyan), and Smith *et al.* (magenta).

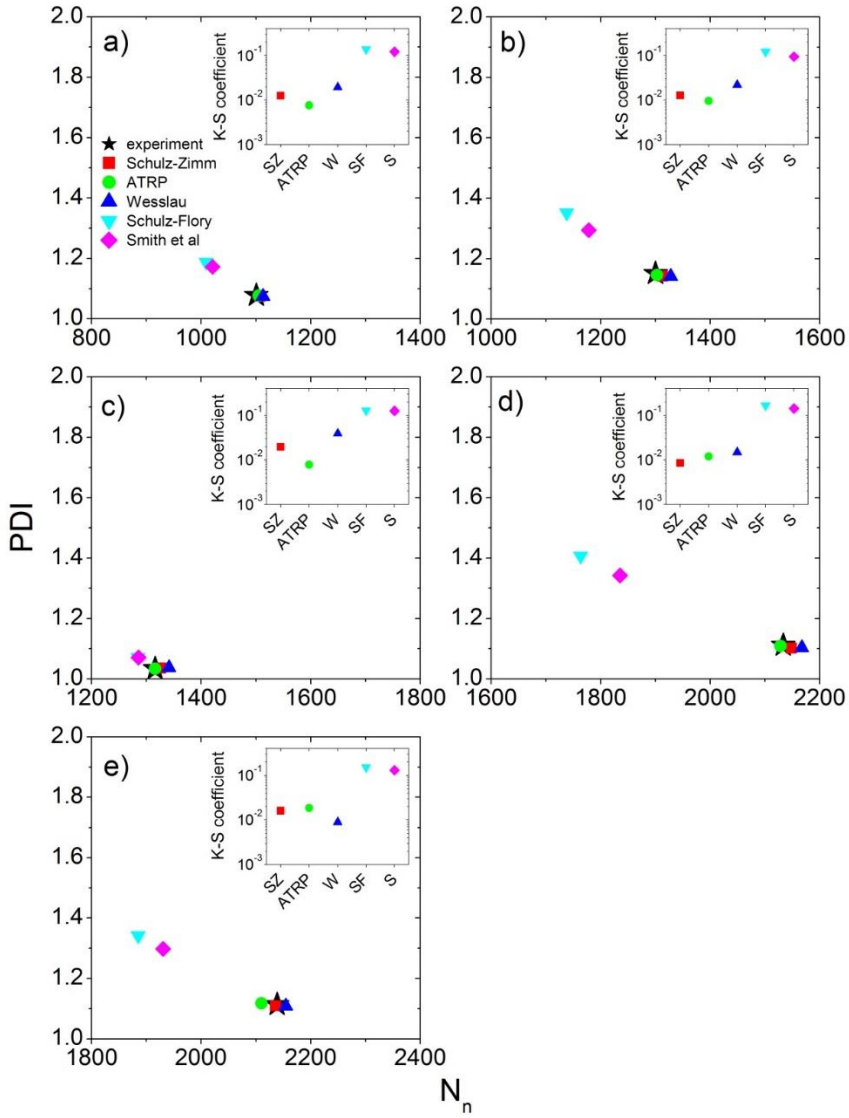

Figure A.5. Polydispersity index (PDI) vs. number average degree of polymerization (N_n) for PMMA chains degrafted from flat surfaces (black star) grown for a) 6, b) 9, c) 16, d) 20, and e) 24 hrs with $Cu^{(II)}/Cu^{(I)}=0$ (see experimental section for details). The experimental data were fitted using the Kolmogorov-Smirnov (K-S) method to distributions featuring the models of Schulz-Zimm (red square), ATRP (green circle), Wesslau (blue up-triangle), Schulz-Flory (cyan down-triangle), and Smith *et al.* (magenta-diamond).

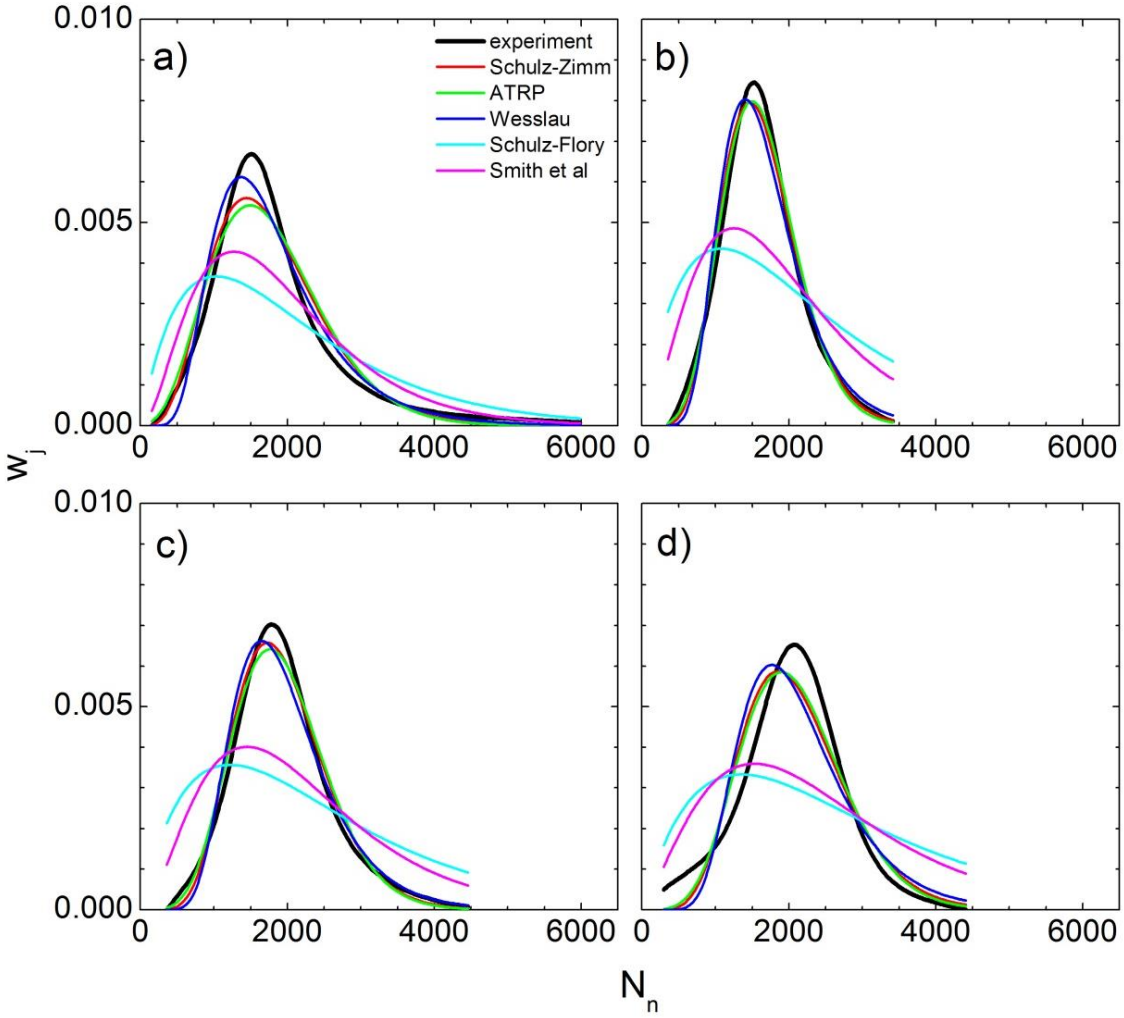

Figure A.6. Weight fraction of PMMA chains (w_j) degrafted from flat surfaces (black lines) as a function of number average degree of polymerization (N_n) for PMMA brushes grown for a) 12, b) 16, c) 20, and d) 24 hrs with $Cu^{(II)}/Cu^{(I)}$=0.005 (see experimental section for details). The experimental data were fitted using the Kolmogorov-Smirnov (K-S) method to distributions featuring the models of Schulz-Zimm (red), ATRP (green), Wesslau (blue), Schulz-Flory (cyan), and Smith *et al.* (magenta).

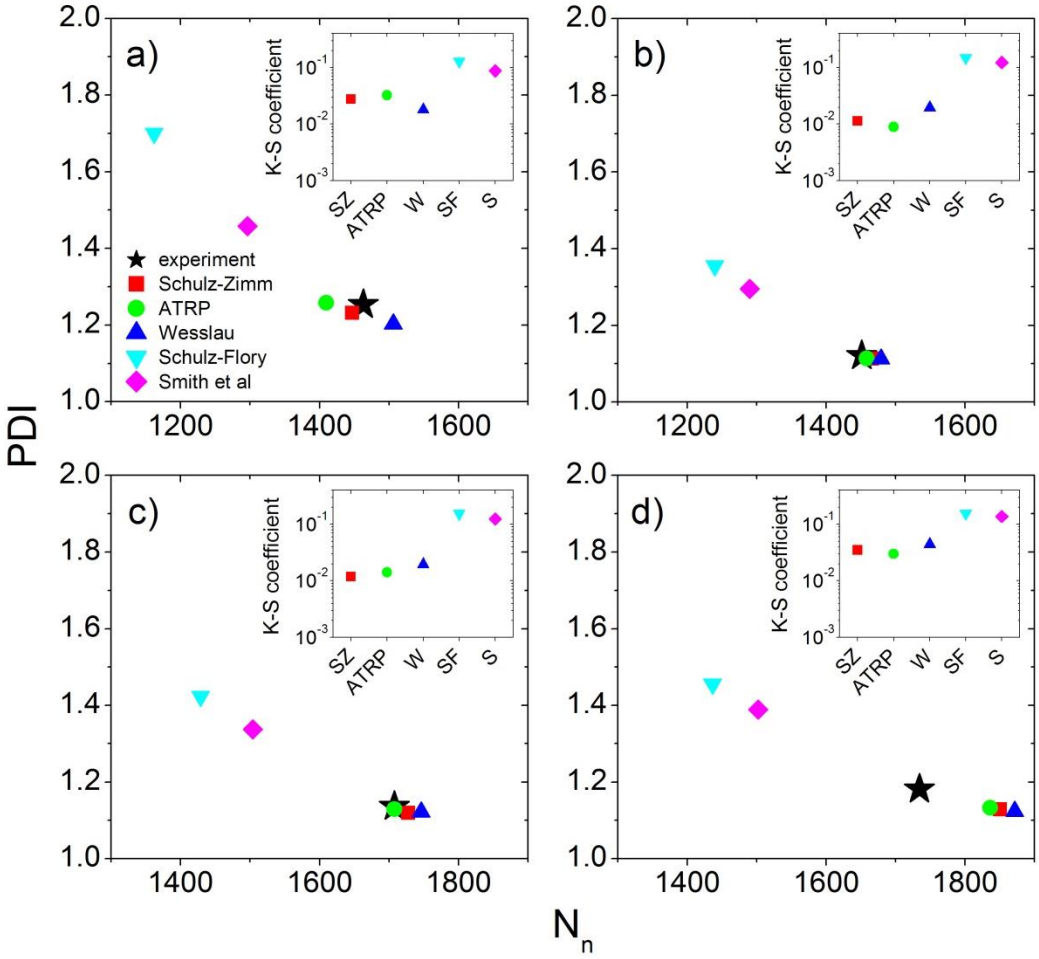

Figure A.7. Polydispersity index (PDI) vs. number average degree of polymerization (N_n) for PMMA chains degrafted from flat surfaces (black star) grown for a) 12, b) 16, c) 20, and d) 24 hrs with $Cu^{(II)}/Cu^{(I)}$=0.005 (see experimental section for details). The experimental data were fitted using the Kolmogorov-Smirnov (K-S) method to distributions featuring the models of Schulz-Zimm (red square), ATRP (green circle), Wesslau (blue up-triangle), Schulz-Flory (cyan down-triangle), and Smith *et al.* (magenta-diamond).

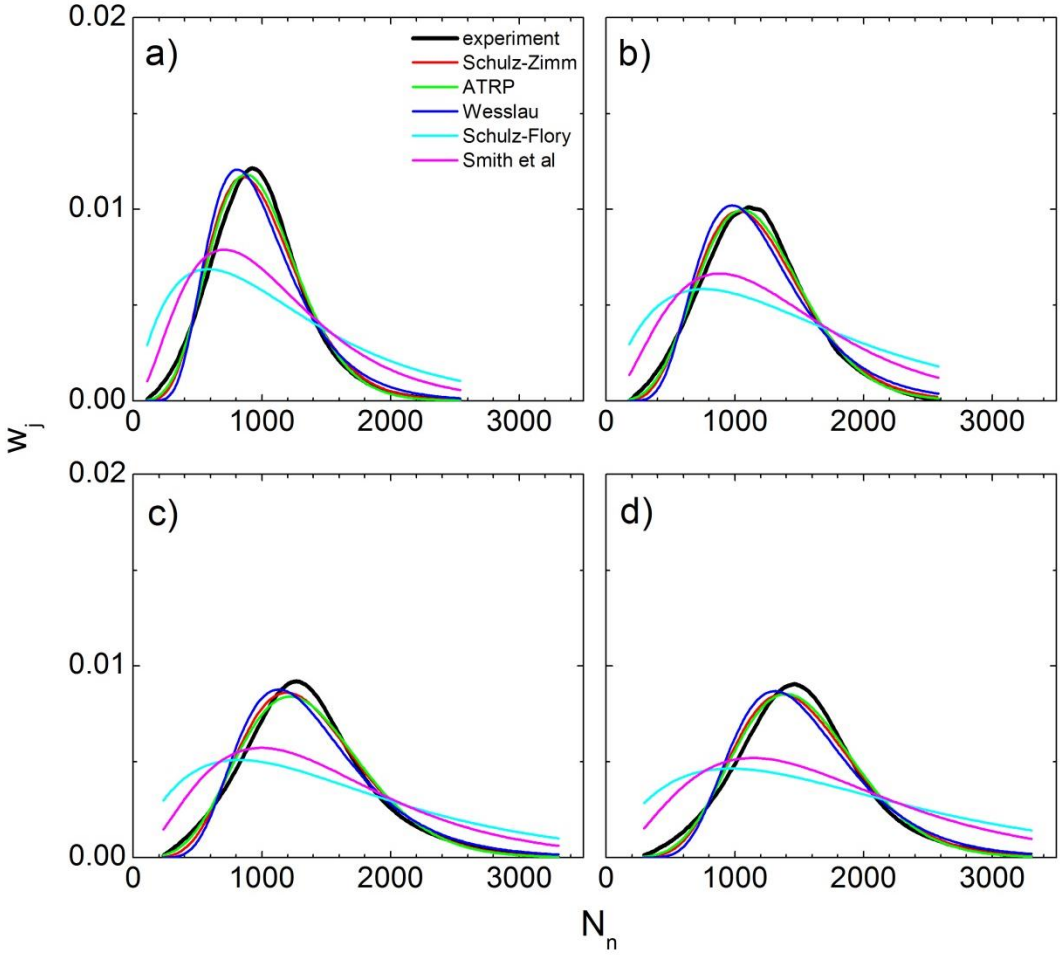

Figure A.8. Weight fraction of PMMA chains (w_j) degrafted from flat surfaces (black lines) as a function of number average degree of polymerization (N_n) for PMMA brushes grown for a) 12, b) 16, c) 20, and d) 24 hrs with $Cu^{(II)}/Cu^{(I)}$=0.015 (see experimental section for details). The experimental data were fitted using the Kolmogorov-Smirnov (K-S) method to distributions featuring the models of Schulz-Zimm (red), ATRP (green), Wesslau (blue), Schulz-Flory (cyan), and Smith *et al.* (magenta).

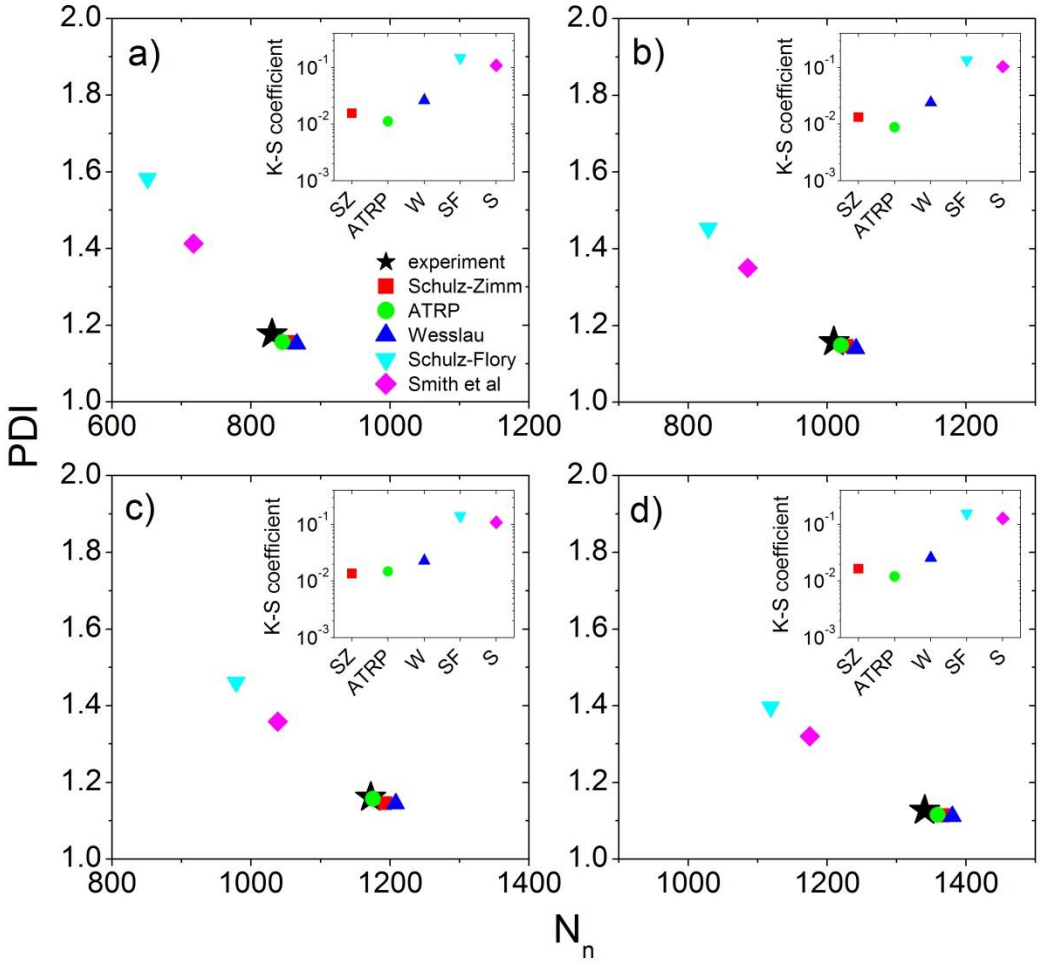

Figure A.9. Polydispersity index (PDI) vs. number average degree of polymerization (N_n) for PMMA chains degrafted from flat surfaces (black star) grown for a) 12, b) 16, c) 20, and d) 24 hrs with $Cu^{(II)}/Cu^{(I)}$=0.015 (see experimental section for details). The experimental data were fitted using the Kolmogorov-Smirnov (K-S) method to distributions featuring the models of Schulz-Zimm (red square), ATRP (green circle), Wesslau (blue up-triangle), Schulz-Flory (cyan down-triangle), and Smith *et al.* (magenta-diamond).

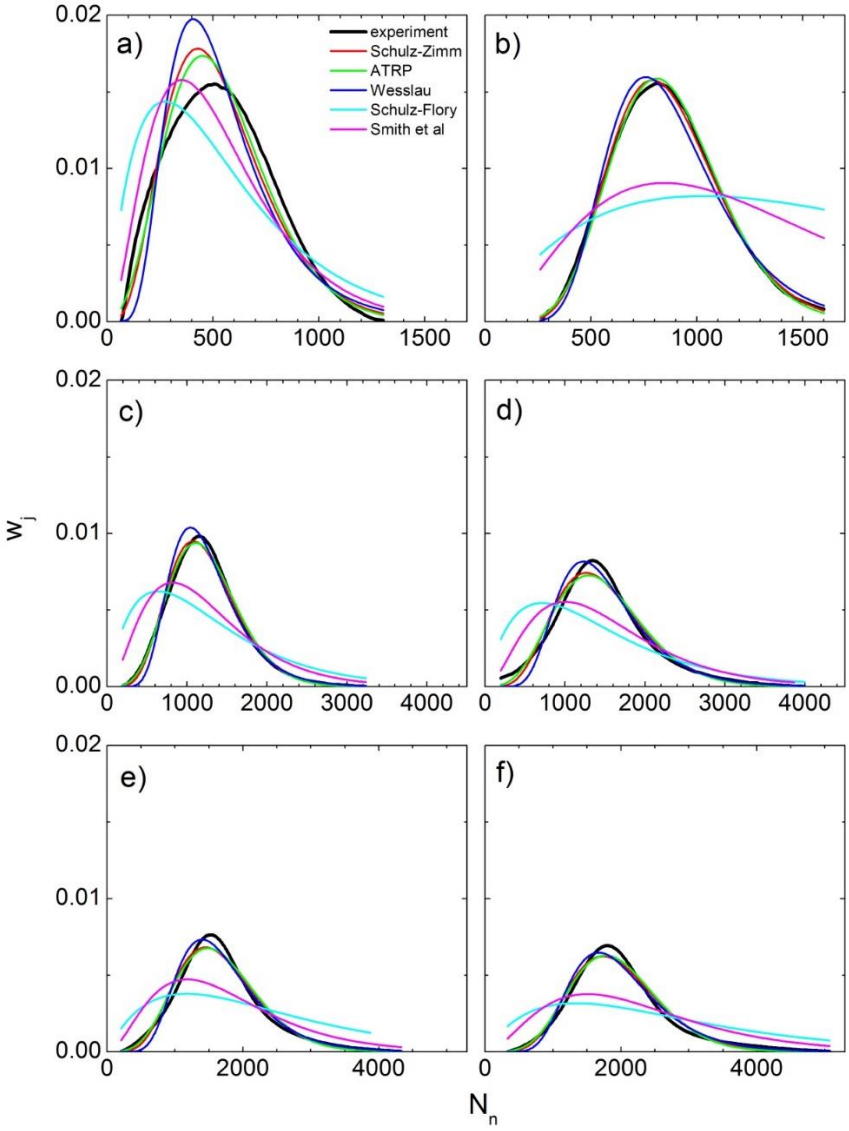

Figure A.10. Weight fraction of PMMA chains (w_j) degrafted from flat surfaces (black lines) as a function of number average degree of polymerization (N_n) for PMMA brushes grown for a) 6, b) 9, c) 12, d) 16, e) 20, and f) 24 hrs with $Cu^{(II)}/Cu^{(I)}$=0.010 (see experimental section for details). The experimental data were fitted using the "chi-squared" (χ^2) method to distributions featuring the models of Schulz-Zimm (red), ATRP (green), Wesslau (blue), Schulz-Flory (cyan), and Smith *et al.* (magenta).

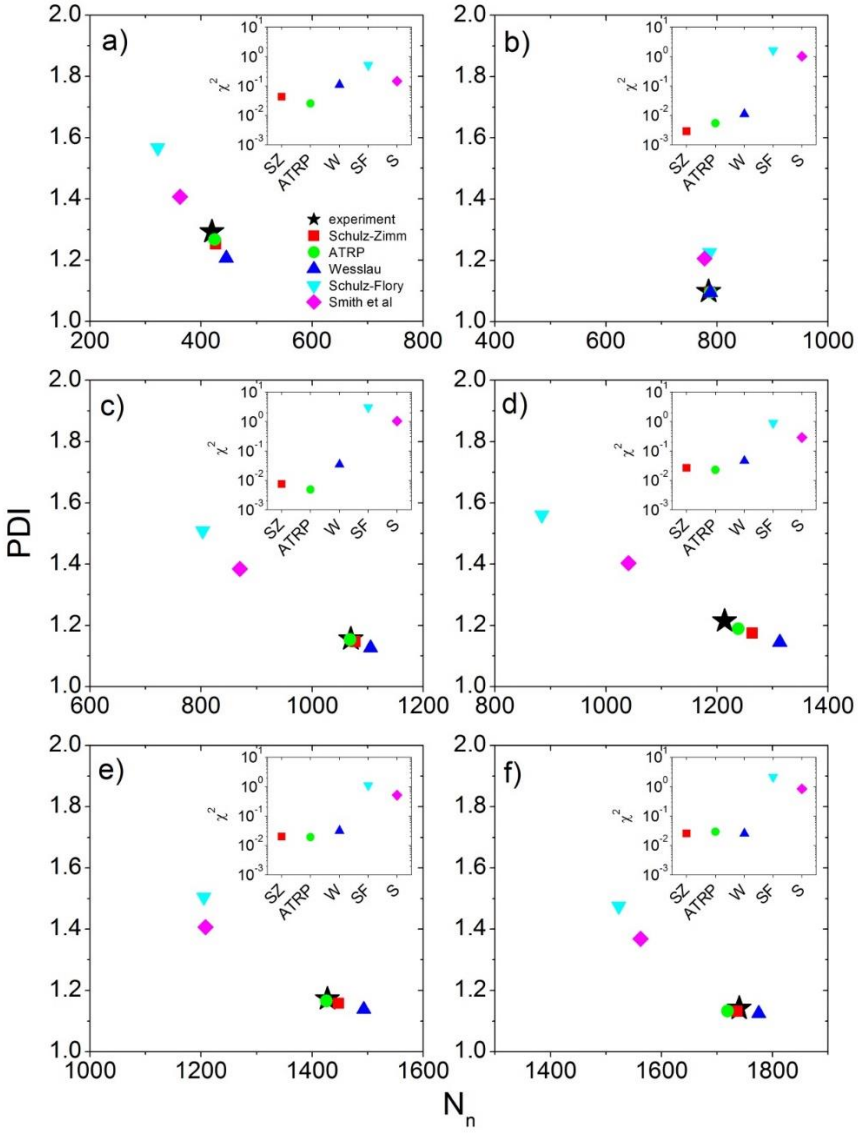

Figure A.11. Polydispersity index (PDI) vs. number average degree of polymerization (N_n) for PMMA chains degrafted from flat surfaces (black star) grown for a) 6, b) 9, c) 12, d) 16, e) 20, and f) 24 hrs with $Cu^{(II)}/Cu^{(I)}$=0.010 (see experimental section for details). The experimental data were fitted using the "chi-squared" (χ^2) method to distributions featuring the models of Schulz-Zimm (red square), ATRP (green circle), Wesslau (blue up-triangle), Schulz-Flory (cyan down-triangle), and Smith *et al.* (magenta-diamond).

A.1 References

(1) Brandup, J.; Immergut, E. H.; Grulke, E. A. John Wiley & Sons: New York, 1999; p V/91 – V/95.

(2) Brandup, J.; Immergut, E.; Grulke, E. In *Interscience, New York*; John Wiley & Sons: New York, 1999; p V/87 – V/89.

(3) Sigma Aldrich http://www.sigmaaldrich.com/chemistry/solvents/tetrahydrofuran-center.html (accessed Oct 9, 2014).

(4) Sigma Aldrich http://www.sigmaaldrich.com/chemistry/solvents/toluene-center.html (accessed Oct 9, 2014).

(5) Hiemenz, P. C.; Lodge, T. P. *Polymer chemistry*, 2nd Editio.; Taylor & Francis: Boca Raton, FL, USA, 2007, 2007.

(6) Schulz–Zimm distribution http://goldbook.iupac.org/S05502.html (accessed Oct 9, 2014).

(7) Mastan, E.; Zhou, D.; Zhu, S. *J. Polym. Sci. Part A Polym. Chem.* **2014**, *52* (5), 639–651.

(8) Most probable distribution (in macromolecular assemblies) http://goldbook.iupac.org/M04035.html (accessed Oct 9, 2014).

(9) Grulke, E. A. *Polymer process engineering*; TPS Publishing Company: Lexington, KY, USA, 1994.

(10) Smith, W. B.; May, J. A.; Kim, C. W. *J. Polym. Sci. Part A-2* **1966**, *4*, 365–374.

(11) Odian, G. *Principles of polymerization*; John Wiley & Sons: Hoboken, NJ, USA, 2004.

(12) Painter, P. C.; Coleman, M. M. *Essentials of polymer science and engineering*; DEStec publications: Lancaster, PA, USA, 2009.

(13) Hollander, M.; Wolfe, D. A. *Nonparametric statistical methods*; Wiley-VCH Verlag GmbH & Co. KGaA: Chicester, UK, 1999.

(14) Greenwood, P. E.; Nikulin, M. S. *A guide to chi-squared testing*; Wiley-VCH Verlag GmbH & Co. KGaA: New York, 1996.

APPENDIX B

B.1 Experimental details

Chemicals

All chemicals were purchased from Sigma Aldrich and used as received unless otherwise specified. Styrene (S) was passed through activated basic alumina to remove 4-tert-butylcatechol which acts as an inhibitor. Methyl methacrylate (MMA) was passed through inhibitor remover column to remove the inhibitor monomethyl ether hydroquinone. Millipore Elix 3 was used to obtain deionized water (DIW) with resistivity >15 MΩ.cm. Anhydrous toluene was prepared by adding molecular sieves (4 Å) activated by heating them using a heating gun for 30 minutes under vacuum. $CuCl_2$ was purified by first dissolving in ethanol and then precipitated in hexanes. (11-(2-bromo-2-methyl) propionyloxyundecyl trichlorosilane (eBMPUS) was purchased from Gelest. ACS grade methanol was obtained from Fisher Scientific. Electronics grade silicon wafers (p-doped, orientation <100>) were purchased from Silicon Valley Microelectronics. Tetrabutyl ammonium fluoride (TBAF) was purchased from Sigma Aldrich as a 1 M solution in THF.

Initiator deposition

In the conventional method a monolayer of the BMPUS initiator was deposited after exposing the silicon substrate to ultraviolet-ozone (UVO) for 15 minutes. A solution of initiator was prepared in anhydrous toluene by adding 1 μl of eBMPUS stock solution (5% w/w in toluene)

per 1 ml of anhydrous toluene. The substrates were placed back to back in disposable glass vials so that the polished sides were exposed to the solution. The vials were sealed with parafilm and placed into freezer at -18°C for 18 hours. After that the substrates were thoroughly rinsed with toluene and dried under a stream of nitrogen gas. In case of degrafting and re-deposition of eBMPUS, the substrates were not treated with UVO but directly incubated in eBMPUS solution.

Growing Polystyrene (PS) brushes

Styrene (60.93 ml, 0.59 mol), DMSO (18.50 ml, 0.24 mol), were added to a round bottom flask. The solution was stirred and degassed by bubbling nitrogen gas for 20 minutes. The ligand PMDETA (0.6 ml, 3.4 mmol), catalyst CuBr (184.6 mg, 1.3 mmol) were added and the solution was further degassed for another 20 minutes. The initiator-containing substrates were placed back to back in a disposable glass vial and the polymerization solution was added. The vial was sealed and stored at room temperature for 24 hours.

Growing Poly (methyl methacrylate) (PMMA) brushes

MMA (32.97 ml, 0.308 mol), Methanol (30.42 ml, 0.751 mol) and deionized water (6.6 ml, 0.367 mol) were added to a round bottom flask, stirred and degassed by bubbling nitrogen gas for 20 minutes. The ligand 2,2'-bipyridyl (1.94 g, 12.4 mmol), catalyst CuCl (0.622 g, 6.29 mmol) and $CuCl_2$ (4.22 mg, 0.031 mmol) were added and the solution was further degassed

for 20 minutes. The $Cu^{(II)}$:$Cu^{(I)}$ molar ratio was 0.005 and total solution was 70 ml. The substrates with deposited initiator layers were placed back to back in glass vials. About 20 ml of solution was added to each of the 3 glass vials which were then sealed and stored at room temperature for 24 hours.

Characterization

The dry thickness was determined by fitting data obtained from the variable angle spectroscopic ellipsometry (VASE, J.A. Woollam Co., Inc.) to a 3 layer model (bottom silicon, intermediate silica (SiO_x), and top "Cauchy" polymer layer). Thermo Nicolet 6700 was uses to obtain FTIR spectra in transmission mode (resolution 4 cm^{-1}) with 32 background scans (silicon wafer) and 512 scans of the sample. The static water contact angle was measured using contact angle goniometer (Ramé Hart, model 100-00) using deionized water as a probing liquid. X-ray photoelectron spectroscopy (XPS) experiments were carried using a SPECS FlexMod instrument with Al Kα source (excitation energy 1486.7 eV) with a takeoff angle of 30° measured relative to the normal. Energy calibration was done by using adventitious carbon as a reference (C 1s line with binding energy of 285 eV). Survey scans were measured with steps of 0.5 eV and 0.04 s dwell per point and pass energy (E_{pass}) setting of 24. High resolution scans were collected with a step size of 0.1 eV, with 0.5 s dwell per point and E_{pass} setting of 20.

B.2 High resolution XPS spectra

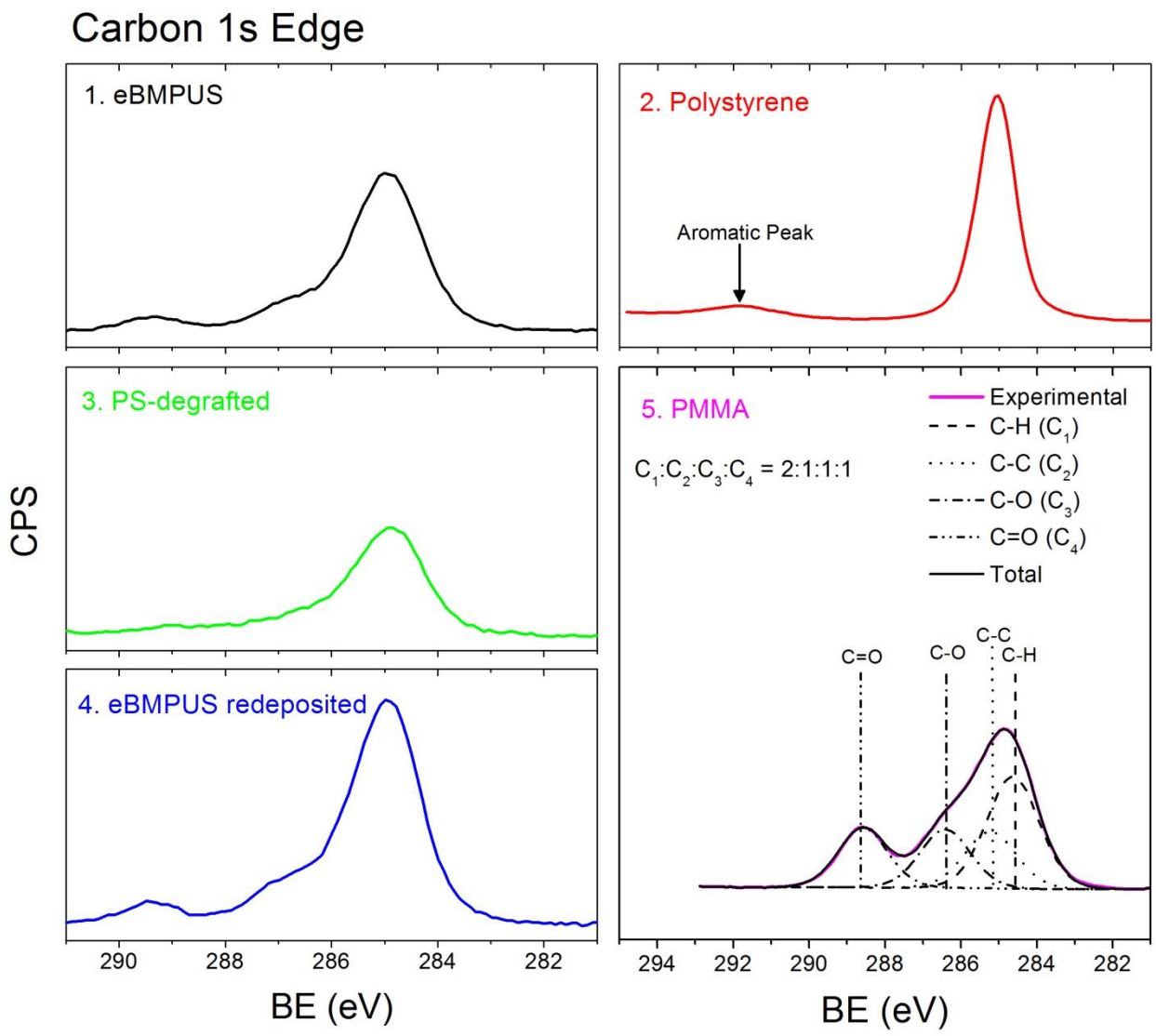

Figure B.1. High resolution C 1s spectra for substrates corresponding to Figure 1. The y axes scales are matched for eBMPUS, PS-degrafted and eBMPUS redeposited while the polystyrene scale is matched with PMMA.

The high resolution spectra for carbon 1s peaks are shown in **Figure B.1** for the 5 substrates displayed in Figure 1 in the paper. The number of photoelectrons is matched on the y axes for

the eBMPUS, the PS-degrafted and the eBMPUS redeposited substrate. There are subtle differences between the shapes of the C 1s peaks for each substrate. For the first eBMPUS and eBMPUS-redeposited substrate a small carbonyl (O–C=O) peak at BE ~289.5 eV is observed. The overall intensity is smallest for the degrafted substrate which indicates the presence of only a small amount of organic material which could feature undegrafted polystyrene chains, undegrafted and uninitiated initiator or simply adventitious carbon. A strong C-C peak is observed for polystyrene at 285 eV along with a small aromatic peak at ~292 eV. In case of PMMA synthetic components for each type of carbon are fitted to experimental data and the ratio of the areas under the peaks matches with the stoichiometric ratio corresponding to its chemical structure. The ratio of peak areas for C-H (dash), C-C (dot), C-O (dash-dot) and C=O (dash-dot-dot) is 2:1:1:1 which is the ratio of the number of C atoms in the structure for PMMA.

B.3 Reusing substrate after degrafting initiator

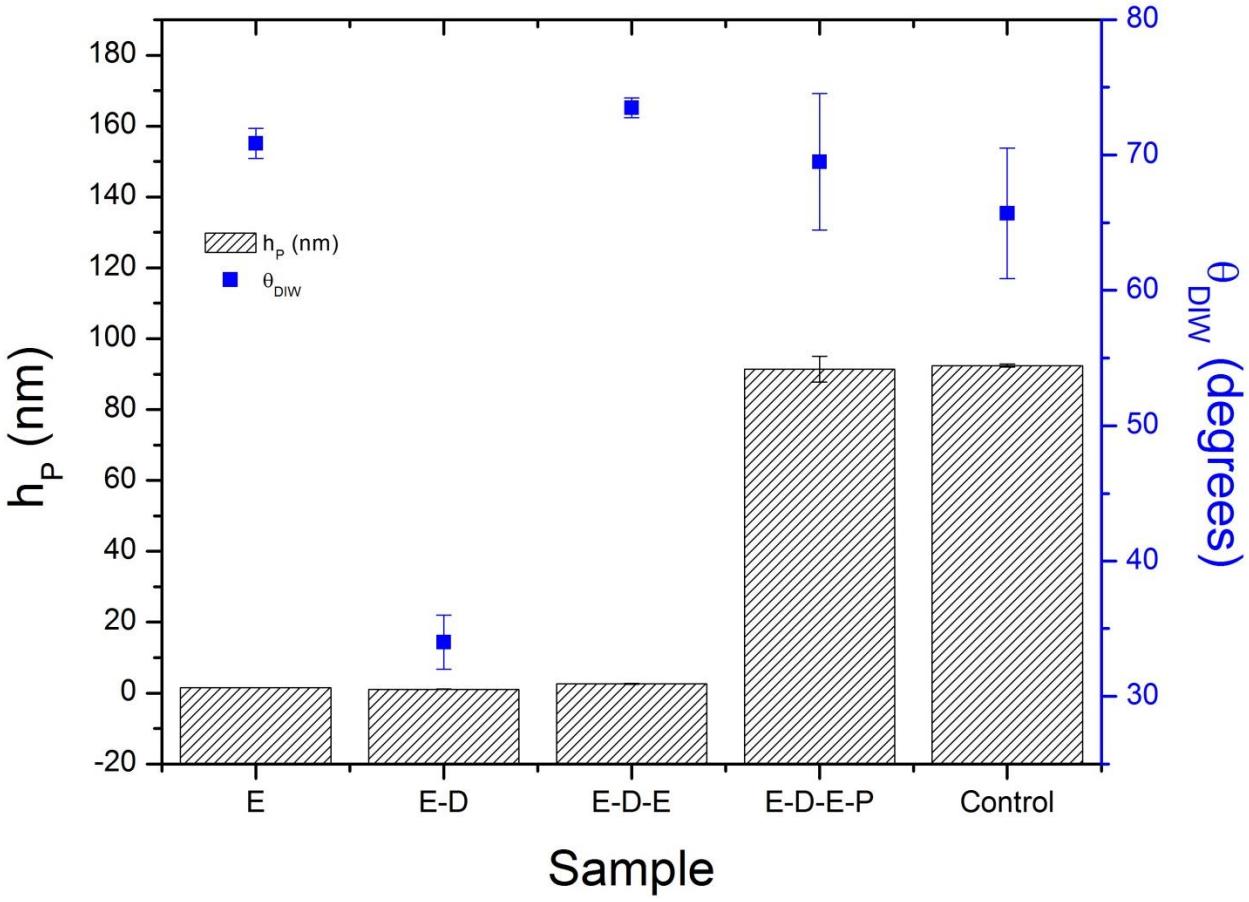

Figure B.2. Dry ellipsometric thickness (h_P) and water contact angle (θ_{DIW}) for eBMPUS (E) initiator degrafting, redeposition and PMMA brush layer (P) grown after degrafting by ATRP.

An alternative experiment to the one described in **Figure 5.2** is shown here in **Figure B.2** where we first deposit eBMPUS (E) using conventional method, *i.e.*, by using ultraviolet-ozone (UVO) to activate the surface. This initiator layer is degrafted (E-D) by incubating the substrate in 0.1 M TBAF at 50°C for 1 hour. After degrafting the ellipsometric thickness decreases from 1.6 ± 0.2 nm to 1 ± 0.05 nm while the water contact angle (θ_{DIW}) decreases

from 71 ± 1 to 34 ± 2 degrees. This substrate is then redeposited by eBMPUS initiator layer (E-D-E) without using UVO treatment which increases its thickness to 2.6 ± 0.15 nm and θ_{DIW} to 74 ± 1 degrees. PMMA is subsequently grown on the initiator layer by ATRP with Cu^{II}:Cu^{I} = 0.005 at room temperature for 24 hours. The resulting layer (E-D-E-P) is 91 ± 4 nm thick and has θ_{DIW}=66 ± 5 degrees, which is comparable to that of the PMMA control sample with conventionally deposited eBMPUS grown in the same polymerization solution.

B.4 OTS pattern to PMMA brush pattern

A complimentary method to that shown in **Figure 5.4** to create surface patterns of polymer brushes involves by first creating a pattern of the initiator by degrafting and then growing brushes. We carried this out by first creating a monolayer of inert n-octyltrichlorosilane (OTS) on silicon substrate (*cf.* **Figure B.3**). A pattern was then stamped onto the substrate using TBAF containing hydrogel stamp which removed the OTS layer. This substrate was then incubated in an eBMPUS solution to create an initiator deposited layer which was then amplified by growing PMMA brush using ATRP. The pattern is visible in the optical images shown in Figure S3, (b) due to a dry thickness of >40 nm.

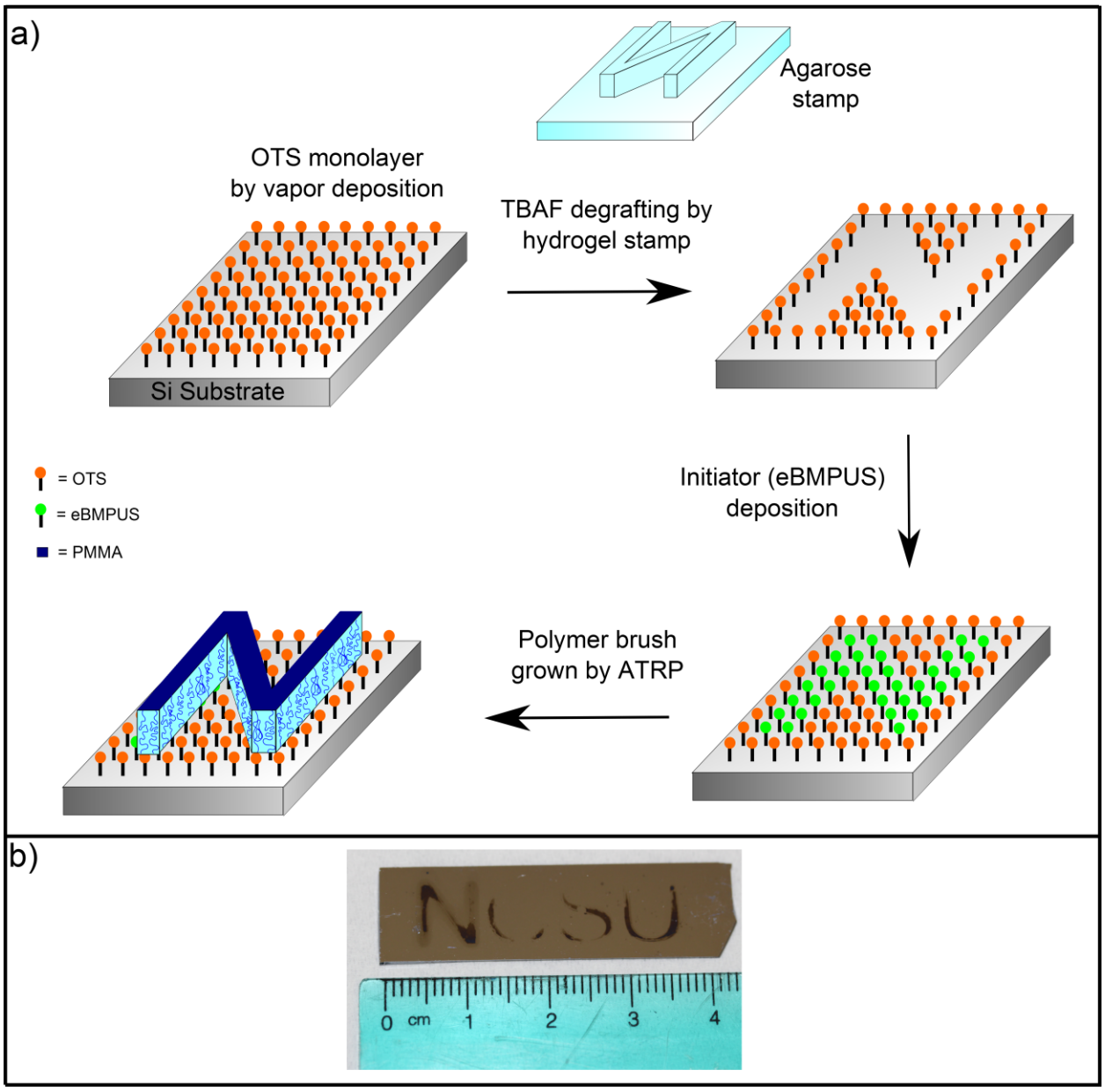

Figure B.3. a) Scheme to create polymer patterns by TBAF degrafting of OTS, initiator deposition and PMMA brush growth, (b) Optical images of the PMMA brush pattern on silicon substrate. The size of the entire substrate is approximately 4.3 cm x 1.2 cm.